MRI-guided Focused Ultrasound Application for Targeted Drug Delivery

Navid Farr

A dissertation
submitted in partial fulfillment of the
requirements for the degree of

Doctor of Philosophy

University of Washington
2014

Reading Committee:

Joo Ha Hwang, Chair

Lawrence Crum

Vera Khokhlova

Program Authorized to Offer Degree: Department of Bioengineering

University of Washington

Abstract

MRI-guided Focused Ultrasound Application for Targeted Drug Delivery

Navid Farr

Chair of the Supervisory Committee:
Joo Ha Hwang, MD, PhD
Associate Professor of Medicine
Adjunct Associate Professor of Bioengineering and Radiology

Pancreatic cancer is one of the most incurable and lethal human cancers in the United

States. Mild hyperthermia (~ 41 °C) has been shown effective as an adjuvant for chemotherapy.

An optimal mild hyperthermia treatment is targeted and non-invasive without tissue damage or

vascular shutoff. High intensity focused ultrasound (HIFU) can non-invasively heat solid

tumors without heating the surrounding organs. Magnetic resonance imaging (MRI) is suitable

for therapy planning and monitoring of HIFU therapy due to its high spatial image resolution

and ability to measure temperature changes in real time. Magnetic resonance-guided high

intensity focused ultrasound (MR-g HIFU) is the novel approach for non-invasive mild

hyperthermia applications. Temperature sensitive liposomes (TSL) release their drug cargo at

the target temperature and in combination with mild hyperthermia may improve drug delivery

to solid tumors.

The objectives of this dissertation were to evaluate the ability of conventional and

multi-parametric MRI techniques to characterize pancreas tumor in three different animal

models. In addition, to develop and implement targeted drug delivery methods using mild

hyperthermia induced by HIFU under guidance and monitoring of MRI in combination with

TSL for pancreatic cancer. Moreover, to assess the short-term tumoricidal activity against tumor in response to MR-HIFU hyperthermia targeted drug delivery.

The characterization of tumor models using conventional and multi-parametric MRI provided valuable information regarding tumor properties that can be use as *in vivo* markers for targeting and therapy monitoring. The combination of hyperthermia induced by MR-HIFU and TSL loaded with chemotherapy resulted in significantly higher tumor drug concentrations compared to TSL alone and free drug. Finally survival studies indicated combination of MR-HIFU and TSL for targeted drug delivery resulted in greater tumor response to the therapy. This technique has potential for clinical translation as an image guided method to deliver drug to pancreas tumor.

Acknowledgements

Navid Farr

December 2014, Seattle, WA

Dedication

I dedicate this thesis to my family which has given me love, joy, and support

throughout my life.

Table of contents

List of Abbreviations

3D	Three-dimensional
ADC	Apparent diffusion coefficient
cisPt	Cisplatin
CT	Computed tomography
DCE	Dynamic contrast enhanced
DNR	Daunorubicin
DOX	Doxorubicin
DPPC	Dipalmitoylphosphatidylcholine
DPPGOG	Dipalmitoyl-sn-glycero-3-phosphoglyceroglycerol
DSPC	Distearoylphosphatidylcholine
DWI	Diffusion weighted imaging
EM	Equivalent minutes
FA	Flip angle
FUS	Focused ultrasound surgery
HBSS	Hanks Balanced Salt Solution
HCC	Hepatocellular carcinoma
HIFU	High intensity focused ultrasound
HPLC	High-performance liquid chromatography
HSPC	Hydrogenated soy phosphocholine
H&E	Hematoxylin and eosin
IACUC	Institutional Animal Care and Use Committee
IFP	Interstitial fluid pressure
IHC	Immunohistochemistry
LTSL	Lysolipid thermosensitive liposomes
lyso-PCs	Lysolipid phosphocholine
MRI	Magnetic resonance imaging

MRgFUS	MRI-guided focused ultrasound surgery
MT	Magnetization transfer
MTD	Maximum tolerated dose
MTI	Magnetization transfer imaging
MTR	Magnetization transfer ratio
Ortho	Orthotopic
PDA	Pancreatic ductal adenocarcinoma
PEG	Polyethyl glycol
PRF	Pulse-repetition frequencies
PRFS	Proton resonance frequency shift
RF	Radio frequency
RFA	Radio frequency ablation
ROI	Region of interest
SNR	Signal-to-noise ratio
Subq	Subcutaneous
SWL	Shock wave lithotripsy
T2WI	T2-weighted imaging
TDox	ThermoDox
TE	Echo time
TR	Repetition time
TSL	Temperature sensitive liposomes, Thermosensitive liposome

List of Figures

List of Tables

Chapter 1. Introduction

1.1 Motivation

The general purpose of the research described in this dissertation was to investigate the biological effects (bioeffects) of hyperthermia induced by high intensity focused ultrasound (HIFU) in conjunction with systemically administered, drug-loaded temperature sensitive liposomes (TSL) in pancreatic cancer tumors, and whether these bioeffects can result in higher concentration and penetration of drug. Identifying the potential mechanisms involved in HIFU-induced, local release of drugs loaded in liposomal carriers or enhancing the penetration of drug into the interstitium of tumors is important for all therapeutic ultrasound applications.

The field of therapeutic ultrasound has been in development since 1917, when, during the development of sonar, Langevin first observed fish death [1]. In 1938, therapeutic ultrasound was first considered for use on humans when Ziess began to study the effects of ultrasound on the eye [2]. Now, therapeutic ultrasound is used in clinics and physical therapy centers around the world to treat a wide range of diseases ranging from prostate cancer, bone metastases, uterine fibroids, and kidney stones to treatment of essential tremor. The main advantage to using ultrasound as a therapeutic agent is that it can produce clinical effects on tissues deep inside the body without damaging the intervening tissue. Ultrasound has additional advantages of being a real-time imaging modality that is relatively inexpensive and can be extremely portable.

The most well-known use of ultrasound is for imaging; however, new and widespread therapies are in various stages of development. While many of the therapeutic anti-tumoral effects of ultrasound are elicited by some degree of hyperthermia (mild or extreme) and ablation of center of the tumor, other therapies utilize acoustically excited bubbles which interact mechanically with the tissues. Bubbles can be used to enhance drug delivery through the formation of transient pores in the cell membrane [2] [3]; aid in the breaking of kidney stones in shock wave lithotripsy (SWL) [4]; and can be used to emulsify cancerous tumors or other unwanted tissues in cavitation cloud and boiling histotripsy [5]. With the new development of liposomal drug carriers therapeutic ultrasound has shown its potential in the field of targeted drug delivery. While the diagnostic ultrasound is a perfect imaging modality, to date It has not been capable of providing real-time tissue temperature estimates, and is thus poorly suited for monitoring thermal therapies.

Magnetic resonance imaging (MRI) is now used to providing the necessary guidance and monitoring for thermal ultrasound therapies. This noninvasive imaging modality has excellent soft-tissue contrast and is used widely for image guided interventions, and can also aid in the treatment planning of focused ultrasound surgery (*FUS*) therapy. Moreover, several MR tissue parameters are altered as a result of ablation and MRI can thus also be used to visualize the severity of tissue damage following treatment. Perhaps the most important utility of MRI for HIFU therapy is its ability to produce high-

resolution *in vivo* temperature maps that can be used to visualize the temperature rise in real-time in any imaging plane within the body [6] [7].

The clinical potential of magnetic resonance imaging (MRI)-guided focused ultrasound surgery (*MRgFUS*) is to provide noninvasive, controlled, safe, and accurate treatment. Clinical MRgFUS systems have been used for *high temperature ablative treatment* of uterine fibroids [8], [9], breast cancer [10], prostate cancer [11], brain tumors, and the treatment of essential tremor [12]–[15]. MRgFUS technology has also been used to perform relatively *low temperature hyperthermia treatments* (*viz.*, to elevate and maintain the temperature to 40-45°C [16]) and, of special interest in this dissertation, to effect hyperthermia-induced targeted drug delivery [17]–[19]. During therapy, vascular shut down, which can occur at hyperthermic exposures as low as 43°C, may be avoided by maintaining the temperature within a narrow temperature range [20], [21].

HIFU can only be used to facilitate release the drug loaded in liposomal carriers, or whether it can also be used to enhance drug penetration into the tumor interstitium, identifying the potential mechanisms involved is an important step toward clinical applications. In addition accurate guidance, monitoring and evaluation of absorption and distribution of the drug and physiological read-outs to evaluate the therapeutic efficacy is a certain need of different MRgFUS therapies. The guiding clinical motivation for the research presented in this dissertation is to examine in the ability to use HIFU mediated hyperthermia under guidance of MRI in combination of TSL drug to achieve controlled release of and consequently higher concentration of the drug in the targeted tumor. This

approach could be applied to improve chemotherapy and the treatment of pancreatic cancer.

1.2 Objectives

This dissertation investigates whether HIFU-induced hyperthermia in conjunction with systemically administered TSL loaded with chemotherapy agent results in higher tissue concentration and penetration of drug compared with other drugs or with no hyperthermia. Microscopic morphologic analysis was performed using standard tissue histology methods as well as florescent microscopy to evaluate the drug release and uptake by tumor cells qualitatively. In addition, quantitative measurements of the drug concentration was performed using high-performance liquid chromatography (*HPLC*).

This dissertation will also characterize the properties of three different pancreatic cancer mouse model using quantitative multi-parametric MR analysis. Moreover, in a feasibility study, this dissertation investigates the ability of multi-parametric MR analysis to assess the HIFU-induced hyperthermia.

1.3 Hypotheses and Specific Aims

The work described in this dissertation has been divided into 4 aims:

Specific Aim 1: Assess the tissue concentration and penetration of doxorubicin in pancreas tumors treated with HIFU to induce hyperthermia in conjunction with systemic administration of either ThermoDox® or free doxorubicin.

Hypothesis: HIFU induced hyperthermia in combination with TSL loaded chemotherapy agent will increase extravasation of drug out of the tumor microvasculature.

Methods: Pancreatic cancer mouse models were treated using clinical MRgFUS system (Sonalleve, Philips Healthcare) to achieve hyperthermia in combination with systemically administered commercial TSL ThermoDox® (Celsion Corp). Treatment guidance and temperature monitoing were performed using 3.0T MRI (Achieva, Philips Healthcare). For control groups free doxorubicin (*DOX*) was administered in combination with hyperthermia. Additionally, sham treatment was delivered to groups after injection of the drug. Mice were sacrificed and samples were collected after each treatment for qualitative evaluation and quantitative analysis.

Specific Aim 2: Assess the response to tumors treated with and without HIFU-induced hyperthermia in conjunction with systemic administration ThermoDox®, Doxil and gemcitabine in a survival study.

Hypothesis: Tumors treated with HIFU-induced hyperthermia in conjunction with systemically administered ThermoDox® will have a greater and more rapid decrease in tumor size compared to tumors treated with HIFU-induced hyperthermia in conjunction with systemically administered Doxil.

Methods: Transgenic mice with pancreatic cancer were treated by clinical MRgFUS system to achieve mild hyperthermia. ThermoDox, Doxil and gemcitabine were

administered to different treatment groups. Sham treatment was performed in all groups. Tumor sizes were measured using ultrasound imaging until the volume doubled after the treatment or reached the IACUC limits.

Specific Aim 3: To evaluate the ability of conventional MRI and newly emerging multi-parametric techniques in characterizing the pancreas tumor in three different mouse models.

Hypothesis: Conventional MRI methods such as T2w-weighted imaging and quantitative values acquired from multi-parametric MRI can serve as valuable *in-vivo* biomarkers of different tumor models with information regarding stroma tissue, blood flow and relative the drug diffusion.

Methods: T2W, Magnetization Transfer (*MT*) Imaging, DW-MRI and Dynamic Contrast Enhanced (*DCE*) imaging were performed to measure the biomarkers related to each organ. The information was compared to histology images of each tumor. Comparison of the quantitative data provide useful information regarding morphological (T2WI), tumor cellularity (apparent diffusion coefficient), ratio of collagen deposition (MT ratio) and relative blood flow (DCE) of each tumor model.

1.4 Organization of the Dissertation

The dissertation is divided into 10 chapters following this introduction.

- Chapter 2 provides information of the pancreatic cancer and the tumor models.
- Chapter 3 is an introduction to therapeutic ultrasound and the biological effects of high intensity focused ultrasound
- Chapter 4 introduces magnetic resonance imaging and the MR-guided HIFU as a treatment platform. This chapter describes the temperature monitoring technique and scans related to therapy. In section 4.5 conventional and multi-parametric MRI scans are described in detail
- Chapter 5 describes the concept of liposomal and temperature induced drug delivery
- Chapter 6 introduces hyperthermia and MR-HIFU drug delivery method
- Chapter 7 evaluates the ability of MRI techniques to characterize tumor models
- Chapter 8 investigates the MR-HIFU induced hyperthermia drug delivery in an acute study
- Chapter 9 assesses the efficacy of MR-HIFU induced hyperthermia drug delivery in a survival study
- Conclusion and possible future studies are discussed in chapter 10

Chapter 2. Pancreatic Adenocarcinoma

2.1 Introduction

Pancreatic ductal adenocarcinoma (*PDA*) is the fourth leading cause of cancer-related mortality and is responsible for 5% of all cancer deaths in the United States. According to the SEER Cancer Statistics Review, in 2010 there were over 42,000 new cases of pancreatic cancer and over 35,000 deaths, despite the standardization of surgical techniques and advances made in systemic treatments [22]. Most pancreatic cancer patients present with inoperable disease and rapidly succumb to a devastating illness characterized by tumor spread, vital organ dysfunction, intractable pain, galloping cachexia, and coagulopathy. The inherent biology of this disease makes it uniformly and rapidly lethal: overall 5-year survival for PDA is less than 5%, with a median survival of 4–6 months. Unfortunately, current treatment options are severely limited. Surgical resection offers a small hope for long-term survival in approximately 20% of patients who qualify, but few survive longer than 5 or 10 years, and the distinguishing features of this subgroup of patients remain a mystery. Systemic chemotherapy provides only temporary benefits in advanced disease. Many chemotherapeutic regimens have failed in treatment of PDA; Gemcitabine, a deoxycytosine analog, is the current standard of care for advanced disease and improves quality of life in a minority of patients, but prolongs survival by only a few weeks. Moreover, despite notable advances in surgical technique and postoperative care, and the use of adjuvant chemical and radiotherapies, virtually all early-stage patients who undergo resection also eventually succumb to recurrent and/or

metastatic disease [23]. The high resistance of the tumor to chemo- and radiation therapy is due to the poor vasculature structure and consequent, lack of perfusion and stroma tissue around the tumor. It is clear that more effective therapies for pancreatic cancer are needed urgently.

2.2 Pancreatic Cancer Mouse Model

Efficacy testing of new agents in oncology drug development relies heavily on mouse models bearing transplanted tumors. However, transplanted tumor models of PDA respond to numerous chemotherapeutic agents, including gemcitabine [24]–[27], which suggests that the predictive utility of such models may be limited. The most common models of PDA utilize human cells xenografted into immunodeficient hosts. In these models, the tumor microenvironment does not resemble the natural development of the tumor and in humans. As an experimental model, tumors have been implanted subcutaneously, primarily in mice. However, disease in these animal models does not adequately resemble human disease, because these tumors are often surrounded by a pseudocapsule, and rarely metastasize [28]. Furthermore, no adjacent major anatomic structures (such as major vessels or gastrointestinal organs) are invaded by the tumor [29].

An orthotopic pancreas tumor model, with the tumor growing in the pancreas itself, was described in 1985 [30]. Orthotopic pancreatic tumors somewhat better resemble the biologic characteristics of human tumors, and thus better represent the clinical situation. Compared with human pancreatic cancer, however, the orthotopic xenograft is not poorly

perfused [31]. Therefore, genetically engineered mouse models of PDA offer an alternative to transplantation models for preclinical therapeutic evaluation.

Genetically engineered strains of the species *Mus musculus* with mutations of KrasG12D; Trp53R172H; Pdx-1-Cre recombinase targeted to the pancreas (KPC mice) develop pancreatic ductal adenocarcinoma. The model closely recapitulates the genetic mutations, clinical symptoms, and histopathology found in human pancreatic cancer [32], [33]. The KPC model remains a nearly ideal way to perform definitive testing of a key hypothesis of this thesis regarding improved drug delivery.

In addition to the KPC mouse model that spontaneously develops pancreatic ductal adenocarcinoma, an orthotopic and a subcutaneous xerograph mouse models were used in these studies. Using tumor cells obtained from mice with the KPC mutation, a rapid and predictable orthotopic model of invasive pancreatic cancer could be produced. For the orthotopic model, immunocompetent mixed 129/SvJae/C57Bl/6 mice of 8-10 weeks age were used. Animals were administered general anesthesia with isoflurane and prepped in sterile fashion. A 2 cm incision was made along the left flank to expose the tail of the pancreas. One million KPC cells in 40 µl Hanks Balanced Salt Solution (HBSS) were injected directly into the pancreatic parenchyma and the incision were closed with sutures. Animals were recovered and monitored by ultrasound and palpation. For the subcutaneous mouse model, the same procedures were followed with the exception of injecting the tumor cells into the flank, close to hind limb. This procedure

was performed without anesthesia and tumor development was monitored visually, as the subcutaneous tumors are fully visible and palpable.

Chapter 3. High Intensity Focused Ultrasound

3.1 Introduction

HIFU, in comparison with the diagnostic ultrasound has significantly higher time-average intensities in the focal region of the ultrasound transducer. Diagnostic ultrasound transducers, based on the mode of imaging (*i.e.* B-mode, pulsed Doppler, or continuous wave Doppler), deliver ultrasound with intensities on the order of 0.1-100 mW/cm^2, corresponding to acoustic pressure in the range of 0.001-3 MPa [34]. In contrast, high intensity focused ultrasound transducers deliver ultrasound with intensities in the range of 100-4000 W/cm^2 to the focal region [2], [35].

The ultrasound field generated by a transducer depends on the size, shape, and vibration frequency of the source. If the diameter of an ultrasound source is much larger than the acoustic wavelength in the medium, then the ultrasonic wave can be focused by reflectors or lenses, or by making the transducer self-focusing [36]. Acoustic lenses are made of materials in which the speed of sound is different from that in the coupling medium, causing the ultrasound beams to focus if the lens shape is appropriate. Another method of focusing ultrasonic beam is by using one- or two-dimensional arrays of transducers, with each element driven by r̲adio f̲requency signals (*RF-signals*) of a specified phase and amplitude, so that the waves emitted by all of the elements are in phase at the desired focal point [36]. Today, phased arrays are the method of choice for clinical devices. The concentric ring design provides control over the depth of focus with

added sectors to provide limited beam steering to make the focal 'coverage' larger [37].

Figure 3.1 represents the ability of electric focusing and beam steering using multiple

elements in a phased array transducer.

FIGURE 3.1. A diagram of a phased array focusing illustrating the ability to control the location of the focus by the phase and amplitude of the RF-signals driving each element. [36]
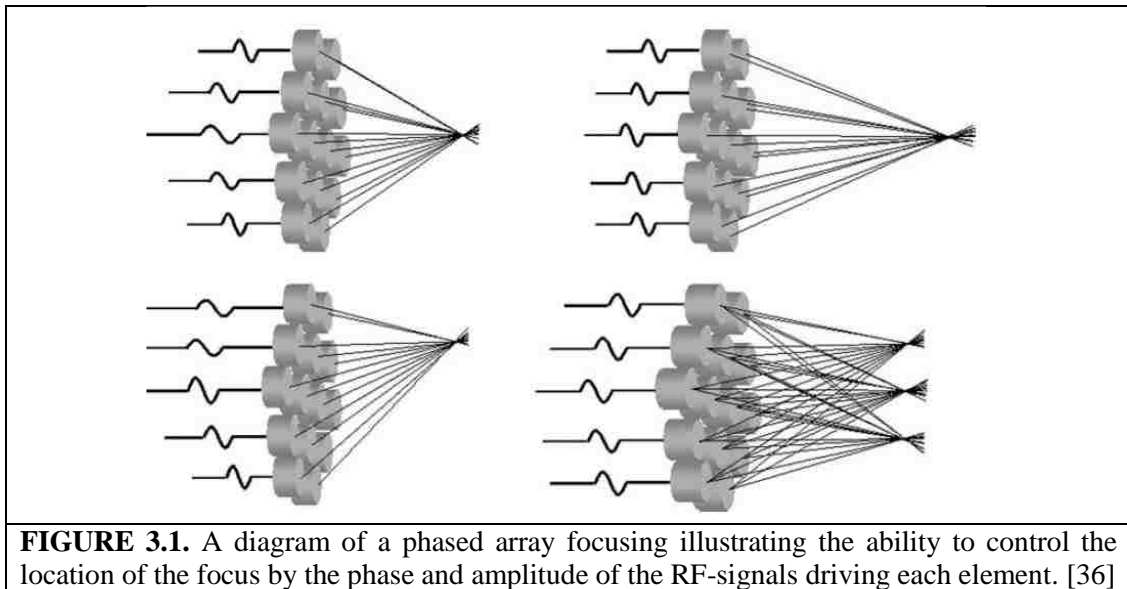
3.2 Therapeutic Ultrasound

Therapeutic ultrasound, or the use of ultrasound for purposes other than imaging or

diagnostics, acts on cells and tissues by thermal and mechanical mechanisms. Ultrasound

enhanced drug delivery uses these mechanisms to cause bioeffects which can improve

targeting and delivery of chemotherapeutic agents [38], [39]. Physical therapists use

therapeutic ultrasound to reduce pain and promote soft tissue healing, although there is

still a debate on whether the bioeffects of ultrasound are beneficial [40]. Therapeutic

ultrasound has also been used to treat glaucoma and tumors in the eye [41], [42] in

addition to being used in applications such as tissue fractionation, renal stone

fragmentation, cauterization, and wound healing [2], [35], [43]. One of the greatest advantages of therapeutic ultrasound is its ability to be focused into a small, well-defined target region in the body and produce clinically significant effects without damaging the intervening tissue as shown in Figure 3.2 [2], [35], [38], [43]. Guidance and monitoring of HIFU therapies are generally accomplished with B-mode ultrasound, or magnetic resonance imaging (MRI) [2], [35]. While HIFU is being used clinically to treat benign prostate hyperplasia and prostate cancer, clinical trials are underway for the treatment of breast cancer, uterine fibroids, and other tumors.
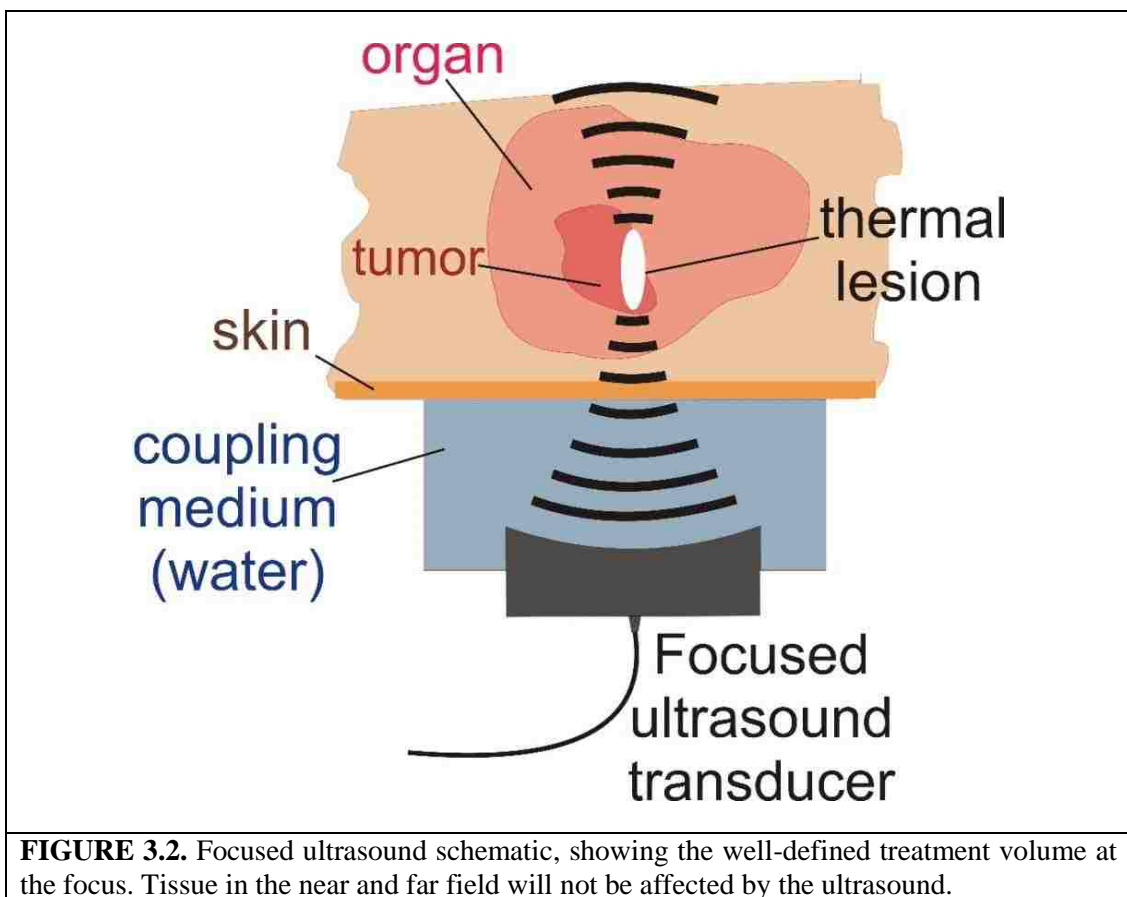
FIGURE 3.2. Focused ultrasound schematic, showing the well-defined treatment volume at the focus. Tissue in the near and far field will not be affected by the ultrasound.

An alternative to tissue denaturation is a mechanical version of HIFU that has the ability to cut through the heart septum [44] and to fractionate tissue by pulsed ultrasound cavitation or shock wave heating and millisecond boiling [5], [45]–[47]. These techniques utilize bubbles to fractionate tissue into submicron-size fragments (*i.e.* no remaining intact cells), with sharp boundaries between the treated and untreated tissues. Histotripsy, or pulsed ultrasound cavitation therapy, fractionates tissue at the focus using *microsecond* pulses at very high acoustic pressures and pulse-repetition frequencies (PRF) to create and maintain a cavitation bubble cloud on the order of several millimeters in size, composed of bubbles on the order of hundreds of microns in diameter [5], [45], [48]. On the other hand, shock wave heating and *millisecond* boiling, hereafter denoted as boiling histotripsy, uses millisecond pulses and lower PRFs and acoustic pressures than cavitation cloud histotripsy to explosively expand a millimeter-size boiling bubble at the focus to fractionate tissue [46], [47]. Figure 3.3 shows the differences in the bubble fields between cavitation cloud histotripsy and boiling histotripsy in a tissue- mimicking polyacrylamide gel.
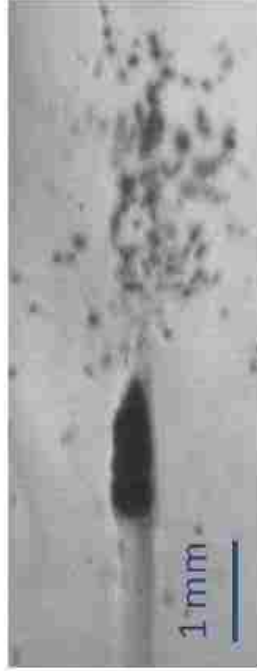
FIGURE 3.3. Images of the bubble patterns for (left) boiling histotripsy and (right) cavitation cloud histotripsy in a tissue-mimicking polyacrylamide gel. In boiling histotripsy, a millimeter-size boiling bubble explosively expands at the transducer focus, and cavitation bubbles form pre-focally. In cavitation cloud histotripsy, many cavitation bubbles of tens to hundreds of microns in diameter form a bubble cloud several millimeters in size. The end result of both techniques is tissue (or gel) fractionation.

The biological effect of therapeutic ultrasound are generally broken down into two categories, *Viz.* thermal and mechanical. Although understanding and ability to control and monitor both of these effects are important, the focus of this work is on HIFU and ultrasound-enhanced drug delivery.

3.3 Interaction of HIFU with tissue (bioeffects)

3.3.1 Ultrasound propagation and tissue heating

The thermal effects caused by ultrasound have been used in many ultrasound surgery applications as well as in hyperthermia as a cancer therapy. In order to cause thermal damage, the exposure at a given temperature must exceed a threshold time, below which the tissue recovers and above which the tissues are damaged irreversibly. The thermal damage threshold depends on tissue type and physiological factors, such as pH and oxygen level. The temperature elevation in a tissue depends on the absorption and attenuation coefficients of the tissue, in addition to the frequency and intensity of the ultrasonic field. Moreover the local blood perfusion rate strongly effects the temperature change.

Tissue interfaces within the beam path may cause reflection due to a mismatch between the acoustic impedance of the two tissues, although the impedances of biological soft tissues are very similar and this effect is mostly negligible in HIFU [49]–[51]. However, ultrasound waves reaching a tissue interface at an angle may be subject to both reflection and refraction [52]–[55]. The reflection will reduce the energy contained in the

transmitted ultrasound beam, whereas refraction will alter the direction in which the transmitted ultrasound waves continue to propagate in the new tissue layer. Thus refraction may shift the focus away from the geometrical focus, dephase and/or distort the focal spot [52]–[55]. If a phased-array transducer is used and the speed of sound in the different layers can be determined (for example with CT imaging [56], [57]); then the focal spot may be recovered at the desired location by applying appropriate phase corrections [52]–[55].

The resulting temperature rise caused by absorption of HIFU energy is often described using Pennes' bioheat transfer equation [58] that takes into account heat diffusion as well as heat loss through perfusion. The relationship between exposure duration and temperature increase for the actual temperature threshold is characterized by a thermal dose equation that describes the thermal exposure as the time in minutes at 43 ℃ that achieves an equivalent bioeffects.

The concept of thermal dose was introduced as a measure of thermal damage by Sapareto and Dewey in 1984 [20]. This model, which is based on the Arrhenius model of physical reaction rates, takes into account not only the current temperature but also the entire temperature history in estimating the thermal damage. The equation describing the thermal dose is written as

$$\text{TD}_{43}(t) = \int_0^t R^{(43-t(\tau))} \, d\tau \qquad\qquad 3.1$$

Where   R = 0.25 (T < 43), R = 0.5 (T > 43) and TD is the thermal dose in equivalent minutes at 43 ºC (EM), t is the time and T(τ) the time-dependent temperature. Due to the logarithmic relationship between the thermal dose and temperature, the spatial distribution of the thermal dose is typically much sharper than for the somewhat diffuse temperature. The thermal dose thresholds for different levels of thermal damage have been shown to differ somewhat between tissues [59]–[65]. However, a threshold of 240 EM is generally considered to be a good representative for full coagulative necrosis [65]–[67]. Similarly, 30 EM has been reported to be a relevant predictor for the onset of tissue damage [65], [68].

In the presence of thermal noise, the logarithmic temperature relationship of the thermal dose will induce errors in the thermal dose estimate if the effect of thermal noise does not average to zero. If a normal distribution of the temperature is assumed, as is commonly done for the temperature estimates obtained from magnetic resonance (MR) thermometry, then the thermal dose increments will follow a log-normal distribution. Normal noise with a standard deviation of σT (°C) will thus on average result in an overestimation of the thermal dose with a factor of

$$\exp\left(0.5\sigma_T^2 \ln^2 2\right)$$

if no compensation is applied [69]. Hence, for a relatively low temperature standard deviation of 1.2 °C, the thermal dose would be overestimated by 40%, whereas for a slightly higher temperature uncertainty, σT = 2 °C, the overestimation exceeds 150%.

The overestimation can, however, be accounted for by dividing the thermal dose obtained from Equation 3.1 with the overestimation factor.

3.3.2 Mechanical effects

During the nonlinear propagation of ultrasound wave in biological tissue, the wave is distorted strongly and a shock wave forms. Great mechanical force is applied on the tissue in the ultrasonic field. The beam also induces a steady force, the radiation force. The radiation force in a standing wave field has been found to cause red blood cells to align in bands with a spacing on ½ of the wavelength [70]. The radiation force can induce detectable tissue motion in a traveling wave. This tissue motion may result in motion on a cellular level when intracellular structures, or gas-filled spaces cause inhomogeneities in the sound field resulting in an imbalance of the macroscopic forces. This can lead to a steady circular flow called acoustic streaming that can induce bioeffects *via* shear forces.

Acoustic cavitation can be defined as the creation or motion of a small gaseous nuclei in an acoustic field [71]; *e.g.*, the oscillatory movement of the bubble in a liquid medium exposed to an acoustic field. There are two forms of cavitation. The first, stable cavitation happens where a bubble is exposed to a low pressure acoustic field resulting in stable oscillation of the size of the bubble. The second form of cavitation is inertial cavitation where the exposure of the bubble to the acoustic field will result in violent oscillations of the bubble with rapid growth of the bubble during negative pressure phase eventually leading to the violent collapse and destruction of the bubble [72], [73].

The center of interest of this work is to induce thermal effects of HIFU in a controlled

manner while minimizing cavitation and other nonlinear effects of ultrasound.

Chapter 4. Magnetic resonance guidance of HIFU therapy

4.1 Introduction

The initial experiments involving magnetic resonance imaging (MRI)-guided HIFU (MR-HIFU) were performed in the early 1990s by a collaboration of investigators at the University of Arizona with investigators at Brigham and Women's Hospital and General Electric [74]–[77]. The feasibility of using a focused ultrasound device within an MRI scanner was demonstrated, focal heating was visualized and the resulting tissue damage was detected by the investigators.

Following these initial studies, substantial work involving methods to improve the MR-HIFU device and the treatment monitoring was performed. Essential work in the area involved developing MR-compatible phased array [37], [78]–[80] and computer control driving systems [81] that can be used to increase the focal heating volume and steer the focal beam, and testing and validating MRI-based temperature imaging [82]–[84] to localize the focal spot [85].

In this chapter the MR-HIFU platform that is used for the experiments as well as treatment planning and temperature monitoring is described.

4.2 MR-HIFU platform

Ultrasound waves cannot propagate in air and need a fluid or gel to couple acoustic path the transducer to the body. In clinical HIFU platforms, this is accomplished by submerging the transducer in a degassed water- or oil-bath that is sealed within an MR -

compatible table top using a thin membrane [86]–[88]. This membrane also acts as an acoustic window through which the ultrasound waves may propagate. Alternative methods where the transducer is confined in a plastic bag inside a table-top have also been suggested [9].

This HIFU table top can be used as any other conventional MR patient table, and can be moved in and out of the MR scanner. A gel pad is often positioned on top of the membrane to improve the acoustic coupling between the water tank and the skin of the patient [86]. Ultrasound gel or degassed water may also be applied at both sides of the gel pad, or alternatively instead of the gel pad, to improve the acoustic coupling at the interfaces between the water tank and the patient [85], [86]. A schematic of a pig positioned on top of the Philips clinical HIFU platform can be seen in Figure 4.1. Intracavitary transducers intended for prostate ablation use an entirely different setup as the casing of the transducer is in direct contact with the wall of the cavity [11], [89], [90].
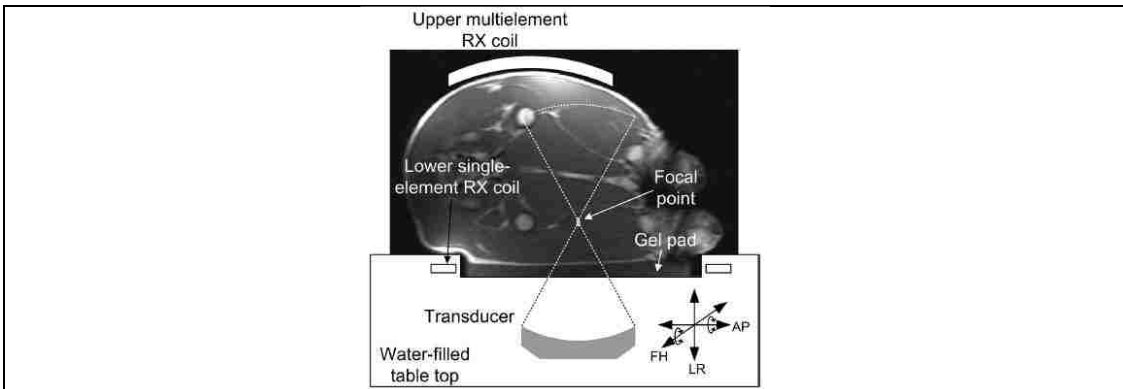
Figure 4.1. Schematic of the Philips clinical HIFU platform viewed in the transverse plane with a pig placed in a left decubitus position on top of the platform. The integrated multi-element MR receive coil is also shown. The lower element is a loop surrounding the acoustic window in the table top through which the ultrasound propagates. The piezoelectric motors which control the positioning allow for three degrees of translational motion and two degrees of rotational motion.

Accurate and flexible positioning of the transducer is a crucial prerequisite for inducing localized thermal damage in the desired target region. Conventional motors cannot be used inside the MR and early positioning devices used hydraulic pistons to accurately position the transducer [87], [88], [91]. More accurate positioning devices have since been developed, and most modern HIFU transducer positioning devices are software controlled and use piezoelectric motors [85][92][93] or robotics [94], [95].

4.3 Therapy planning

The excellent soft-tissue contrast provided by MRI makes this noninvasive imaging modality ideal for identifying and localizing the abnormal tissue to be targeted for any form of image guided therapy or treatment. High-resolution MR images can therefore be used for accurate planning of the MR-HIFU therapy if the relationship between the coordinate system of the planning images and the coordinate system of the ablation device, *i.e.* the transducer, is known. A graphical user interface to which these planning images are imported can then be used to create the MR-HIFU treatment plan by defining the position and angulation of the planned ablations, and examining the corresponding beam paths for acoustic barriers such as bone or air filled cavities. The efficiency and accuracy of this treatment planning can be improved by creating graphical overlays of the transducer and beam path on the planning images, which are updated according to the actual transducer position. The time needed for transducer positioning can be reduced and planning efficiency further improved if the transducer positioning is software controlled. Such a setup as outlined above allows for visualizing and interactively

adjusting the treatment plan and transducer position in reference to the target region anatomy, much in the same manner as in stereotactic surgery.

4.4 Treatment monitoring by magnetic resonance thermometry

Since both the relaxation properties and chemical environment of the signal in MRI are sensitive to Brownian motion and the associated molecular tumbling rates, MRI techniques are intrinsically sensitive to temperature.

The objective of any thermal therapy is to adequately treat the target while sparing adjacent healthy tissue. However, the heat diffusion, absorption, and perfusion of the tissue all vary as a function of tissue architecture, tissue composition, local physiological parameters and temperature. These parameters may furthermore change due to coagulation or necrosis. This makes predicting the temperature distribution exceedingly difficult. Continuous acquisition of temperature maps during treatment would therefore significantly improve the control of the thermal therapy outcome by estimating the temperature distribution near and at the target.

Of the many MR parameters that can provide temperature-sensitive contrast, the temperature dependence and sensitivity of several parameters in particular, have proven useful for temperature change monitoring in soft tissue, such as relaxation constants, diffusion, and resonance frequency. By choosing the MR imaging sequence appropriately, continuous dynamic MR imaging can provide real-time information on the instantaneous *in vivo* temperature distribution in any imaging plane at a good spatial and

25

temporal resolution. MR temperature imaging, or thermometry, has been suggested for monitoring hypothermia during cryosurgery [96] as well as for monitoring hyperthermia induced by laser [97], microwave [98], radio frequency (RF) [99], [100], and HIFU [6] treatments. The use of MR for thermometry was initially suggested by Parker et al. in 1983 [101], even though the temperature dependency of several MR parameters had already been established earlier [102]–[104]. The method suggested by Parker was based on monitoring the longitudinal relaxation constant (T1). Since then several other methods of thermometry have been suggested. The most widely used of these methods is thermometry based on the diffusion constant as first suggested by Le Bihan et al. [105], thermometry based on the proton resonance frequency shift (PRFS) as suggested by Ishihara et al. [7], as well as thermometry based on the longitudinal relaxation constant.

PRFS thermometry is by far the most widely used method of thermometry, and is the method used in the experiments described in this dissertation. Because of this, discussion on other forms of thermometry is here omitted. Details on T1- and diffusion constant based- thermometry, as well as other methods of thermometry, can be found in the excellent reviews of Quesson et al. [106], Denis de Senneville et al. [106], and Rieke et al. [107].

4.4.1 Proton resonance frequency shift

PRFS temperature dependence was first observed by Hindman in 1966 [103] when studying intramolecular forces and hydrogen bond formation between water molecules.

A hydrogen nucleus is screened more efficiently from the main magnetic field by the electron cloud when part of a free water molecule, than when in a water molecule that is hydrogen bonded to another water molecule. This is because the hydrogen bonds distort the electronic configuration of the water molecules, thereby reducing the electronic screening. The fraction of water molecules that are hydrogen bonded depends on the temperature. An increase in temperature causes the hydrogen bonds to bend, stretch, and break, thus reducing the average time spent by the water molecules in a hydrogen bonded state.

The decrease in the local magnetic field due to the change in the temperature dependent chemical shift will also lower the proton resonance frequency that is linearly dependent on the local magnetic field. This temperature dependent shift in resonance frequency and thus also the chemical shift can be calculated using the phase information from the MR images of a gradient echo sequence.

The temperature sensitivity of the PRFS method is very good as for a typical signal-to-noise ratio (SNR) of 40, field strength of 3 T, and echo time of 20 ms, the theoretical standard deviation is as low as 0.3 ℃. The inverse of the SNR is proportional to the temperature standard deviation, and a low SNR will therefore result in a high temperature uncertainty. It is important to note that the PRFS technique is only capable of calculating relative temperature change, and not absolute temperature. The core body temperature is therefore typically used as the starting temperature to which the temperature variation maps are added in order to obtain absolute temperature maps.

In principle any gradient echo sequence can be used for acquiring the phase information necessary for these temperature maps, as long as stimulated echoes can be neglected. However, short repetition times and flip angles close to the Ernst angle are typically used, which makes efficient RF spoiling of the signal becomes crucial in order to avoid contaminating the phase information with stimulated echoes from previous excitations. A spin echo sequence cannot be used for measuring the temperature induced phase change as the spins will be refocused at the time of image acquisition, leaving the phase image independent of chemical shift and thus also independent of temperature.

A very important advantage of the PRFS method of thermometry is that the temperature dependent chemical shift α is nearly independent of tissue type and is also not affected by coagulation. Typical values of the temperature dependent water PRF shift vary between -0.009 and -0.01 ppm/ºC. However, the PRF shift is only tissue independent for aqueous tissues, as the temperature dependent PRF shift stems from changes in the hydrogen bonds which are absent in lipids. The PRF of lipid hydrogen is thus almost independent of temperature and the presence of lipids in the phase images may therefore lead to errors in the PRF temperature images. Fortunately, fat suppression or spectral selective excitation can be used to image only water protons, thereby enabling accurate PRF thermometry in tissue where both fat and water protons are present.

The need of a reference phase also poses some problems, as the phase is assumed only to be influenced by changes in temperature. However, the external magnetic field of currently available MR scanners will drift in time when the gradients are utilized

28

intensively, resulting in phase drift and an apparent temperature change. This phase drift can be compensated by subtracting the average phase change seen in either an external phantom in thermal equilibrium or an internal non-heated region. If the phase drift varies in space, an improved compensation can be obtained by fitting a polynomial curve to the spatial distribution of the phase drift in the non-heated reference region and subtracting this fitted phase from the acquired phase images. An alternative approach to PRF thermometry is to not use a phase reference image at all, but instead use a polynomial fit of the phase or complex data from the non-heated area to estimate the background phase in the heated area. The background phase, which is the estimated phase in the heated area had it not been heated, is then used as the reference phase. This so called *referenceless* thermometry does therefore not need a phase drift correction, as the temporal field drift is already included in the non-heated area from which the reference phase is estimated. A disadvantage of this method is, however, that a high SNR is required and the heating needs to be confined to a small well-defined area for the polynomial fitting of the phase reference to be reliable.

Organ motion is, the most prevalent problem for PRFS thermometry. Several abdominal organs are prime candidates for MR-HIFU but are subject to both rigid and non-rigid motion during the respiratory cycle. Not only does this motion need to be compensated and the images aligned with the reference image to avoid artifacts in the temperature images, but a correct reference phase must also be used since the local magnetic field experienced by the organ will vary as the organ moves through the

inhomogeneous magnetic field inside the body. Removal of non-temperature related phase perturbations is thus imperative for accurate PRFS thermometry of moving objects.

In this dissertation, the temperature monitoring is performed using PRFS thermometry method in a 3 T MRI to accurately monitor the therapy during hyperthermia exposures.

4.5 Conventional and multi-parametric MRI techniques

4.5.1 T2-weighted imaging

T2-weighted imaging (T2WI) relies upon local dephasing of spins following the application of the transverse energy pulse. The contrast of a T2WI is predominantly dependent on T2 and can be increased by using a long echo time. The value of echo time (TE) effectively determines the sensitivity of the sequence to the process of T2-relaxation. Water has a very high T2 constant, therefore has very high T2 signal and thus appears bright on a T2 contrast image. Thus this scan is important and suitable for evaluating cyst contents (fluid, septa) and the pancreatic ductal system.

Traditionally, T2WI has been used to provide morphological information about the zonal anatomy of the cancer and highlight suspected areas. T2WI with and without fat suppression will provide good delineation of organ contour and the presence of peripancreatic inflammation. As pancreatic tumor may present a broad spectrum of appearance the small hyperfuctioning parts of pancreatic tumor may not be visible on

T2WI [108]. In such case combination of T2W and other imaging techniques may be beneficial.

4.5.2 Diffusion Weighted Imaging and Apparent Diffusion Coefficient

Molecular diffusion and microcirculation in the capillary network result in a distribution of phases in a single voxel in the presence of magnetic field gradients. This distribution produces a spin-echo attenuation [109]. The diffusion weighted MRI (DW-MRI) is sensitive to water diffusion because each image voxel has an image intensity that reflects the rate of water diffusion at the location. This scan demonstrates pathology based on fluid motion states at the cellular level. It is known that tumor water diffusion is associated with tumor cellularity. DW-MRI has a potential to be useful at all stages of a cancer and could be survival indicators. In addition DW-MRI is quantifiable and can be repeated easily. In living tissue the diffusion process is superimposed by capillary pseudo diffusion and gross motion to which the MR measurement is also very sensitive. In this thesis, the apparent diffusion coefficient (ADC) values were measured, the underlying hypothesis being that it could be a good marker to monitor early changes in the tissue. Comparing the ADC value of different tissues with the tumor we can acquire diffusion properties of cancer tissue.

Yoshikawa *et al.* [110] reported that cancerous pancreatic tissues had an ADC value higher than that of normal pancreas, although the study included only a small number of patients. However depending on the area where a value is measured, one expects decrease

of the ADC value to correlate with lower diffusion in a region containing high fibrosis. .

The b-value, a factor of diffusion weighted sequence, is a parameter that adjusts the strength, duration and time of the diffusion gradients. Sequences with low b-values are relatively sensitive to diffusion; sequences with high b-values are sensitive to even minor water displacements. It has been reported that high–b value DWI is different from morphologically oriented imaging techniques in that it can sensitively depict disease associated changes of random translational molecular motion, known as diffusion or Brownian water motion [111]. The authors of several studies have reported that quantification of diffusion as ADC values is useful in tissue characterization [112] [113].

A minimum of two b-values must be acquired in order to process the ADC map or calculate the ADC values. Typically the first b-value is very low (0-100) and the second is optimized to the pathology. Multiple b-values can be acquired in a single pulse sequence; however, scan time increases as number of b-values increases. SNR decreases as b-value increases. Due to its nature this scan is extremely sensitive to gross movement of the patient. Therefore in this scan motion compensation techniques or proper gating is required to eliminate the effect of motion with longer scan times.

4.5.3 Other imaging methods

Magnetization transfer imaging (MTI) is based on the interaction of macromolecules with the proton spins of liquid pools through exchange processes and can be an indicator

of the structural integrity of the tissue being imaged. In this thesis, Magnetization transfer ratio (MTR) is the method used to assess potential changes in macromolecules.

A common characteristic of PDA is tumor desmoplasia with a marked increase in fibrotic connective tissue that penetrates and envelopes the neoplasm. This extracellular matrix facilitates disease progression [114], metastasis [115], and confers drug resistance [31]. PDA-associated desmoplasia leads to threefold increases in collagen deposition compared with normal pancreas tissues [116] [117].

MT-MRI can be used to noninvasively probe dynamic physical processes involving the exchange of magnetization between subpopulations of free water protons and those water protons bound to tissue macromolecules. MT-MRI studies in cartilage degeneration [118] and regeneration [119] and liver fibrosis [120] have each demonstrated that MT contrast can be highly sensitive to tissue collagen concentration, the primary component of desmoplasia. Thus, we hypothesized that fibrosis levels in PDA may be directly reflected in MT-MRI MT ratio (MTR) measurements. In chapter 9, MTR values are measured to determine if it can serve as a marker that can differentiate the amount of fibrosis and stroma tissue in different mouse models.

Dynamic contrast-enhanced MR imaging (DCE-MRI) has emerged as a promising method for diagnosis and prognosis of cancer. As with other modalities of perfusion imaging, DCE-MRI uses repeated imaging to track the entrance of diffusible contrast agents into tissue over time. A paramagnetic contrast agent, gadolinium-DTPA injected

intravenously circulates through the body and diffuses over time into the extravascular extracellular space. From the known properties of the imaging sequences it is possible to convert the relative signal increase into a quantitative measure of contrast agent over time in tissue. From these curves, one can obtain semi quantitative analogs of blood flow, or, if similar concentration curves are obtainable from arterial blood, one can use the two compartment tracer kinetic theories of Kety [121] [122] to obtain more quantitative indices of blood flow and capillary permeability. The DCE-MRI will be a good marker for blood flow and relatively the drug diffusion into different type of tumor models.

Chapter 5. Temperature sensitive liposomal drug delivery

5.1 Liposomes for cancer therapy

Liposomes were developed initially by Alec Bangham as closed vesicle models with which to study cell membranes [123], but are now widely used as biocompatible carriers. These carriers are composed of a lipid bilayer membrane encapsulating an aqueous volume [124], [125] and have been used as possible therapeutic intervention vehicles and as molecular MRI contrast agents [126]–[130]. A liposome can trap hydrophobic molecules of a few nanometers in diameter within the bilayer; it can hold hydrophilic agents of several hundred nanometer diameter in the relatively large interior compartment [125], [131]. Coating the lipid bilayer with water-soluble polymers (polyethyl glycol (PEG)) led to development of 'stealth' liposomes, so-called because the polymers prevent the attachment of plasma proteins which label foreign matter for removal by immune system cells. Moreover, peptides which target specific biological targets may also be attached to the polymers [125]. Safinya et al., 2012 published an outstanding illustration on the evolution of liposomes, Figure 5.1 [125].
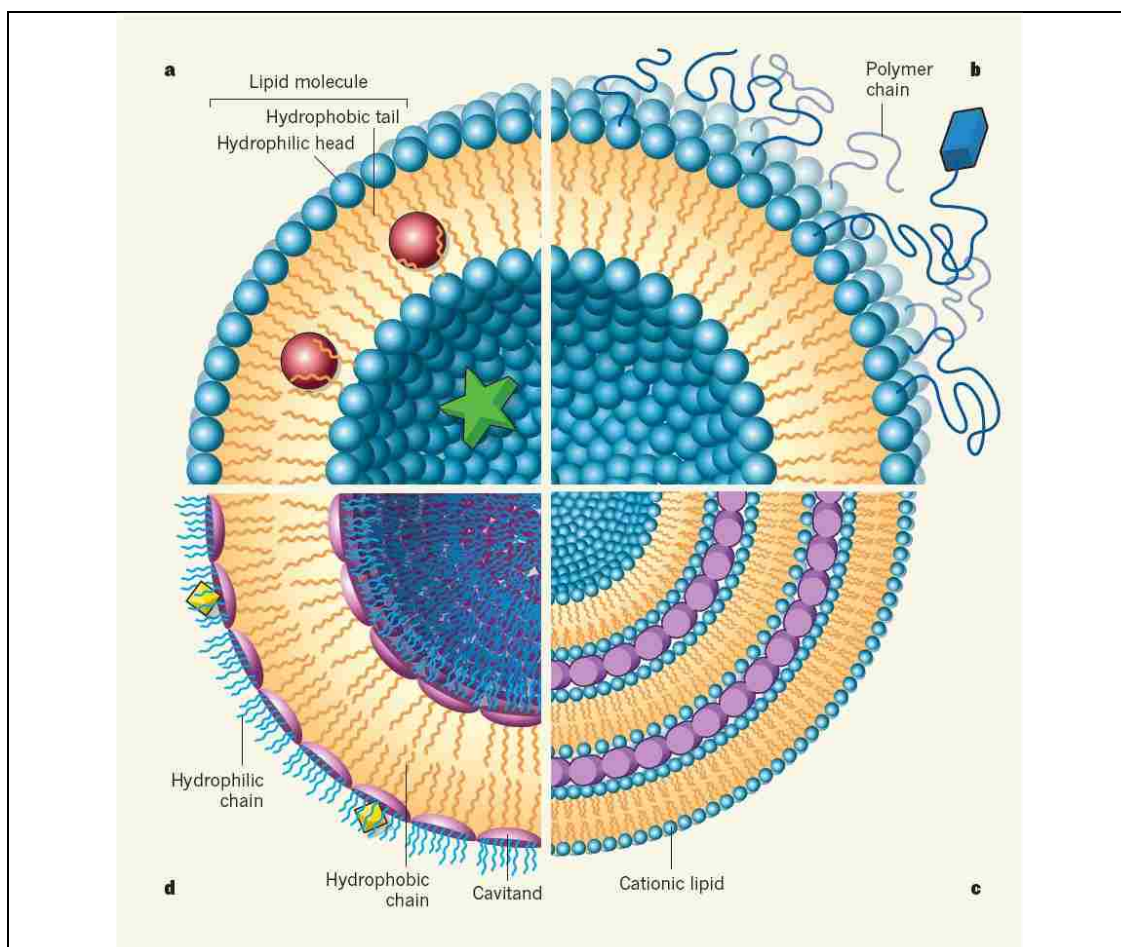
Figure 5.1. a, Simple liposomes are vesicles that have a shell consisting of a lipid bilayer. A liposome can trap hydrophobic guest molecules a few nanometers in diameter (red spheres) within the hydrophobic bilayer, and hydrophilic guests up to several hundred nanometers (green star) in its larger interior.

b, In 'stealth' liposomes developed for drug-delivery applications, the lipid bilayer contains a small percentage of polymer lipids. Peptides (blue rectangle) that target specific biological targets may also be attached to the polymers.

c, Most cationic liposome–DNA complexes have an onion-like structure, with DNA (purple rods) sandwiched between cationic membranes.

d, Kubitschke *et al.* report liposomes in which the bilayer assembles from cavitands — vase-shaped molecules — to which the authors attached hydrophobic and hydrophilic chains. The cavitands can trap angstrom-sized guest compounds (yellow diamonds) in their hydrophobic cavities. These vesicles can therefore encapsulate guest molecules of different sizes in the cavitands, the bilayer and the liposome's interior.

When used as carriers of anti-tumoral drugs, the prolonged circulation time of stealth liposomes in the blood can result in accumulation of the liposomes in the interstitium of tumors. Release of their content in the targeted region can then be effected by various means. Despite the fact that the concentration of drug inside PEGylated liposomes can be much higher than would be possible were the drug to be administered systemically in 'free' form, liposome-encapsulated drugs are not bioavailable to the tumor cells absent a mechanism to release the liposomal contents [132]. Approved liposomal forms of doxorubicin (DOX) for the treatment of cancer (Doxil, DaunoXome and Myocet) reduce the cardiac toxicity associated with DOX, but these vesicles do not necessarily improve drug efficacy of cancer treatment [126]. Absent an active release-triggering mechanism, drug escapes from the accumulated drug carriers in the tumor tissue *via* slow, passive diffusion, or *via* slow degradation of the lipid shell. While this can be advantageous with some drugs (*e.g.,* cell cycle-specific drugs such as Vincristine), it may be of little benefit when using non-cell cycle specific drugs such as DOX and cisplatin (cisPt) [133]–[135]. The lack of drug efficacy explains the failed phase III clinical trial of liposomes loaded with cisplatin [136]. Therefore, triggered release of the drug to control the amount as well as the time and location of the release is necessary. Triggering mechanisms have included pH changes, light, and mild heating [137]–[140], the latter being the focus of this dissertation.

5.2 Thermosensitive liposomes

Thermosensitive liposomes (TSL) consist of lipid membranes which undergo phase transition and melt from a relatively 'solid' and impermeable gel form to a liquid phase at a transition temperature, T_m, which varies with the lipid composition of the membranes. Bilayer structural changes occur at T_m, increasing dramatically the permeability of the membrane and resulting in the release of liposomal contents [141]. Although the maximal release happens at $T \geq T_m$ [142], [143], significant amounts of drug escape the liposomes at temperatures 1-2 degrees below the bulk T_m of the bilayer. This is due to the inhomogeneous structure of the lipid bilayer plane; *i.e.,* there exist minute domains whose properties differ from the bulk or average properties of the bilayer as a whole, and thermally-induced permeability increases can occur in these domains at somewhat lower temperature than required to melt the entire membrane [144].

Early TSLs were formulated with dipalmitoylphosphatidylcholine (DPPC), having a T_m of 41.5 °C. These were suitable for applications of very mild hyperthermia while remaining below 43 °C [145], [146]. When DPPC formulations are modified by the addition of other lipids (*e.g.*, distearoylphosphatidylcholine (DSPC; T_m of 54.9 °C), and hydrogenated soy phosphocholine (HSPC)), these modifications produce greater lipid packing incompatibility relative to 'single-species' formulations, and this increases their permeability at elevated temperature. In turn, this increases drug release in tumors in response to TSL and hyperthermia therapy [147]–[149].

The first PEGylated, long-circulating TSL was developed by Unezaki et al. [150]. Although the addition of DSPC to DPPC can increase the permeability of the liposomal membrane, the phase transition temperature of these membranes is formulation-dependent, and increases with increasing molar fraction of DSPC [151], which is generally undesirable. These liposomes have a relatively broad transition temperature (43-48 °C) with the center T_m close to 46 °C [152], and slow drug release kinetics [153]. However, the required release temperature range of such liposomes (43-45 °C) can be associated with the development of thermal doses sufficient to damage healthy tissues surrounding a tumor. Therefore, TSL formulations with lower drug release temperature thresholds (*i.e.*, in the range of mild hyperthermia (39-42 °C)) were needed.

To this end, lysolipids were incorporated into PEGylated DPPC membranes to lower the phase transition temperature and thereby promote rapid drug release under mild hyperthermic conditions [153], [154]. These were termed lysolipid thermosensitive liposomes (LTSL). Inclusion of lysolipids into the liposome membrane has several effects on the physicochemical properties of the bilayer. It has been shown that DPPC liposomes containing 10 mol% lysolipid phosphocholine (lyso-PCs) and corresponding alkyl or acyl analogues decreases the melting phase transition temperature and broadens the transition temperature range [155]. Other studies on the combination of mild hyperthermia and LTSL-localized DOX demonstrated DOX release within a few seconds, with 50% DOX release occurring within 20 s of heating to 42 °C [153], [154], [156]. Preclinical experiments clearly demonstrated the improved efficacy of this type of

drug delivery [153], [155], [157]–[159]. However, studies on the pharmacokinetics of LTSLs in human plasma indicated rapid DOX leakage at body temperature [160]–[162]. This shortcoming led yet again to new formulations of TSLs.

TSLs composed of dipalmitoyl-sn-glycero-3-phosphoglyceroglycerol (DPPGOG) and DPPC/DSPC improved the serum stability at 37 °C relative to LTSLs. Additionally, liposome formulations containing DPPGOG had longer circulation times in blood, leading to higher plasma levels of DOX compared with other TSL formulations. [163], [164].

ThermoDox® (Celsion Corporation, Columbia, MD) is a commercially developed LTSL loaded with DOX (LSTL-DOX) that has demonstrated great promise in both preclinical and clinical studies. Pre-clinically, LTSL-DOX enhanced the delivery and therapeutic efficacy of DOX in multiple xenograft models (colon HCT116, squamous cell FaDu, prostate PC-2, ovarian SKOV, mammary 4T07) [165], [166]. In addition, in canine solid tumors LTSL-DOX demonstrated favorable toxicity profiles, pharmacokinetic properties, and efficacy [167]. This array of promising *in vivo* studies has led to the further investigation of LTSL-DOX (ThermoDox®) in human clinical trials. It is currently being tested in combination with focused microwave induced hyperthermia in a multi-center Phase I/II trial for the treatment of loco-regional recurrent breast cancer (ID: NCT00826085). A corresponding Phase I trial already established a maximum tolerated dose (MTD) of 50 mg/m^2 and demonstrated promising tumor response activity. In a different set of trials, LTSL-DOX (ThermoDox®) is being

investigated in combination with radiofrequency ablation (RFA) for the treatment of hepatocellular carcinoma (HCC). A Phase I trial completed in 2009 also determined the MTD to be 50 mg/m^2, demonstrated a promising toxicity profile, and showed promising efficacy results [168]. A Phase III HCC trial is ongoing and Celsion has also announced a randomized Phase III study of LTSL-DOX (ThermoDox®)/RFA for the treatment of colorectal liver metastases. Lastly, Celsion is working with Phillips Healthcare for a Phase II clinical study investing ThermoDox® in combination with Philips Sonalleve MR-HIFU technology for the treatment of prostate cancer metastases to the bone. These promising early results strongly recommend the clinical investigation of this therapeutic strategy for the treatment of pancreatic cancer.

In addition to ThermoDox®, there is an ongoing attempt to produce a LTSL co loaded with Dox and gadolinium as MR contrast agent [144], [169], [170].

Chapter 6. Temperature induced drug delivery using MR-HIFU

6.1 Hyperthermia

Hyperthermia is broadly accepted to be elevation of, and maintenance of the tissue temperature at 40-45 °C [20], [59], [171]. Increased tissue temperature leads to a number of vascular responses which alter blood flow. Moreover, the responses differ in normal and tumor tissue. In normal tissue, hyperthermia causes vasodilation, increased blood flow, and increased vascular wall permeability [172]. This response happens over a relatively a wide range of temperature (37-45°C), with specific responses depending on the tissue [173]. Elevation of temperature to a higher range may result in vascular damage.

Hyperthermia-induced changes in the blood flow in tumors are considerably different from those of normal tissue [172], [174]. Tumor vessels are ill-formed, and are usually devoid of smooth muscle [174]. Historically, this was thought to preclude vasodilation. However, under relatively low temperature heating regimes, blood flow increases slightly in some types of tumors [174]. Mild hyperthermia (41-42 °C) results in increased tumor blood flow [175] and increased tumor oxygenation during the treatment [176]. This change is expected to enhance liposome penetration into the tumor *via* the tumor microvasculature and thus to carry more liposome-encapsulated drug into the tumor. In healthy tissues under conditions of mild hyperthermia, blood vessel structure will not allow the extravasation of liposomes. In tumors, however, hyperthermia has been shown

to enhance tumor microvascular permeability [177], [178] in addition to increasing blood flow. The increase in blood flow peaks in the mild hyperthermia temperature range, but microvascular permeabilization continues to increase with increasing temperature until thermal vessel damage occurs and blood flow stops. These aspects can be further used to enhance the delivery of the liposomes to the tumor site.

6.2 MR-HIFU drug delivery

Targeted release from TSLs has been studied extensively with different heating modalities, including water baths [149], [154], [157], external electromagnetic applicators (microwaves or radio waves) [167], localized interstitial hyperthermia applicators with ultrasonography guidance [179], [180], and therapeutic focused ultrasound.

HIFU can be used noninvasively to heat deep tissue in a small focal volume relative to that achievable with other hyperthermia devices; *i.e.*, spatial control capability can be quite good. By controlling the duration and magnitude of ultrasound exposure, HIFU can also effect tissue heating with a high degree of temporal and amplitude control. Therefore, HIFU has emerged as a leading modality for heat-triggered drug release from TSL. To maintain the target temperature, accurate measurement at the focal point is needed. In some studies, temperature measurement was limited to point measurements made by invasive thermocouples or optical probes [181]–[183]. These studies provided useful information, but better temperature monitoring technology is required for clinical

use. Therefore noninvasive monitoring of the temperature in the target volume has been a high priority area of research.

MRgFUS is a powerful tool for controlled applications of hyperthermia. MR imaging offers superior tissue contrast compared with ultrasound imaging, which makes it better for treatment guidance. Moreover, MR thermometry offers a noninvasive method to monitor temperature changes and to provide real-time treatment feedback. Effective treatment of *in vivo* tumors using MRgFUS and TSL has been demonstrated in recent studies [165], [166], [170], [184], [185]. In these experiments, tumors in the treatment groups receiving both MRgFUS and drug-loaded liposome demonstrated the greatest uptake of drug when compared with liposome only and/or free drug treatments.

Chapter 7. Characterization of three pancreatic cancer mouse model using conventional and multi-parametric MRI techniques

7.1 Introduction

Pancreatic cancer is one of the most lethal human cancers and continues to be a major unsolved health problem at the start of the 21st century. Although much effort has been devoted to increase the sensitivity for detecting early-stage pancreatic adenocarcinomas with conventional imaging techniques, such as sonography, computed tomography (CT), or magnetic resonance imaging (MRI), the detection sensitivity is still insufficient [186]. This topic was discussed in Chapter 2.

Faced with such a poor prognosis, new treatment strategies for pancreatic cancer have been studied extensively. Development of different tumor models and different properties of each tumor model have been discussed in Chapter 2.2. Pancreatic tumor models that somewhat better resemble the biologic characteristics of the human tumor, and thus better represent the clinical situation in patients are among top choices for new studies. Characteristics such as perfusion, intra tumoral diffusion, the amount of stroma, genetic mutations, clinical symptoms, and histopathology of tumor and comparison of each with the one found in human pancreatic cancer are relevant for different types of studies.

Efficacy testing of new agents in oncology drug development relies heavily on mouse models bearing transplanted tumors. Therefore evaluating a tumor's characteristics is also

very important to help evaluate different therapies and what type of therapy is most appropriate. In this thesis research, evaluation of tumor characteristics lead us to better targeting of the tumor while avoiding liquid cystic areas and necrotic cores of the tumor. Characterizing the tumor tissue can also be used to predict the response to chemotherapy [187]. Differentiation between cancer and pancreatitis is both important and difficult with CT. MR imaging is excellent in the delineation of small pancreatic tumors. Moreover due to its superior soft tissue contrast, MRI is often the method of choice to detect cystic masses or pancreatitis, which can lead to different types of treatment such as surgery, or chemo and radiation therapy in combination.

MRI is capable of providing the necessary guidance and monitoring for focused ultrasound therapy. This noninvasive imaging modality is widely used for image-guided interventions, and can also aid in the treatment planning of HIFU therapy. Moreover, several MR tissue parameters such as the spin-lattice relaxation time, T, the equilibrium magnetization, M_0, and the molecular diffusion contrast are altered as a result of temperature change and ablation. Thus MRI can also be used to visualize the severity of tissue damage following treatment. Perhaps the most important utility of MRI for HIFU therapy is, however, its ability to produce high-resolution *in vivo* temperature images that can be used to visualize the temperature rise in real-time in any imaging plane within the body[6] [7].

In addition, several MRI modalities have been explored in various cancer models for the early detection and therapy response. Diffusion weighted MRI helps differentiate

normal pancreas from pancreatic cancer [188]. Tumor growth curves constructed from serial T2-weighted MR measurements are used to measure the tumor therapeutic response. The inhibition of growth indicates therapeutic response [189]. T1 imaging has been used to assess treatment in brain tumors [190]; by evaluating the changes in vascular volume after cancer therapy, dynamic contrast enhanced (DCE) MRI has been used to assess response to cytotoxic and cytostatic therapies [191].

The general hypothesis guiding this research was conventional MRI methods such as T2-weighted imaging and quantitative values acquired from multi-parametric MRI can serve as valuable *in-vivo* biomarkers of different tumor models with information regarding stroma tissue, blood flow and relatively the drug diffusion.

The MR imaging techniques have been described in Chapter 4.5. Briefly, T2-weighted images (T2WI) provide morphological information about the tumor. This scan defines the organ boundaries, the tumor and cystic components due to high water contrast and addition of fat suppression. Diffusion weighted imaging (DWI) provide quantitative method to characterize the tumor and other organs. The magnetization transfer ratio (MTR) in magnetization transfer imaging (MTI) is used to identify collagen deposition and fibrosis in the different tumor models. Dynamic contrast enhanced (DCE) MRI was used to characterize blood flow and diffusion into different types of tumor models.

7.2 Methods and materials

In addition to transgenic KPC mice which spontaneously develop PDA, orthotopic xenograft and subcutaneously implanted mouse models were used. Mice with tumors larger 500 mm^3 and smaller than 1000 mm^3 in volume were prepared for imaging. Before scanning, the mouse was anesthetized with a mixture of 1.5% isoflurane in oxygen delivered at 1 liter/min through a nose cone (Novaplus). An eye lubricant was administered to each animal to prevent corneal desiccation while under anesthesia. Mouse temperature was controlled with a built-in heating system maintaining physiologic body temperature. A water circulation system embedded in the gradient coil housing controlled the temperature of the RF coil. Water temperature was controlled by a heated water bath. Heart- and respiration rates were monitored with an MRI-compatible small animal gating system (SA Instruments, Stony Brook, NY).

For *in vivo* imagining, a 14T MR System, (spectrometer with a micro imaging accessory, 600 MHz Bruker Avance III) was used in combination with a 25 mm coil and the coil holder. The high-field MRI has the benefits of higher signal-to-noise ratio, contrast-to-noise ratio and spectral resolution for certain application. In most cases, these benefits facilitates higher spatial and temporal resolution.

Turbo Spin Echo T2-weighted images were acquired in the coronal plane, with no interslice gap and identical fields of view of 40 x 40 mm. The acquisition was done under respiration gating.

With higher field strength, it was possible to acquire multi b-value diffusion weighted images which can be processed in low and high b-value ranges. Diffusion-weighted imaging was performed with different b-values to assess their ability to characterize the tumor. Two different diffusion weighted imaging protocols were performed in a coronal plane using a spin-echo single-shot echo-planar imaging sequence with two sets of diffusion gradients, a low b-value (b=0 s/mm^2), and a middle b-value (b=400 s/mm^2). Another scan with a low b-value (b=0 s/mm^2) and a high b-value (b=1000 s/mm^2). Diffusion-weighted gradients applied in slice directions. In order to reduce the effect of motion, the scans acquired with respiration and ECG gating. After initial studies demonstrated that ECG gating was superfluous, only respiration gating was used.

All raw MR scans were processed using Image-J (Rasband, W.S., ImageJ, U. S. National Institutes of Health, Bethesda, Maryland, USA, http://imagej.nih.gov/ij/, 1997-2012) [192]. The detection of diffusion by the spin-echo technique on the MR signal was calculated a technique similar to that described by Bihan D Le *et al.* 1986 [109]. The MT MRI pulse sequence with offset frequency 7000Hz. MTR measured by the technique described by Li *et. al* [193]. Briefly Voxel-wise MTR maps were calculated as follows: 100 x (1 − MT/M0), where MT represents the signal intensity for the image acquired following application of the MT pulse and M_0 is the signal intensity image acquired without MT saturation. For an imaging slice through the center of each tumor, a region of interest (ROI) was drawn to circumscribe the entire tumor. The mean MTR value is reported for each tumor.

The dynamic contrast-enhanced (DCE-MRI) time course was acquired using T1-weighted RF-spoiled gradient echo. Five different T1 scans with different flip angles were acquired (FA=2, 5, 10, 20, 40). From these scans, T1 maps were calculated using ImageJ software. 700 time points were acquired after injection of the contrast agent giving a total imaging time of 10 minutes. For contrast enhanced imaging, 200μl of the paramagnetic contrast agent, Gadolinium (Gd-DTPA), was injected *via* a tail vein catheter. A compartmental analysis was used to analyze dynamic contrast-enhanced T1-weighted data. The transfer constant, and the extravascular extracellular space fractional volume and the rate constant were calculated from the data. The transfer constant has several physiologic interpretations, depending on the balance between capillary permeability and blood flow in the tissue of interest. In high-permeability situations, the transfer constant is equal to the blood plasma flow per unit volume of tissue. With these values a two compartment tracer kinetic theories of Kety [121] [122] was used to obtain more quantitative indices of blood flow and capillary permeability.

These mice were later used in Aim 2. After the final study, microscopic morphologic analysis was performed using standard tissue histology methods. For the histological analyses, tumors were excised, snap-frozen and cut into 5 μm sections utilizing a cryostat (CM1950, Leica, Bannockburn, IL). H&E staining was completed using standard protocols for gross histological assessment of cellular density, necrosis and fibrosis. The sections were examined using a Nikon H550L light microscope (Nikon, Melville, NY). Consecutive cryosections from the sample were collected for Masson's trichrome

staining for evaluation of the stroma layer in the tumor. Immunohistochemistry (IHC) was performed to visualize the vasculature structure.

Masson's trichrome staining samples were imaged, and using Matlab software (MatWorks, Natick, MA), fibrotic tissue areas were quantified within each slide. The total tumor tissue area (A_{total}) was also measured. The percentage of fibrotic tissue was defined as the ratio $A_{fibrosis}/A_{total}$ x 100. These measurements were repeated for each animal. The percentage were compared with the MT ratio for each group.

In order to improve the study's ability to resolve differences between different tumor model properties, 8 animals in each group were measured. With 90% power and a significance level = 0.0125, between treatment variance = 36, within treatment variance = 25. The treatment variance and between treatment variance in this calculation is estimated.

The MRI data were expressed as mean $\pm$ SD. One-way analysis of variance was used to compare MTR measurements. All statistical analyses were performed with Stata software (Stata11, Stata-Corp, College Station, Tex). In order to have a baseline and distinct value from the tumor the ADC values of tumor were compared with values of liver, spleen and kidney.

7.3 Results

Eight mice in each tumor group (orthotopic, subcutaneous xenograft, or transgenic) were imaged. Figure 7.1 shows the coronal view T2W images of three different tumor model. Red dashed line indicates the tumor and surrounding organs are visible in the plane. By reducing the slice thickness and acquiring more slices 3D reconstruction of each tumor is possible. The 3D image of each tumor is shown in Figure 7.2 and can be used to calculate the volume of each tumor.

Using fully automated acquisition of T2 series, followed by a semi-automatic image analysis T2-map of the tumor was generated and overlaid on the T2WI. A representative example is shown in Figure 7.3. T2 measurements are helpful in detecting pathological tissues due to their elongated T2 relaxation time (e.g. degenerative changes of cartilage, muscular atrophy, and high signal intensity in tumors). T2 relaxation time of the tumor in each model is shown in Figure 7.4. There is no different between T2 relaxation time of three tumor models. But there is a different in relaxation time of tumors and other organs (*Viz.* spleen and muscle).

ADC value of each tumor was calculated and the result is presented in Figure 7.5. KPC mice have the lowest ADC value and subcutaneous mice tumor has the highest ADC value. This is due to the higher density of the KPC tumor in comparison with the other tumor models.

Representative tri-chrome histology slides for KPC, orthotopic and subcutaneous mice are shown in Figure 7.6. These slides clearly depict the fibrotic stroma seen histologically as blue-stained bands of collagen enveloping the tumor cells in each tumor model. KPC model consistently demonstrated significantly greater levels of fibrosis and associated collagen deposition; the percentages of fibrotic tissue area measure for these specific examples were 1.4, 5.21 and 7.8 for subcutaneous, orthotopic and KPC tumors, respectively.

A summary of both MTR measurements and histologic measurements of fibrotic tissue area for each tumor type is shown in Figure 7.7. MTR measurements from the tumors in KPC mice (45.4 ± 5.1) were higher than MTR measurements in orthotopic mice (38.4 ± 3) and tumors in the subcutaneous mice (26.3 ± 2.8). The comparison of MTR and histologic data indicates there is a correlation (r=0.87) between MT ratio and the amount of stroma in each tissue. The data confirms that the transgenic KPC model has the highest stroma level among other type of tumor.
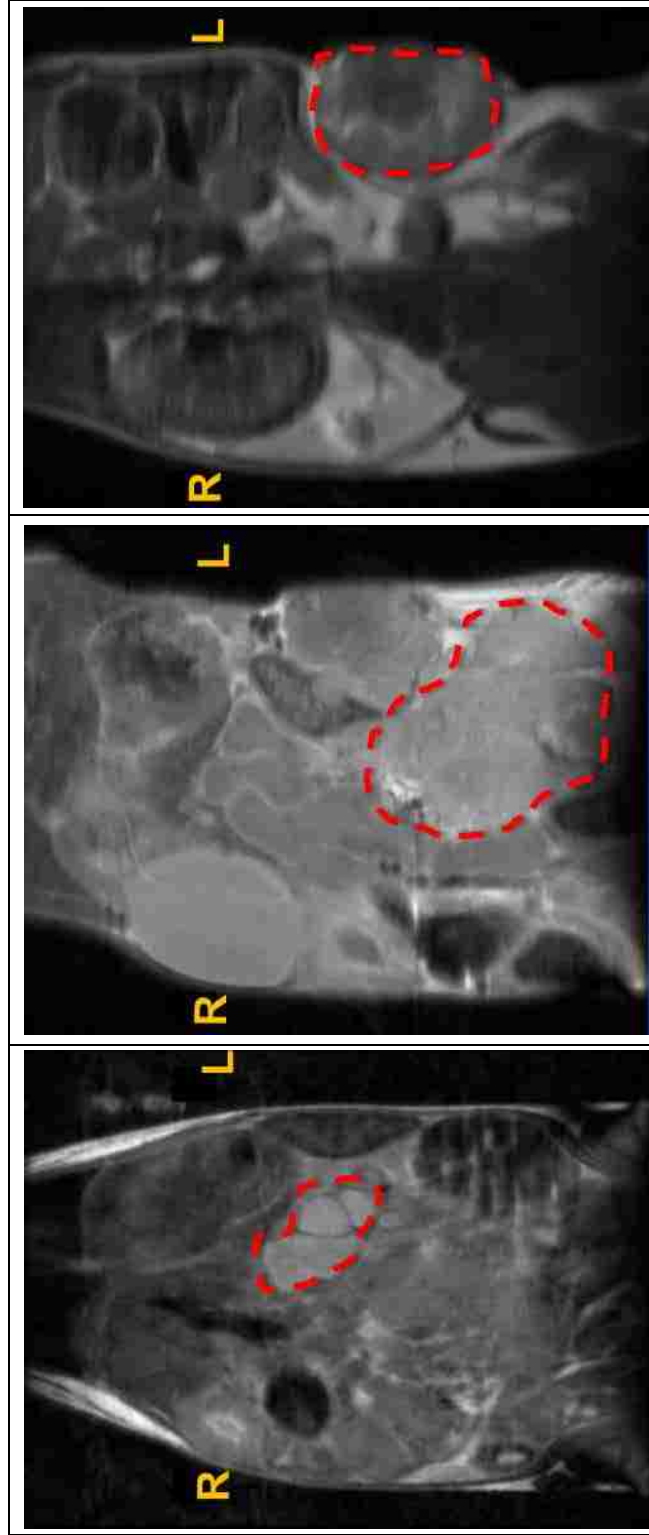
Figure 7.1. T2-weighted images of three different mouse model in coronal view. (**Right**) Subcutaneous, (**Middle**) Orthotopic, (**Left**) KPC mice. Red dashed line identifies the tumor growing on the flank (right) tail of pancreas (middle) and pancreas (left).
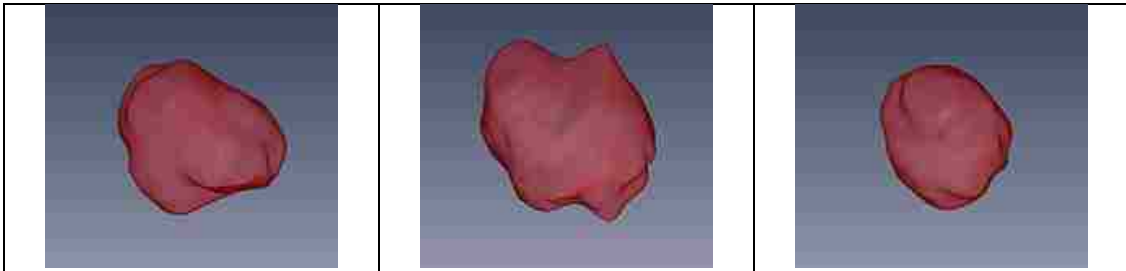
Figure 7.2. Representative 3D volumetric image of the tumor grown in each model can be used to calculate the volume of the tumor. **(Right)** Subcutaneous, **(Middle)** Orthotopic, **(Left)** KPC mice.
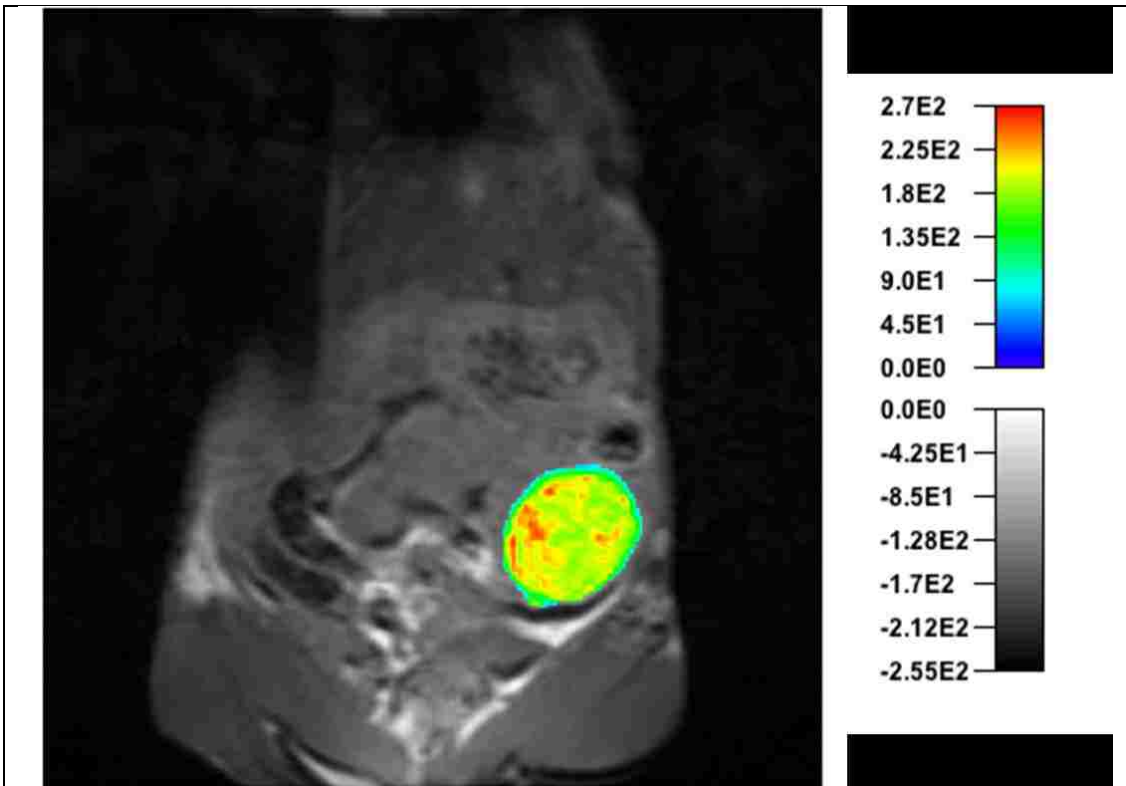
Figure 7.3. T2 relaxation time of the tumor overlaid on the T2WI. T2-map calculated semi-automatically from series of T2 acquisitions.
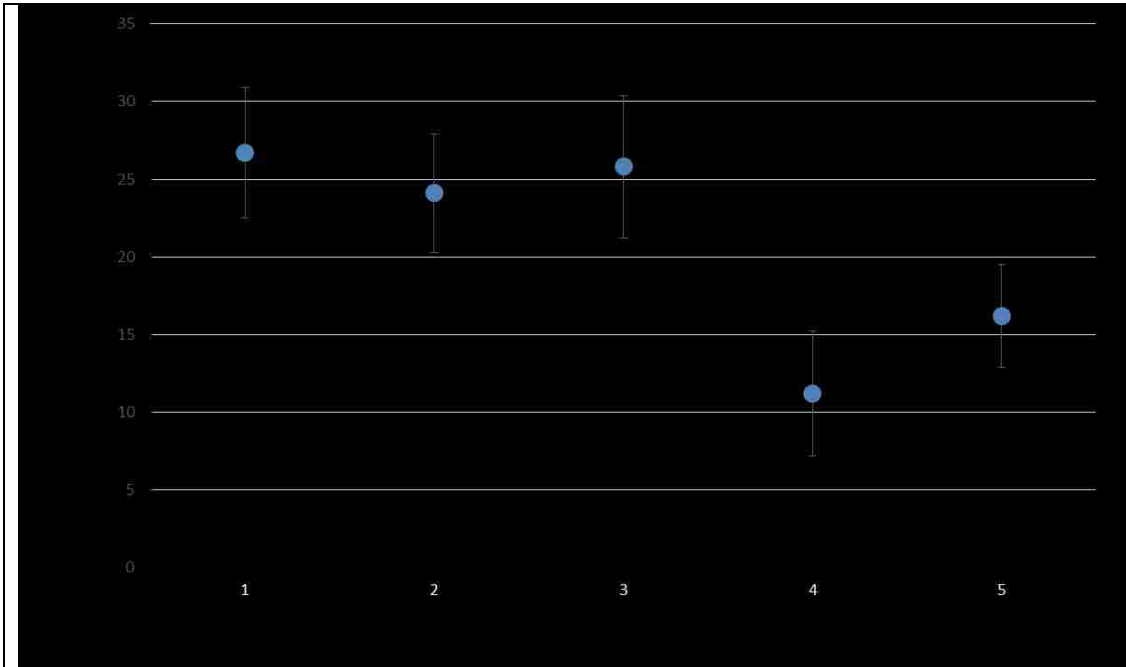
Figure 7.4. T2 relaxation time of the tumor in three different mouse model and two organs (*Viz.* spleen and muscle) in all animals.
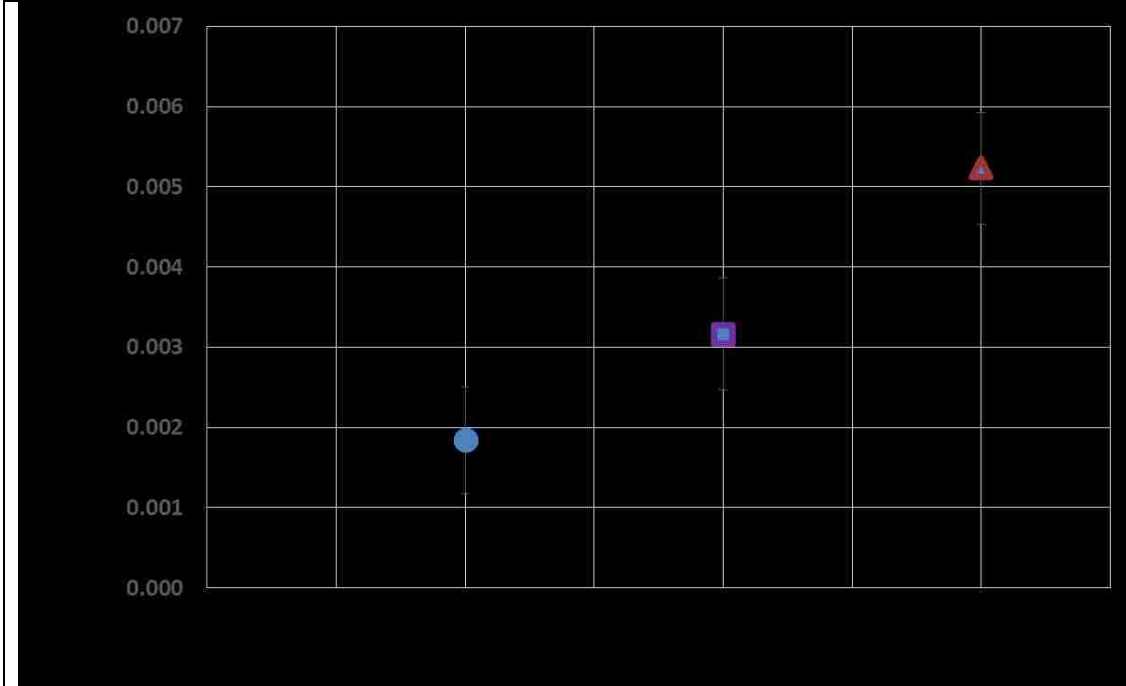
Figure 7.5. ADC value of the tumor in three different mouse model.
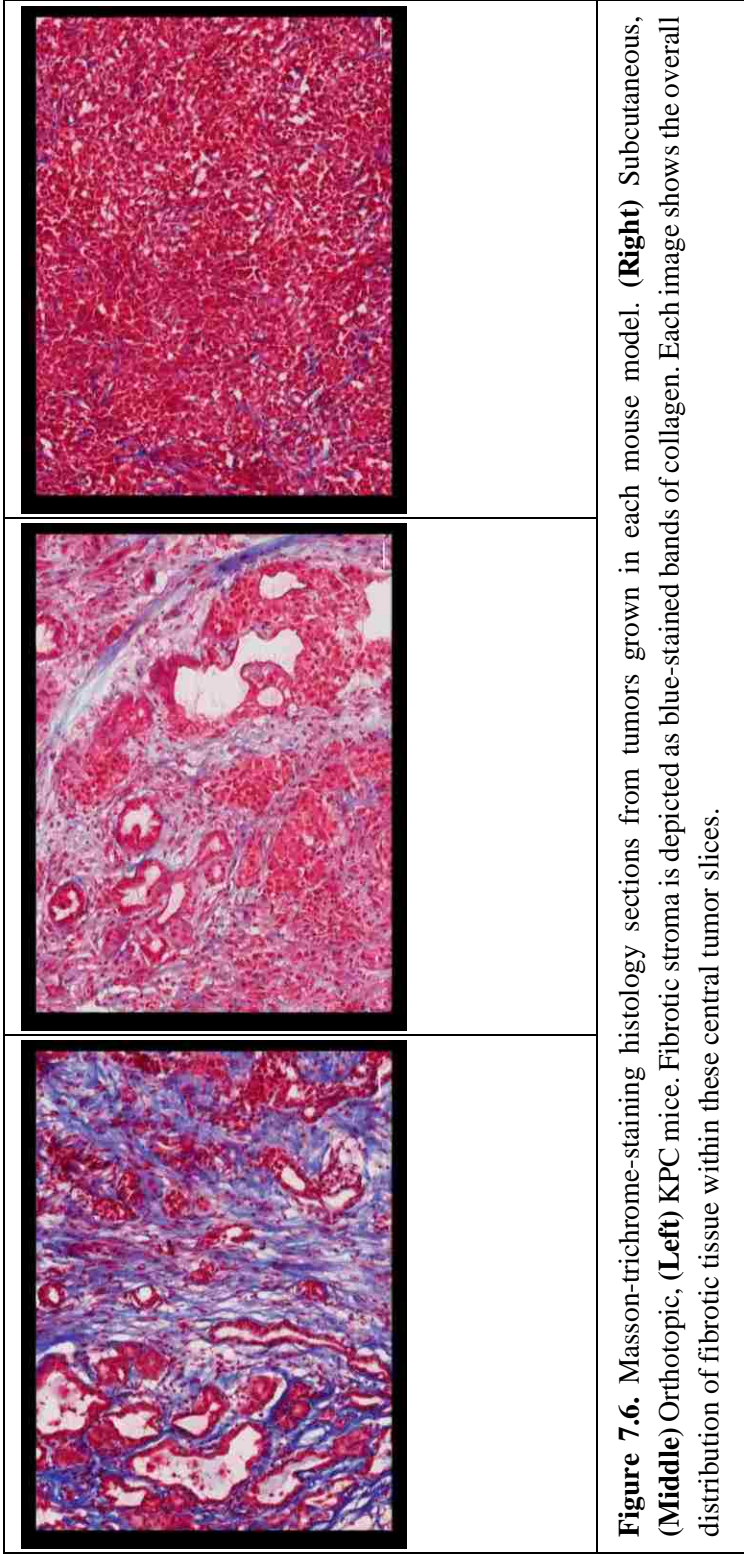
Figure 7.6. Masson-trichrome-staining histology sections from tumors grown in each mouse model. (**Right**) Subcutaneous, (**Middle**) Orthotopic, (**Left**) KPC mice. Fibrotic stroma is depicted as blue-stained bands of collagen. Each image shows the overall distribution of fibrotic tissue within these central tumor slices.
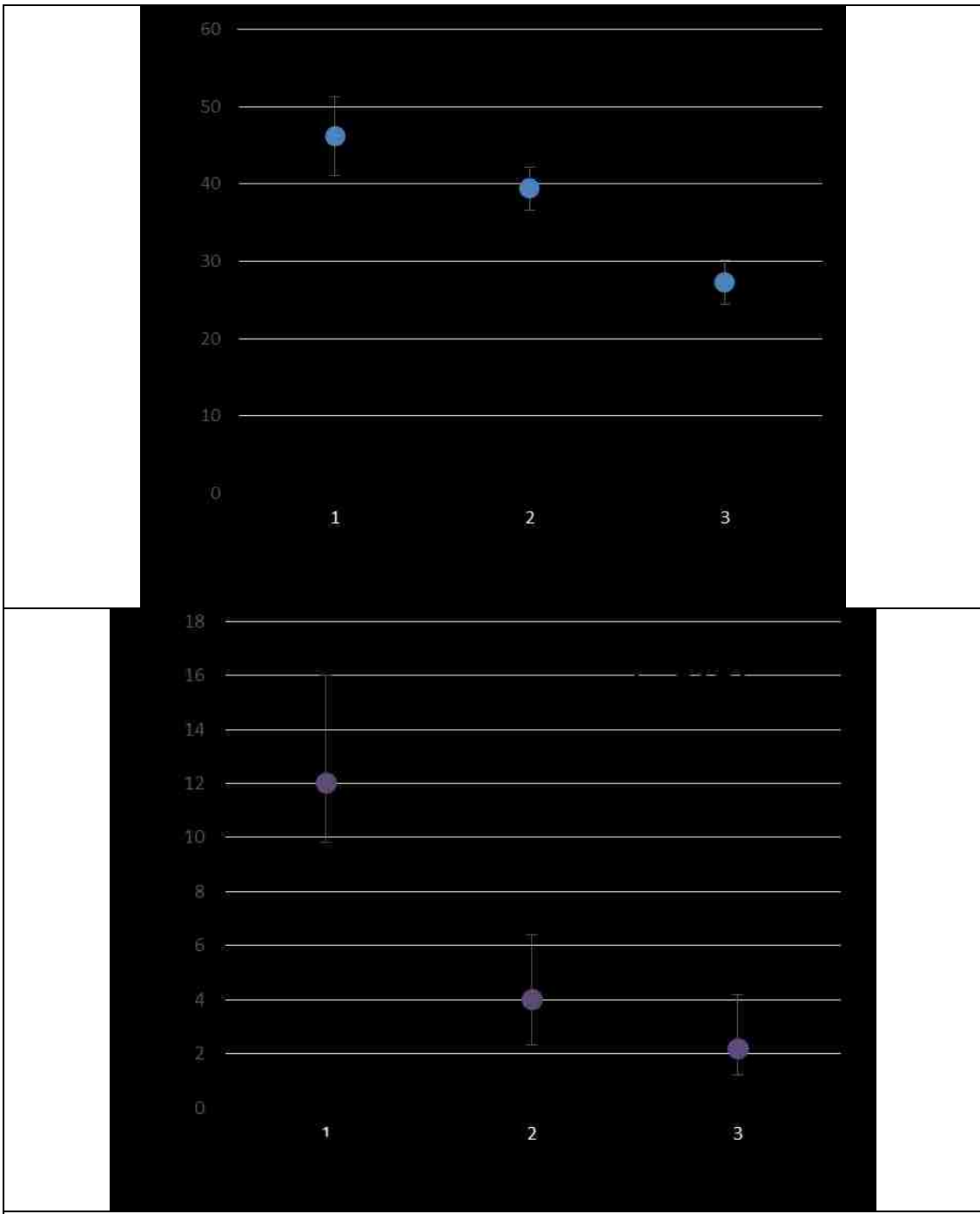
Figure 7.7. MTR measurements **(top)** and histologic fibrotic tissue area measurements **(bottom)** for each of the three mouse model. There is a correlation between MT ratio and the amount of stroma in the tumor (r=0.87).

Chapter 8. MR-HIFU induced hyperthermia for enhanced drug delivery in the pancreatic cancer mouse model

8.1 Introduction

Pancreatic ductal adenocarcinoma (PDA) is one of the most lethal types of cancer, in part because it is insensitive to many chemotherapeutic drugs [194], [195]. The current standard of care therapy, gemcitabine, improves survival by only a few weeks [195], [196]. It relies on systemic delivery with limited tumor specificity that may result in negative side effects in normal tissue and insufficient drug delivery to the tumor [197], [198]. In addition, previous pre-clinical studies have demonstrated that doxorubicin has activity against human pancreatic adenocarcinoma cell line [199], [200]. The literature describing such findings and barriers to DOX delivery into the tumor is reviewed in Chapter 2. To reiterate briefly, a special structure of the tumor, the desmoplastic stroma, is an effective barrier to doxorubicin delivery into the tumor. Advances in cancer therapies such as localized heat induced drug delivery, discussed in Chapter 6, can offer a solution in the non-invasive treatment of PDA, and may increase treatment options by greatly increasing the effectiveness of drugs such as doxorubicin which are otherwise ineffective.

In an implanted rat model treated with MR-guided HIFU to achieve hyperthermia, tumor concentrations of doxorubicin were compered in animals administered TSL containing doxorubicin and gadolinium [170]. The results implied that MR-guided,

HIFU-induced hyperthermia was successful in releasing doxorubicin and gadolinium from temperature-sensitive liposomes in implanted tumors.

The general hypothesis guiding this research was HIFU induced hyperthermia in combination with TSL loaded chemotherapy agent will increase extravasation of drug out of the tumor microvasculature. Figure 8.1 is a schematic presentation of the drug release in the heated zone of the tissue by HIFU (the image is not drawn to the correct scale).

Figure 8.1. (1) Encapsulated TSL with doxorubicin, (2) Open TSL, (3) Free doxorubicin, (4) Doxorubicin uptake by cell nuclei, (5) Cancer cells, (6) Red blood cells, (7) Ultrasound wave Yellow zone indicates the heated zone.
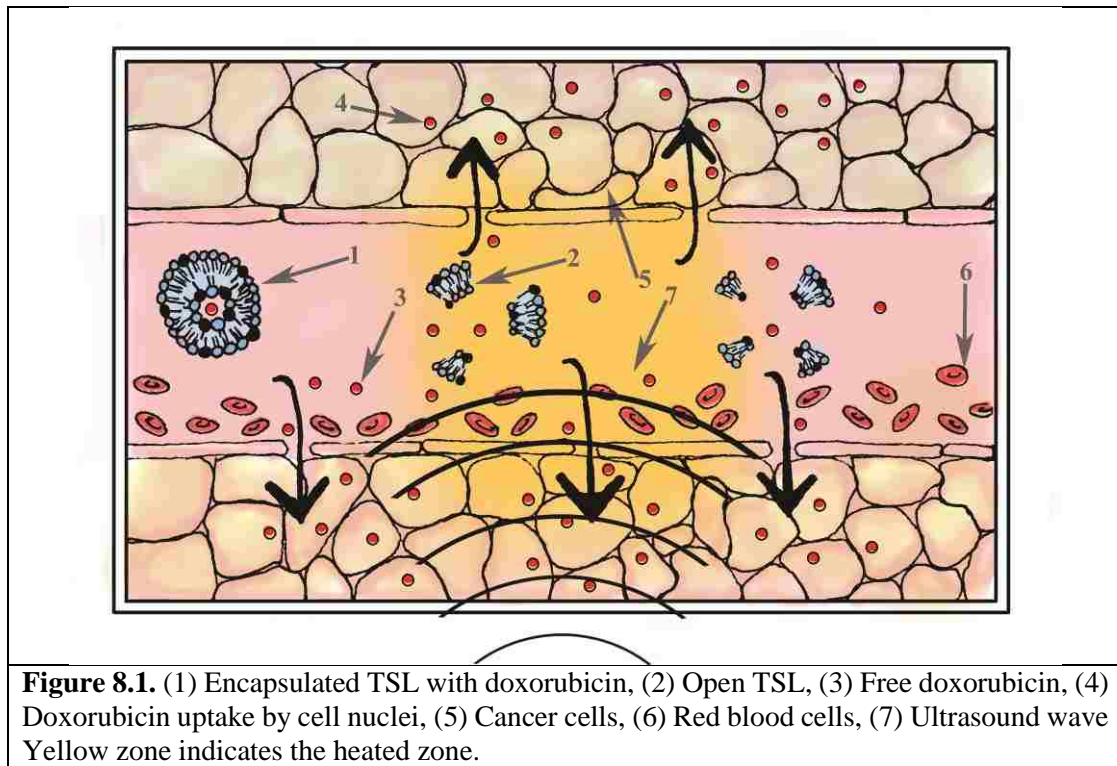
8.2 Methods and materials

Study design

KPC and orthotopic mice were assigned randomly into treatment and control groups, with 4 mice in each group. Two different doses of doxorubicin loaded TSL were used. Initial studies used a dose of 15 mg/kg to facilitate detection and quantification of autofluorescence after treatment. Subsequent studies used a more clinically relevant, and better-tolerated, dose of 5 mg doxorubicin/kg. Free doxorubicin was injected at both dosages in KPC mice but only at the 5 mg/kg dose in orthotopic animals. Moreover a PEGylated liposomal form of doxorubicin, Doxil, was injected at only the 5 mg/kg dose. Each disease model type of animal in each injection dose group was assigned to MR-HIFU hyperthermia treatment or no hyperthermia treatment (Table 8.1).

Dose	KPC	Orthotopic
15 mg/kg	TSL + MR-HIFU	TSL + MR-HIFU
	TSL	TSL
15 mg/kg	Doxorubicin + MR-HIFU	
	Doxorubicin	
5 mg/kg	TSL + MR-HIFU	TSL + MR-HIFU
	TSL	TSL
5 mg/kg	Doxorubicin + MR-HIFU	Doxorubicin + MR-HIFU
	Doxorubicin	Doxorubicin
5 mg/kg	DOXIL + MR-HIFU	DOXIL + MR-HIFU
	DOXIL	DOXIL

Table 8.1. Study design. Each tumor model was assigned randomly to eighteen different treatment and control groups. Two different doses of doxorubicin were used for TSL drug.

Animal model

The protocol used for animal experiments was approved by the Institutional Animal Care and Use Committee (IACUC) at the University of Washington. Two different pancreatic cancer mouse models were used in the study. The first was the KPC transgenic mouse mode that spontaneously developed PDA. The second was the orthotopic model. This model was used to provide a basis for comparison between previously published results using the xenograph model and the result of the present study.

Both of these models were described thoroughly in Chapter 2.2.

Chemotherapeutic agents

A lyso-lecithin containing LTSL formulation (ThermoDox®, Celsion Corp., USA) was provided through a collaborative agreement. The concentration as provided was 1.8 mg doxorubicin/mL. Doxorubicin hydrochloride (Doxorubicin) was served as free drug.

In a separate study, a TSL drug co-loaded with doxorubicin and gadolinium as an MR contrast agent from The Eindhoven University was also examined.

***In vivo* setup**

MR-HIFU hyperthermia treatments were performed on a 3T clinical MR-HIFU system (Sonalleve® V1, Philips Healthcare, Vantaa, Finland). Anatomical and temperature imaging at a spatial and temporal resolution sufficient for mice was facilitated by using a dedicated small animal research coil setup. For this study, a special mouse support was fabricated, with design considerations focusing on body temperature

control, the acoustic pathway to the pancreas, and provisions for adequate animal monitoring. Figure 8.2 represents an schematic view of the *in vivo* setup.
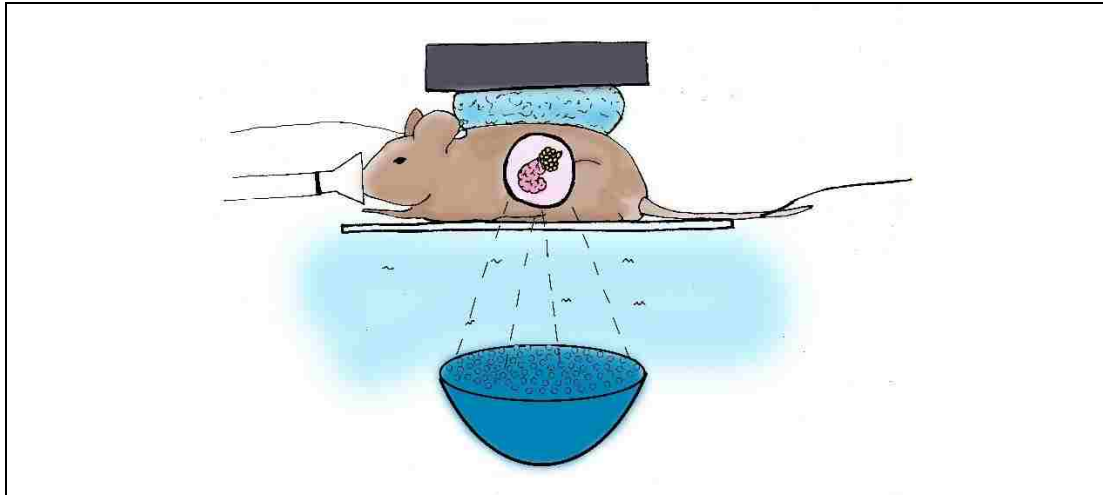
Figure 8.2. *in vivo* experiment setup. Animal was placed on the positioning tray. Acoustic coupling was achieved by using degassed distilled water and degassed ultrasound gel. An acoustic absorber was placed on top of the ultrasound gel on the back of the animal to control the exit wave and minimize the movement. Respiration was monitored by MR-compatible small animal monitoring system.

In further detail, the supporting animal bed was made of non-stretching, thin plastic sheeting (Saran Wrap, Dow Chemical, Terneuzen, the Netherlands) gripped in a rectangular plastic frame (Figure 8.3 A+B). The bed was filled with a mixture of degassed water and degassed ultrasound gel (Aquasonic 100, Parker Laboratories, Fairfield, USA) in order to achieve good coupling of the ultrasound beam into the animal and to minimize water convection caused by local heating (Figure 8.3 C). A water circulation system was installed along the sides of the plastic frame to allow maintain the water temperature close to mouse body temperature (Figure 8.3 D). The ultrasound gel was added to minimize water convection caused by local heating. The mice were anesthetized with a 1.5% mixture of isoflurane in oxygen (1 L/min) delivered through a

nose cone (Isoflurane Vaporizer Novaplus). The mouse anesthesia inhalation mask was positioned and held in place at the top end of the frame (Figure 8.3 E). The mouse was positioned in the center of the circulation tubing, with the lower body, including the target area, submerged in the gel-water mixture and with its head supported by a thin foam strip (Figure 8.3 H). When bowel gas was present in front of the target area, a gel dome (10% polyacrylamide) was placed underneath the animal, pushing the gas to the sides. Degassed ultrasound gel was put alongside and on top of the animal to minimize any air-tissue interface. This results in a lower occurrence of artifacts during MR imaging and temperature mapping. Additionally, a piece of quality assurance ultrasound gel (Parker Laboratories, Inc. NJ. USA) was placed alongside the animal for positioning of a baseline drift reference region for correction of the measured temperature changes for main magnetic field drift (Figure 8.3 G). An ultrasound absorber was placed on top of the gel on the posterior of the animal to control the exit of the ultrasound wave and to keep the animal from moving during treatment (Figure 8.3 J). A plastic strip with a small balloon sensor (Graseby, Smiths Medical, St Paul, USA) was placed on the mouse head / upper back to monitor the animal respiration rate during treatment (Figure 8.3 F).

Figure 8.3. The MR-HIFU animal support.

65
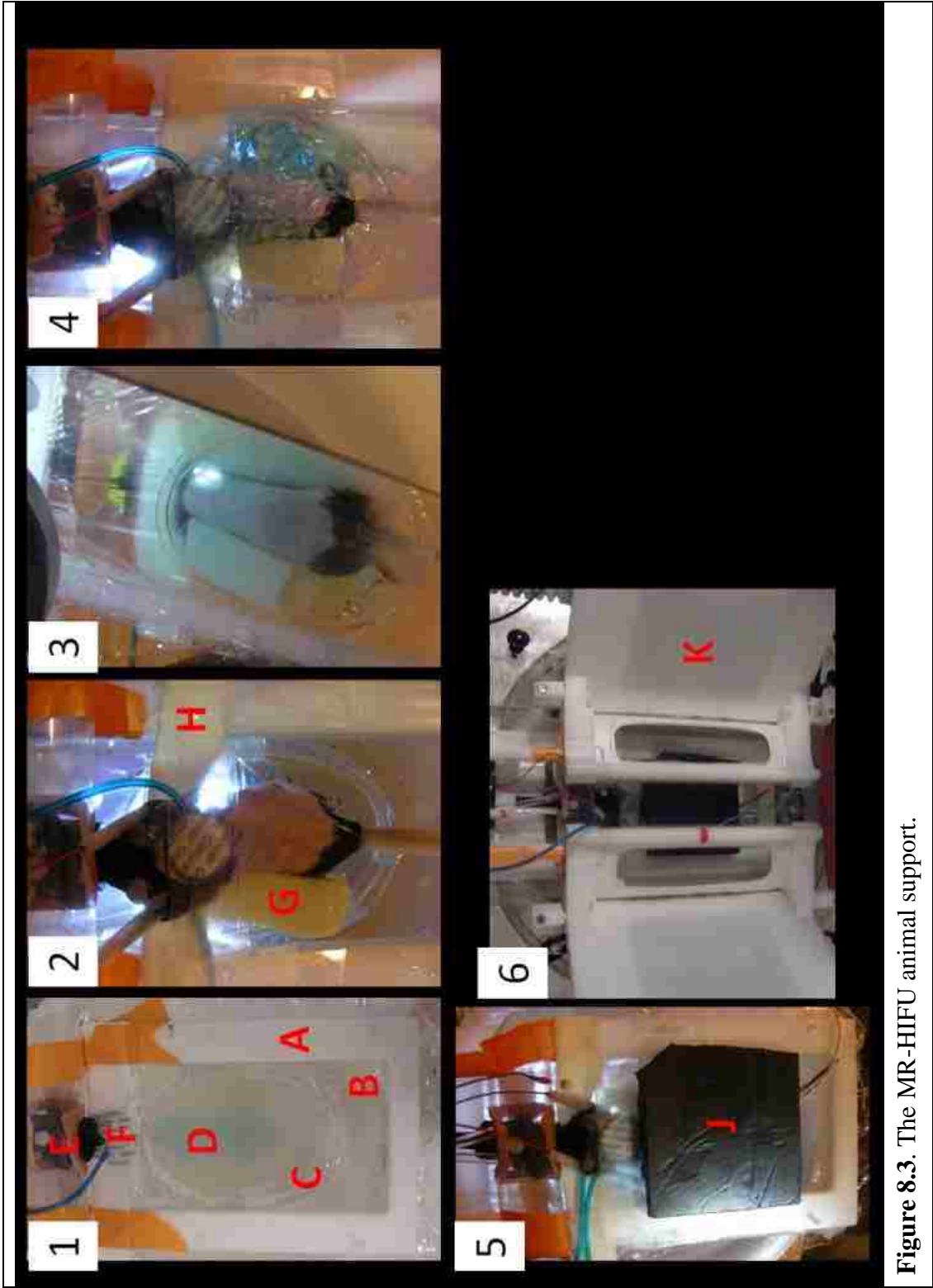
Treatment planning, and application monitoring

After positioning the mouse in the small animal setup, a quick survey scan was acquired followed by a susceptibility sensitive scan (T1W 3D steady-state gradient-echo; TR/TE: 15/12 ms; FA: 10°; FOV: 150 x 150 x 40 mm^3; voxel size: 1.1 x 1.1 x 2.0 mm^3; slices: 20; acquisition time: 2 min) to check for the presence of air bubbles in the ultrasound beam path. HIFU treatment was planned on a proton density weighted image set acquired with a gradient echo sequence (Fast field echo; orientation: coronal; TR/TE: 1791/13 ms; FA: 20°; FOV: 40 x 48 mm^2; voxel size: 0.25 x 0.25 x 1.00 mm^3; parallel imaging (SENSE) factor: 2 (RL), saturation bands: 3; slices: 20; acquisition time: 5 min).

An ellipsoidal HIFU treatment volume (known as a 'cell') was targeted inside the mouse tumor. Depending on tumor size and the proximity of air cavities in the bowel, a 2 or 4 mm diameter treatment cell was used (cell length ≈ 2.5 times the diameter). Several low power test sonications (continuous wave ultrasound, acoustic frequency = 1.2 MHz, acoustic power = 10 W; duration = 20 s) were performed prior to therapeutic sonication to assess for, and if necessary, to correct for miss-registration between the heated volume and planned treatment location.

The temperature change in the target region was monitored by continuous acquisition of one tomographic slice perpendicular to the beam axis and one slice parallel to the beam axis, all centered on the target volume (RF-spoiled gradient echo with EPI readout; EPI-factor: 7; TR/TE: 62/20 ms; FOV: 100 x 100 mm^2; voxel: 0.9 x 0.9 x 4.0 mm^3; fat suppression: spectral pre-saturation with inversion recovery (SPIR); SENSE-factor: 1.8;

SENSE-direction: RL; number of averages: 2; saturation bands: 2; dynamic scan time: 1.8 s). The temperature maps were calculated online using PRFS thermometry and displayed on the therapy control workstation. PRFS thermometry method has been described in Chapter 4 Section 4. The temperature images were corrected for baseline drift by subtracting the drift calculated from the reference region positioned in ultrasound gel from the actual temperature data. Parallel imaging was added to the temperature mapping sequence to improve dynamic scan time. This gain in imaging speed was in turn traded for the use of saturation bands in case of interference from bowel air or respiratory motion.

Once the treatment was planned and co-registered, animals were injected with TSL (5 mg/kg or 15 mg/kg) *via* a tail vein catheter (model MTV-03, SA instrument Inc., Stony Brook, NY). Therapeutic sonication (continuous wave ultrasound, acoustic power = 7 W) was started within five minutes post injection. For prolonged hyperthermia treatment, a binary feedback control algorithm was used that compared the feedback temperature with pre-defined threshold temperatures (T_{min} = 40 °C, T_{max} = 42 °C) and switched the transducer power on or off accordingly. After five or ten minutes of mild hyperthermia, the sonication was stopped for recalibration of temperature elevation measurement to readjust the baseline temperature and also to control the animal's condition. Sonication was continued for five or ten more minutes as needed (total hyperthermia time: 15-30 min); (Figure 8.4).
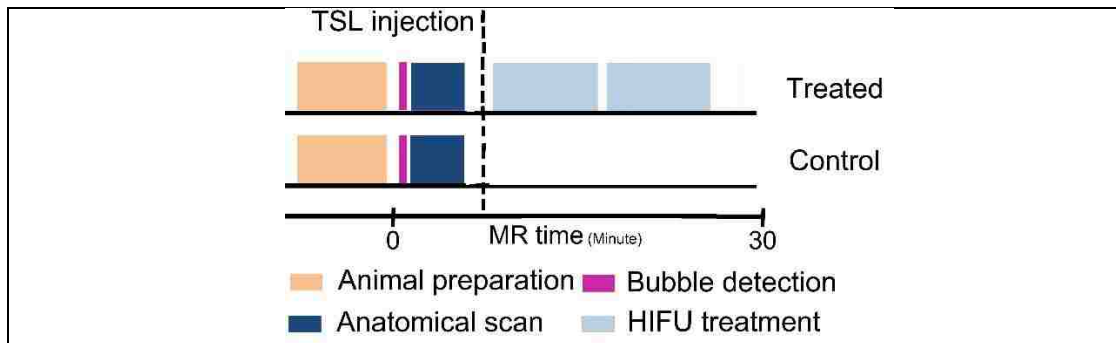
Figure 8.4. Schematic representation of experimental time line. Following animal preparation and anatomical scans after a slow infusion of drug, hyperthermia (5-10 min) was interleaved with 2 minutes of cooling period. The cooling time was used to control the animal's condition and readjust the baseline temperature. This was repeated for total of 15-30 min of heating. Mice were euthanized after the experiment and tissues were harvested for histological analysis and quantitative analysis of drug concentration using HPLC.

Treatment planning and monitoring with Eindhoven drug

The same animal models and setup described above was also used for this part of the study. During MR-HIFU planning and treatment after checking for air bubbles and prior to injection and treatment, maps of the longitudinal relaxation rate (R1) where acquired of both the HIFU targeted tumor area and the bladder (single slice steady state inversion-recovery Look-locker sequence with EPI read-out, EPI-factor: 5, TR/TE: 9.0/3.4 ms, interval time: 100 ms, flip angle α: 10°, FOV: 50x69 mm^2, matrix: 64x65, fat suppression: SPIR, slice thickness: 3 or 5 mm (depending on HIFU treatment cell size), number of averages: 2, acquisition time: 2:36 min). The bladder was used as an internal control for contrast agent release from the liposomes (upon release, Gd-HPDO3A gets excreted by the kidneys into the urine, resulting in a local R1 change).

The Look-Locker scans were triggered using the *Physiological Simulator* module available in the Philips Achieva scanner software (number of R-R intervals: 1, duration:

68

6010 ms, heart phases: 10). Fast gradient echo based images were acquired for more detailed anatomical reference to the R_1-maps (Fast field echo, orientation: transverse, TR/TE: 98/7.2 ms, FA: 20°, FOV: 40x48 mm^2, voxel size: 0.5x0.5x1.0 mm^3, parallel imaging (SENSE) factor: 2 (RL), saturation bands: 3, slices: 3, acquisition time: 29 sec) at the same positions as the Look-Locker scans. These images where used to check for animal movement between different HIFU heating periods, and as a fast qualitative snap-shot of the local T1-times.

In initial experiments, animals were pre-heated to $T_{ave} \approx 41°C$ for 2 minutes before injection of the liposomes. However, this was removed from the protocol as injection of the liposomes could not be done during heating (due to interference of the liposomal Gd with the temperature mapping), while the expected benefit of increased perfusion is not likely to remain after cool down from short-term hyperthermia. Therapeutic sonication was performed as described in previous section. After five minutes of mild hyperthermia, the sonication was stopped and a fast FFE scan was acquired. Subsequently, sonication was continued for five more minutes, followed by two additional ten minute periods (total hyperthermia time: 30 min). The heating periods were interleaved by short FFE anatomical scans and R1 maps of the target location to check for contrast agent release (Figure 8.5). Finally, R1 maps of the bladder were acquired and the animals were taken out of the MR-HIFU setup.

The effective T1-time (T1*) as well as the effective R1 values (R1* = 1/T1*) were calculated from the signal recovery on a voxel-by-voxel basis using an in-house created

IDL-based software tool (IDL version 6.3, RSI, Colorado, USA). The longitudinal relaxation rate R1 was calculated from the effective R1* (R1 = R1* + ln(cos(α))/TR, with α = 10° and TR = 100 ms).

Figure 8.5 MR-HIFU treatment schedules.

Post treatment procedures

Following treatment, the mouse was removed from the coil and sacrificed immediately. The chest cavity was then opened and a 10 mL intracardiac injection of PBS administered to clear the vasculature of drug/liposomes. Necropsy was performed immediately after euthanasia. Skin and organs were examined for damage and metastasis. Tumor and tissue samples from spleen, liver and kidney were collected. Samples were snap frozen and then stored at -80°C until histopathology and high-performance liquid chromatography (HPLC) analyses. For the experiment with the Eindhoven drug in some cases urine was collected to evaluate the presence of gadolinium.

Qualification and quantification analysis

For histological analysis and fluorescent microscopy, tumors were excised, snap-frozen and cut into 5 μm sections utilizing a cryostat (CM1950, Leica, Bannockburn, IL). Hematoxylin and eosin (H&E) staining was completed using standard protocols for gross histological assessment of cellular density, necrosis and fibrosis. The sections were examined using a Nikon H550L light microscope (Nikon, Melville, NY). Consecutive cryosections from the sample were collected for doxorubicin distribution assessment using florescent microscopy as well as Masson's trichrome staining for assessment of stroma layer in the tumor. Immunohistochemistry (IHC) was performed to visualize the vasculature structure.

Quantification of doxorubicin was achieved by HPLC. Tissue homogenization and sample preparation for HPLC were carried out as reported previously [201]. Briefly, samples were homogenized, doxorubicin extracted and quantified with HPLC using an internal standard daunorubicin (DNR) [166].

Following data reduction, tissue drug concentration values are reported as the mean drug concentration per weight of tissue ± SD, unless otherwise indicated. Within each injection dosage group, doxorubicin concentration effects were compared between groups of animals using the Mann-Whitney U test. This determines if the type of drug or HIFU treatment would affect the drug concentration. Sample size calculations were performed to achieve a power of 0.8 (1-β), significance level of 0.05 (α), with the assumption that a 2-fold increase in doxorubicin concentration would be achieved in the

71

ThermoDox® group. This assumptive is conservative estimate based on preliminary results and existing literature.

8.3 Results

MR-guided hyperthermia

Hyperthermia therapy in a small animal was successful using a clinically available MR-HIFU system; the mild hyperthermia heating algorithm resulted in a tight target temperature range (41 ± 0.5 ℃, target = 40 - 41℃) which was homogeneous (SD = 1.0 ℃) within the ROI. Approximately 20 s were required to achieve the target temperature (Figure 8.6).

Figure 8.6. Image guided hyperthermia. Example of temperature elevation during a sonication. Following a short heat-up period, stable mild hyperthermia was achieved in the target region through binary feedback control.
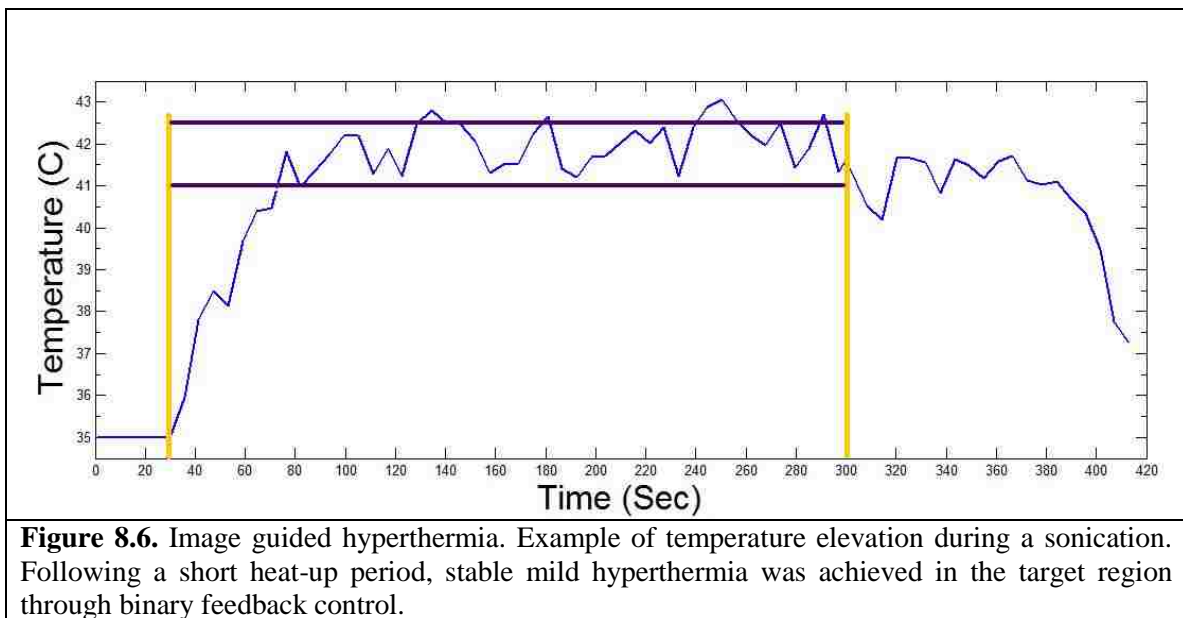
Histopathology analysis

H&E staining performed on tissue from transplanted and KPC mice models, demonstrated tumor consisting of viable tumor tissue and a well-defined tumor border. To better identify stroma tissue in the tumor, Masson's trichrome staining was used to differentiate the stroma tissue and tumor tissue. The fluorescence images of doxorubicin illustrated targeted drug distribution. The red spots in the Figure 8.7 indicates the doxorubicin uptake by the tumor nuclei, and has higher intensity in the target region of the LTSL + MR-HIFU group.

Doxorubicin appears to accumulate in all parts of the tumour and within the stroma matrix, by comparing the Masson's trichrome staining with the fluorescence images (Figure 8.7).

Figure 8.7. Example of enhanced fluorescence resulting from doxorubicin uptake into the tumor (left) that corresponds to regions containing dense stromal matrix (right). The right image has been stained with a Masson's trichrome stain which highlights collagen. The green annotations highlight structural features that can be used as landmarks.
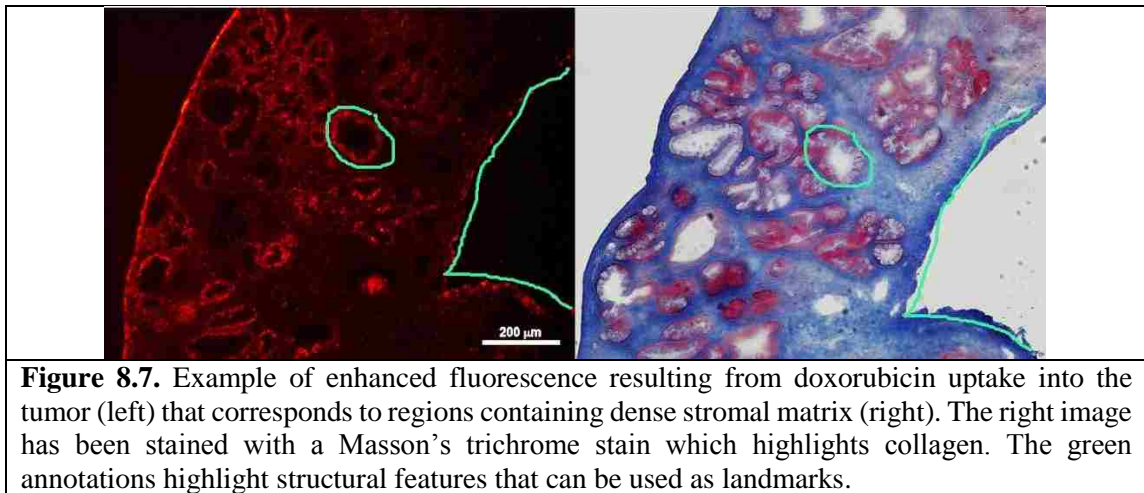
Fluorescence evaluation of the samples revealed increased focal nuclear uptake of doxorubicin in tumors treated with MR-HIFU hyperthermia with systemically administered doxorubicin loaded TSLs (Figure 8.8).
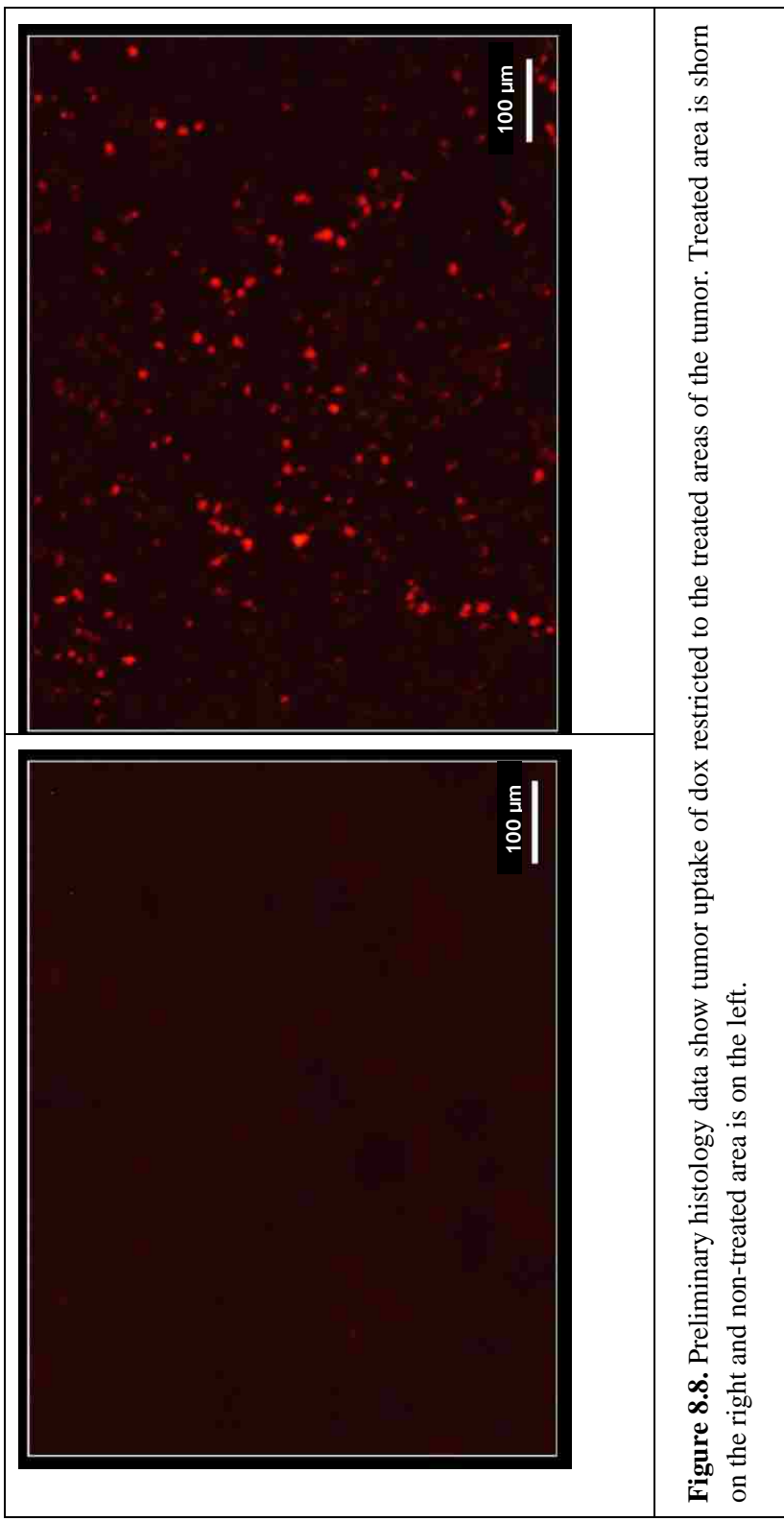
Figure 8.8. Preliminary histology data show tumor uptake of dox restricted to the treated areas of the tumor. Treated area is shorn on the right and non-treated area is on the left.

75

Drug concentration

Tumor doxorubicin concentrations were measured as µg doxorubicin per gram tissue.

The data for free doxorubicin, LTSL and LTSL +MR-HIFU is represented in table 8.2.

Animal model	Treatment type	Drug Dose	Doxorubicin Concentration µg/g
KPC	TSL + MR-HIFU	15 mg/kg	9.21 ± 7.98
	TSL	15 mg/kg	0.41 ± 0.32
	DOX + MR-HIFU	15 mg/kg	5.13 ± 2.60
	DOX	15 mg/kg	1.97 ± 1.32
	TSL + MR-HIFU	5 mg/kg	0.68 ± 0.26
	TSL	5 mg/kg	0.50 ± 0.83
	DOX + MR-HIFU	5 mg/kg	1.23 ± 0.96
	DOX	5 mg/kg	0.18 ± 0.17
	DOXIL + MR-HIFU	5 mg/kg	0.33 ± 0.42
	DOXIL	5 mg/kg	0.08 ± 0.10
Orthotopic	TSL + MR-HIFU	15 mg/kg	0.81 ± 0.24
	TSL	15 mg/kg	0.31 ± 0.53
	TSL + MR-HIFU	5 mg/kg	1.71 ± 1.10
	TSL	5 mg/kg	0.09 ± 0.05
	DOX + MR-HIFU	5 mg/kg	1.08 ± 0.67
	DOX	5 mg/kg	0.87 ± 1.23

Table 8.2. Doxorubicin detected in pancreatic tumor following different treatment regimens. The data are shown as the mean doxorubicin concentration in the tumor with standard error of mean (n = 4 in each group) *$P<0.05$.

A total of 64 mice were treated successfully with the Philips MR guided ultrasound system. There were some deaths due to a reaction to the ThermoDox (TDOX). From these mice, which were injected with a lower TDOX concentration, it was determined that the deaths were caused by a hypersensitivity to the TDOX. In response to these findings, the protocol was revised to include a corticosteroid to prevent any deaths when using higher doses of the injected drug.

The concentration of doxorubicin in the tumor of each group of animals is summarized graphically in the following figures. Each chart in the figures represent box-and-whisker plots of drug concentration. The horizontal line through each box represents the median value and box represents data from the 25th to the 75th percentile (middle 50% of observations). The whiskers represent data from the minimum to the maximum.

The concentration of doxorubicin in the tumor treated with TDOX and free DOX in KPC mice injected with the larger dose (15 µg/g) has been compared to control in Figure 8.9. The group treated with hyperthermia and TSL shows statistically significant difference compared to other groups. This indicates the effect of hyperthermia treatment in combination with TSL on increasing the drug concentration in treated tumor. Additionally the group treated with heat and free DOX showed an increase in doxorubicin concentration compared to the group that didn't receive hyperthermia treatment. This indicates the positive effect of hyperthermia in targeted drug delivery. The doxorubicin concentration in the tumor treated with the larger dose (15 µg/g) in KPC and orthotopic mice treated with TSL has been compared with control in Figure 8.10. Although the orthotopic mice treated with TSL and heat shows a greater drug concentration to control but this concentration is lower than KPC mice treated with TSL and heat. This can be due to the fact that KPC tumor has higher interstitial fluid pressure (IFP); drug released from liposomes flushes out of low pressure tumor with the blood flow while trapes in the tumor because of higher pressure and extravasates to the tumor cells. Figure 8.11 represents drug concentration in KPC tumor treated with lower dose of

drug (5µg/g). Animals treated with TSL or free DOX were compared to control. Although the median value of animals treated with heat and drug is higher than when there is no hyperthermia treatment but there is no statistically significant difference between any of the groups. Figure 8.12 shows drug concentration in orthotopic tumor treated with lower dose of drug (5µg/g). Similar to the result in KPC mice treated with lower dose the data between TSL and free DOX is not statistically significant. There is a statistically significant difference between TSL and heat treatment and control. All of these results suggests that hyperthermia has a positive effect on increasing drug concentration. The result of KPC mice treated with Doxil and hyperthermia treatment has been compared to control group in Figure 8.13. Doxil as a long circulating liposomal form of doxorubicin accumulates more in the tumor treated with hyperthermia but the short duration of acute studies is not enough for this type of drug to show its effect.
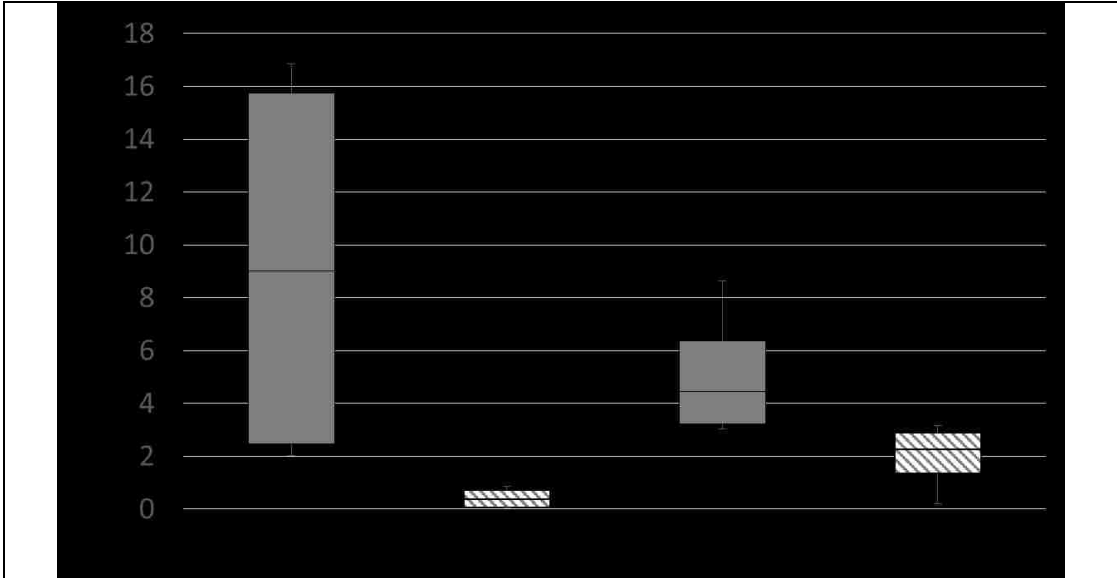
Figure 8.9. Doxorubicin concentration in the tumor of KPC mice treated with ThermoDox and free DOX compared to control. Higher dose of injection (15µg/g).
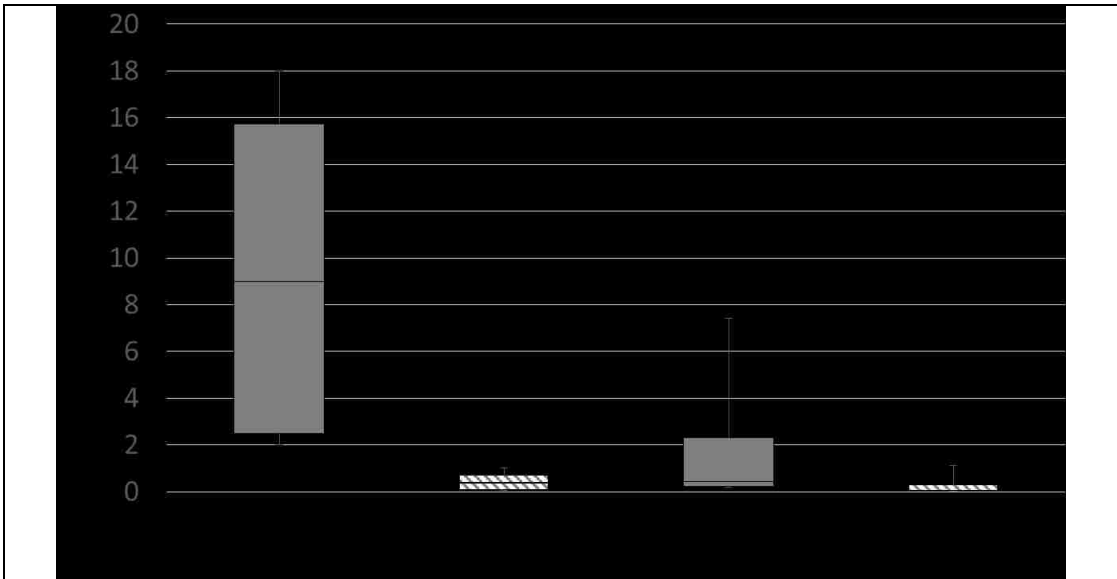
Chart 8.10. Doxorubicin concentration in the tumor of KPC and orthotopic mice treated with ThermoDox compared to control. Higher dose of injection (15µg/g).

Chart 8.11. Doxorubicin concentration in the tumor of KPC mice treated with ThermoDox and free DOX compared to control. Lower dose of injection (5µg/g).

Chart 8.12. Doxorubicin concentration in the tumor of orthotopic mice treated with ThermoDox and free DOX compared to control. Lower dose of injection (5µg/g).
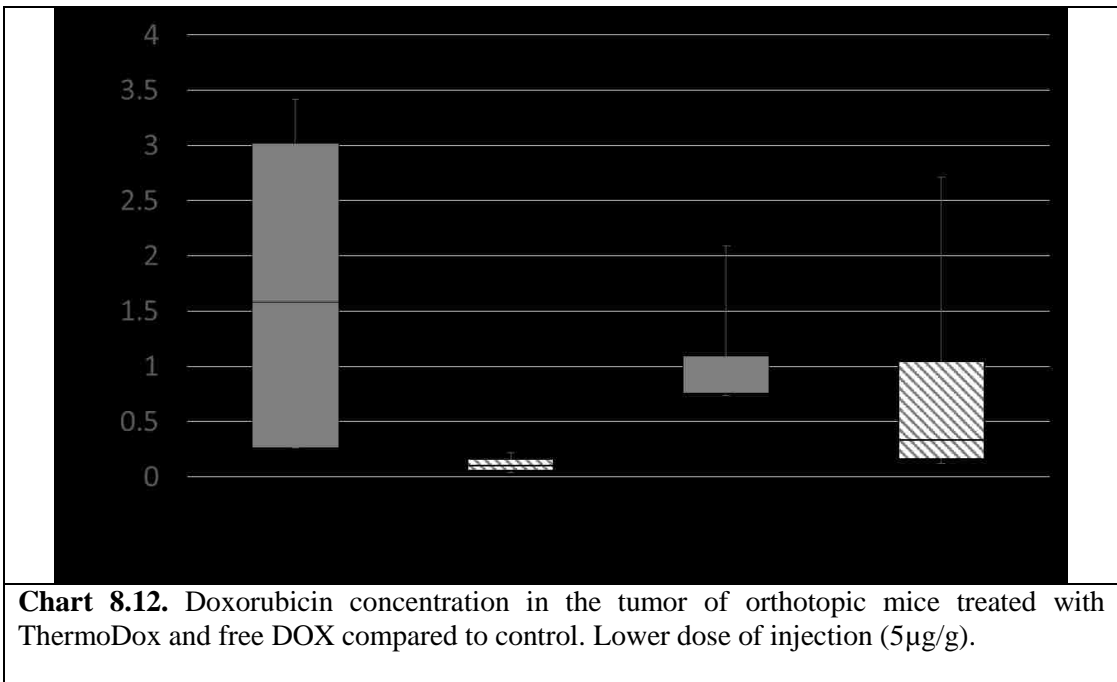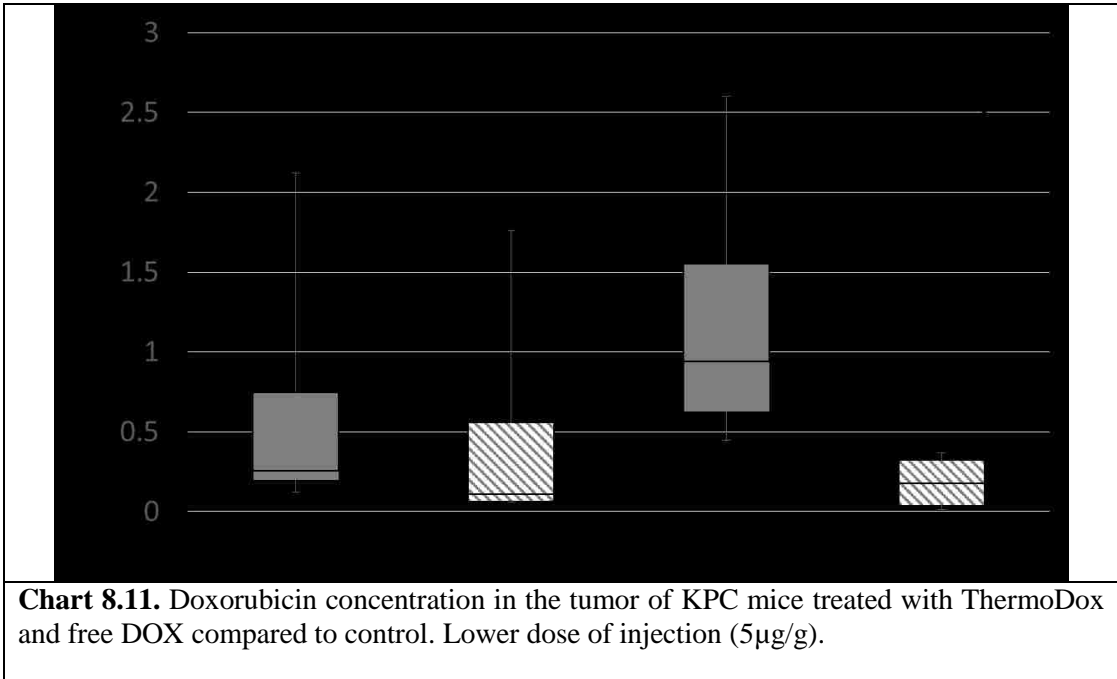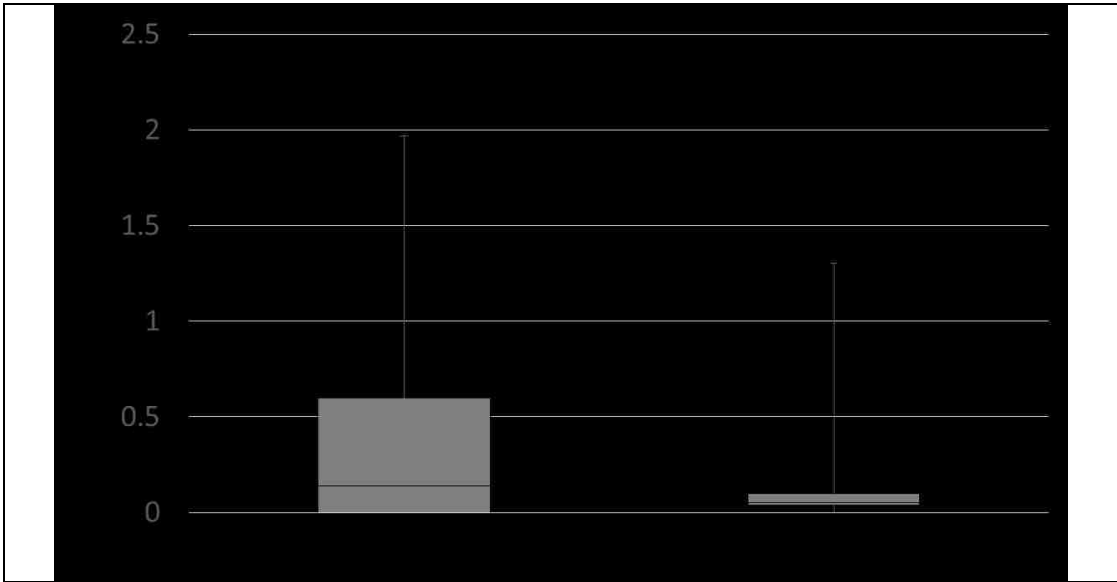
Chart 8.13. Doxorubicin concentration in the tumor treated with Doxil (5µg/g) of KPC mouse.

Drug release monitoring with the Eindhoven liposome

R1 maps of the tumor were acquired pre-injection of the TSLs as well as at multiple time points after injection and subsequent hyperthermia treatment. For some animals, the R1 maps of the bladder were also acquired pre- and post-treatment.

Only one of the animals (Ortho 1199) for which both injection and hyperthermia treatment were successful, showed a significant decrease of R1 values in the tumor right after the first treatment($p = 0.032$, one-tailed T-test). However, the R1 change was not localized to the tumor volume, indicating heating outside the tumor area, or an increased in overall body temperature.

Animal Ortho 1203 showed a significant ($p = 0.000$, one-tailed T-test) R1 drop 30 minutes after treatment; however as the R1 of the surrounding gel and water also clearly decreases, the reliability of this R1 drop is questioned.

The other animals showed either no or mildly increasing values of mean R1 over the treatment; none of these apparent R1 changes were significant. However, as can be observed in Figure 8.14, for all animals that were monitored the R1 of the bladder showed quite large increases after the treatment, indicating release of [Gd(HPDO3A)(H2O)]. In one of the animals that was used as a control in the subcutaneous tumors group (SubQ 1089) also showed a R1 increase in the bladder, only starting from 15 minutes after injection compared to immediately after treatment as was observed in treated animals. This indicated leakage of [Gd(HPDO3A)(H2O)] from the liposomes *in vivo*.
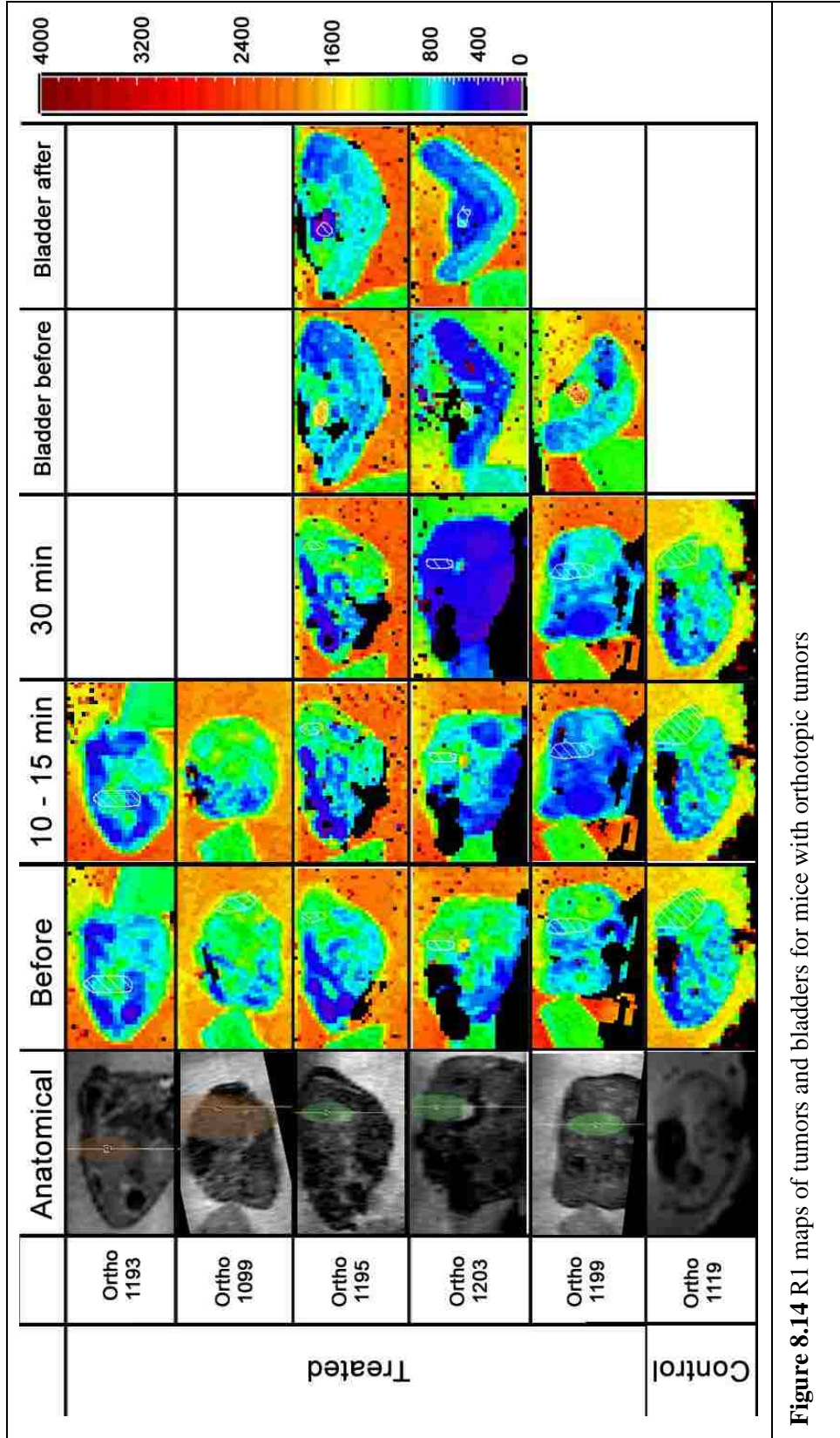
Figure 8.14 R1 maps of tumors and bladders for mice with orthotopic tumors

83

8.4 Discussion

The objective of this study was to test the hypothesis that hyperthermia induced by high intensity focused ultrasound in combination with temperature sensitive liposomes will enhance the drug accumulation in the pancreatic cancer tumor. These results provided a base for the next aim of this research; to investigate the effectiveness of the therapy in a survival study.

In all results, the combination of heat and drug therapy has a greater effect on accumulation of DOX concentration in the tumor. Figure 8.9 indicates the treatment with LTSL + MR-HIFU resulted in significantly greater doxorubicin delivery to the target compared to free doxorubicin (2-fold) or LTSL alone (8-fold) treatments (P<0.05, Mann-Whitney). Results of lower dosage of drug injection (5µg/g), plotted in Figure 8.11 and Figure 8.12, indicate large variability within each treatment. Nonetheless there is a larger concentration of drug in {Drug+HEAT} groups compared to {Drug Only} groups. This wide range of drug concentrations suggests that the lower dose of drug injected with 10 minutes of heating does not cause the maximum effect. Results suggests that the extraction factor needs to be investigated. Moreover part of the drug flushes out of the tumor after release or releases prior to getting inside the tumor in other organs.This could be due a number of reasons. Even though the temperature during the treatment were monitored with 2 slices placed at the focus and one slice post focus to avoid excessive heating in the post-focal region, it was observed that during the treatment the overall temperature of the mouse increased, in some cases to 39 ºC, which is the critical

temperature for ThermoDox. These lower elevations in temperature, occurring at the periphery of the treatment zone, constitute a relatively large area in the mouse. This means that relatively greater amounts of drug would have released before getting into the target zone. Some of these issues, such as whole body heating, would not be relevant in clinical application, but in order to avoid pre-focal release and extraction of drug from the target following approaches might be considered. The first is to use larger area of heating if possible, although in the mouse tumor this approach is not feasible. Second is using higher intensities of ultrasound to use the additional benefit of radiation force, described in chapter 3, section 3.3. However, higher intensities of ultrasound will result in much rapid heating and internal organ damage if not controlled and monitored correctly. Rapid heat generation can be significantly reduced to sub-cytotoxicity levels with pulsed HIFU exposures, where relatively short duty cycles allow non-damaging thermal mechanisms to predominate, such as acoustic radiation force. Then same closed loop feedback algorithm can be used to achieve hyperthermia treatment.

The results of studies with orthotopic tumor model plotted in Figure 8.10 follows the same pattern. But in comparison with studies of KPC mice at larger (15µg/g), Figure 8.10, or lower doses (5µg/g), plotted in Figure 8.11, both shows irregularity in the data pattern. The greater concentration in orthotopic tumors relative to KPC tumors in the case of lower dose injections could be due to differences in the vasculature structure of each tumor. Orthotopic tumor models are more perfused, have lower amounts of stroma

therefore lower IFP, and in comparison with KPC tumor, are not hypovascular. This can cause different reaction to hyperthermia treatment and drug extravasation into the tumor.

For the acute studies using the Eindhoven drug no significant change in tumor R1 time could be measured after hyperthermia treatment. However, the nuclear uptake of doxorubicin in the tumor on histology and the R1 change in the bladder do suggest Gd-release from the liposomes upon heating. It is possible that Gd-release does not take place inside the targeted tumor area, but in a heated part somewhere else in the body thus precluding a measurable effect on the tumor R1. This could easily occur as the temperature monitoring is performed in only two 4mm slices, covering the expected ultrasound beam pathway. Local heating to hyperthermic temperatures outside this area would not have been visible.

Another plausible explanation for not detecting an effect of release on tumor R1 would be the shorter half-life of the MR contrast agent in the mouse body. According to Tweedle et al., Gd-DTPA half-life is about 5-6 minutes in mice, as opposed to 20 minutes in rats. Therefore, the contrast agent could have been cleared from the tumor tissue into the bladder during the time required to start the R1 map acquisition (which took about 3-5 minutes to start due to the Physiological Simulator). Furthermore, a higher spatial resolution R1 map could help achieving higher signal from the contrast agent. With the current protocol, we used a 3 or 5 mm thick imaging slice in order to gain enough signal to noise for accurate R-1 measurement. However, if the area of local release was smaller, the effect of the Gd would be averaged out by the non-affected tissue inside the imaging

voxel (i.e. partial volume effect). Several attempts were made to check this hypothesis, including acquisition of a fast FFE based sequence immediately after the first five minutes of heating. Thus with current setup the null hypothesis cannot be rejected. Unfortunately, no clear explanation could be found based on current results. Also, the extravasation of Gd-HPDO3A from the tumor vasculature (reflected in the k-trans value) might be different in KPC tumors as compared to the tumors treated so far in subcutaneous rat models. If the k-trans value is very low, Gd-HPDO3A might not extravasate, resulting in faster contrast agent clearance. Doxorubicin, on the other hand, has a much higher free volume of distribution, and travels *via* perfusion. This way, the doxorubicin uptake would be much less affected by low k-trans values. More research is necessary, including measurement of the tumor perfusion and k-trans signal using, e.g, dynamic contrast enhanced (DCE) MRI.

8.5 Conclusions

Activation of ThermoDox® using MR-guided HIFU is a promising and appealing method for treatment of unresectable pancreatic cancer. This aim evaluated the feasibility and efficacy of this approach in a transgenic KPC and an orthotopic mouse model of pancreas cancer. The successful execution of this aim provided substantial support for *viz.* Aim 3 to Assess the response to tumors treated with and without HIFU-induced hyperthermia in conjunction with systemic administration ThermoDox®, Doxil in a survival study.

Chapter 9. MR-HIFU induced hyperthermia for enhanced drug delivery in pancreatic cancer mouse model survival study

9.1 Introduction

Although Aim 1 studies produced positive results demonstrating a 2-fold increase in the tumor concentration of doxorubicin in KPC mice, activity against the tumor was not assessed in these studies. The general hypothesis guiding the experiments described in this chapter was that the increase in DOX concentration in the tumor site after treatment of TSL+HEAT will result in slower growth tumor rates and greater and more rapid decrease in tumor size compared to tumor treated with none temperature sensitive drugs. These experiments were designed to evaluate for short-term tumoricidal activity against the KPC tumor.

9.2 Methods and materials

Study design

The transgenic KPC mouse pancreatic cancer model, was used in this study. Mice were assigned randomly into treatment and control groups after the tumor size reached the critical size, 250-500 mm^3. ThermoDox as the temperature sensitive liposomal form of doxorubicin and Doxil as a PEGylated liposomal form of doxorubicin were tested. Each animal in each type of drug group was assigned to MR-HIFU hyperthermia treatment or no hyperthermia treatment (Table 9.1).

Drugs	Treatment Groups	
ThemoDox	TSL + MR-HIFU	TSL Alone
Doxil	Doxil + MR-HIFU	Doxil Alone

Table 9.1. Study design. Each anima was assigned randomly to four different treatment and control groups. Two different types of chemotherapy agent were used.

Once animals developed tumors that are larger than 250 mm^3 and smaller than 500 mm^3 in volume, they were assigned randomly to one of the groups described in table 9.1 and undergo treatment.

The system as described in previous chapter was used for this study. Also the same treatment protocol and parameters described in Chapter 8.2 was used for the treatment groups of "Drug + MR-HIFU". Briefly, animals which underwent HIFU-induced hyperthermia were anesthetized with isoflurane and placed on the specially designed tray for small animals that includes a small animal coil for imaging. The tray was advanced into the magnet for imaging. As part of treatment planning, MR imaging was performed. After acquisition of the MR images the target was evaluated and the ultrasound path was adjusted to ensure than an adequate acoustic window exist for HIFU therapy. In addition, critical surrounding organs (*viz.*, spine and lungs) were controlled to be out of the pre- and post-focal heating zones. The target zone for heating was then placed. ThermoDox (at a doxorubicin dose of 5 mg/kg) or Doxil (at a doxorubicin dose of 5 mg/kg) were administered intravenously *via* tail vein injection. The previously assigned target tumor was exposed to HIFU to achieve a temperature of 42°C for 10 minutes. During the treatment animal respiration and body temperature was monitored using an MR-compatible small animal monitoring system. After treatment, the mouse was recovered

from anesthesia and checked for any skin burn or unwanted damage. The healthy and undamaged animals were returned to the vivarium for ongoing monitoring. Animals randomized to the non-HIFU experimental arm were sedated and administered the appropriate drug *via* tail vein injection then recovered and returned to the vivarium for ongoing monitoring.

The primary end-point of this study was number of days for the tumor volume to double the size, from 250 mm^3 to 500 mm^3. Tumors were monitored with twice weekly ultrasound examinations until the tumor volume doubled or reached the IACUC protocol limits. After statistical reduction, the data are presented as median days for the treated tumor to double in volume. Comparative statistics used the Mann-Whitney U test to determine if the number of days differed between groups. Sample size calculations were performed to achieve a power of 0.8 (1-β), significance level of 0.05 (α), with the assumption that a 2-fold increase in number of days the ThermoDox® group would require over Doxil to reach a volume of 500 mm^3.

9.3 Results

The mice treated with Doxil and heat survived the longest among other groups (14 days). Among the mice treated with ThermoDox the group that received heat and drug combination survived longer than the ones treated with TSL injection and didn't receive hyperthermia. In one case the mouse in {TSL Only} group survived longer than {TSL + Heat} group. This was due to the fact that the tumor in the second group was treated at a larger size and the endpoint reached before the tumor size doubles. Figure 9.1 represents

the tumor growth rate of these two animals. This figure indicates that the mouse that underwent the hyperthermia and TSL treatment had slower tumor growth compared to control.
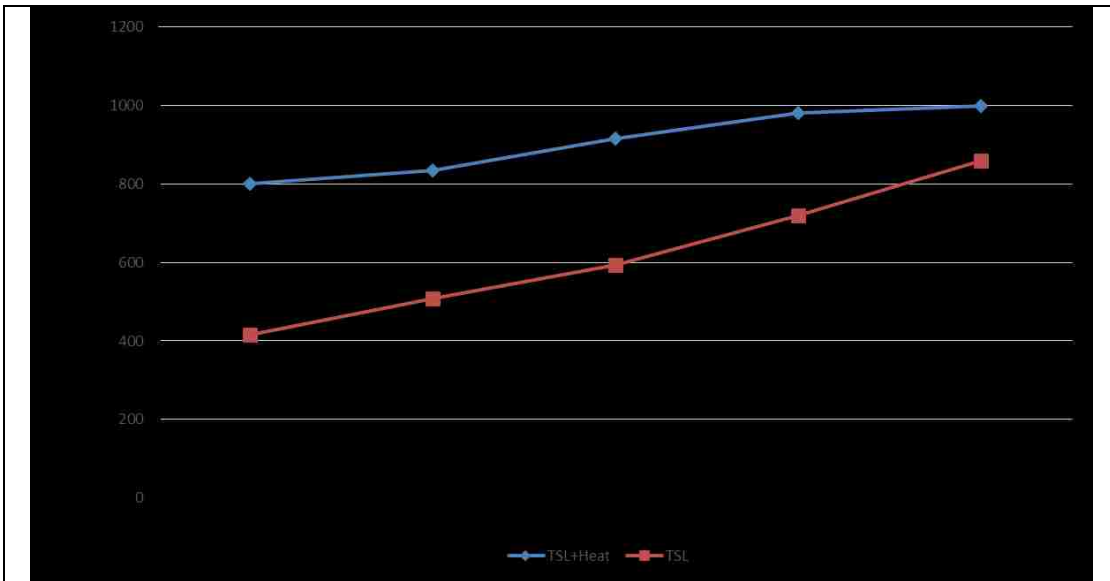
Figure 9.1. Tumor growth rate as measured by ultrasound imaging. KPC mouse treated with TSL and heat in blue and TSL alone in red as control.

9.4 Discussion

Activation of ThermoDox® using MR-guided HIFU is a promising and appealing method for treatment of unresectable pancreatic cancer. Successful execution of this project would provide substantial support for an FDA IND/IDE to evaluate ThermoDox® and MR-guided HIFU for palliation of unresectable pancreatic cancer in humans. Depending on the results MR-guided HIFU induced hyperthermia with Doxil may get support for and FDA IND/IDE study.

Chapter 10. Conclusions and future studies

Conclusions

The overall aim of the research presented in this dissertation was to investigate the effectiveness of MR-guided, HIFU-induced hyperthermia in combination of liposomal drug vehicles for drug delivery in a pancreatic cancer tumor. The overarching hypothesis was that HIFU-induced hyperthermia in combination with temperature sensitive liposome could be used to achieve higher concentration of drug in the targeted tumor and thus improve the cancer therapy.

The specific objectives of this research were to:

- Evaluate the ability of conventional and multi-parametric MRI to characterize pancreas tumors of three different 'types',

- Investigate the effectiveness of MR-HIFU drug delivery,

- Assess the response to tumors treated with MR-HIFU hyperthermia TSL.

The study presented in chapter 7 demonstrated the significant by great value of the KPC tumor model in comparison to the orthotopic and xenograft subcutaneous mouse models. It is anticipated that this findings will aid efficacy testing of new agents in oncology drug development. By evaluating a tumor's characteristics it can help evaluate different therapies and what type of therapy is most appropriate. In our studies evaluating tumor's characteristics leads us to better targeting the tumor while avoiding liquid cystic

areas and necrotic cores of the tumor. Moreover this study guided us to choose KPC mice for survival studies over orthotopic model.

The first drug delivery study (chapter 8) examined the effectiveness of hyperthermia induced by MR-HIFU in combination with TSL and free doxorubicin by comparison to control treatments of no heat. Histological analysis and quantitative analysis of the drug concentration in the targeted tumor generally supported the hyposis that {HIFU hyperthermia + TSL} could systemically increase drug concentration in targeted tumor.

A study assessing the growth response to tumors treated with or without HIFU-induced hyperthermia in conjunction with systemic administration of ThermoDox® and Doxil indicated the effectiveness of the treatment in a pre-clinical setting (Chapter 9).

Future studies

Based on the series of studies presented in this dissertation, it appears possible that HIFU-induced hyperthermia could be used for enhancement of drug delivery especially in combination with the temperature sensitive drug carriers. However, the overall outcome of the chemotherapy can be optimized using different HIFU exposure to achieve the maxim level of drug concentration into the tumor.

Development of pulsed HIFU-induced hyperthermia exposures that maintain the temperature without damaging the tissue will be needed to study the effectiveness of combination of thermal and mechanical bioeffects of HIFU in drug therapy.

Additionally, multi-parametric MRI proved to be a valuable method for *in vivo* monitoring of the treatment quantitatively. Therefore development of scans for identification of MR-HIFU hyperthermia is highly needed. The outcomes of these studies will determine if further development and refinement of drug delivery techniques in clinical studies is warranted.

Bibliography

[1]   K. F. Graff, W. P. Mason, and R. N. Thurston, "A history of ultrasonics," *Phys. Acoust.*, vol. 15, 1981.

[2]   M. R. Bailey, V. A. Khokhlova, O. A. Sapozhnikov, S. G. Kargl, and L. A. Crum, "Physical mechanisms of the therapeutic effect of ultrasound (a review)," *Acoust. Phys.*, vol. 49, no. 4, pp. 369–388, Jul. 2003.

[3]   R. Deckers and C. T. W. Moonen, "Ultrasound triggered, image guided, local drug delivery.," *J. Control. Release*, vol. 148, no. 1, pp. 25–33, Nov. 2010.

[4]   O. A. Sapozhnikov, V. A. Khokhlova, M. R. Bailey, J. C. Williams, J. A. McAteer, R. O. Cleveland, and L. A. Crum, "Effect of overpressure and pulse repetition frequency on cavitation in shock wave lithotripsy," *J. Acoust. Soc. Am.*, vol. 112, no. 3, p. 1183, 2002.

[5]   A. D. Maxwell, T.-Y. Wang, C. a Cain, J. B. Fowlkes, O. A Sapozhnikov, M. R. Bailey, and Z. Xu, "Cavitation clouds created by shock scattering from bubbles during histotripsy.," *J. Acoust. Soc. Am.*, vol. 130, no. 4, pp. 1888–98, Oct. 2011.

[6]   H. E. H. E. Cline, K. Hynynen, C. J. Hardy, R. D. Watkins, J. F. Schenck, and F. A. Jolesz, "MR temperature mapping of focused ultrasound surgery," *Magn. Reson. Med.*, vol. 31, no. 6, pp. 628–636, Jun. 1994.

[7]   Y. Ishihara, A. Calderon, H. Watanabe, K. Okamoto, Y. Y. Suzuki, and K. Kuroda, "A precise and fast temperature mapping using water proton chemical shift," *Magn. Reson. Med.*, vol. 34, no. 6, pp. 814–823, Dec. 1995.

[8]   E. Stewart, W. Gedroyc, C. Tempany, B. Quade, Y. Inbar, T. Ehrenstein, AShushan, J. Hindley, R. Goldin, and M. David, "Focused ultrasound treatment of uterine fibroid tumors: Safety and feasibility of a noninvasive thermoablative technique☆," *Am. J. Obstet. Gynecol.*, vol. 189, no. 1, pp. 48–54, Jul. 2003.

[9]   L. Zhang, W.-Z. Chen, Y.-J. Liu, X. Hu, K. Zhou, L. Chen, S. Peng, H. Zhu, H.-L. Zou, J. Bai, and Z.-B. Wang, "Feasibility of magnetic resonance imaging-guided high intensity focused ultrasound therapy for ablating uterine fibroids in patients with bowel lies anterior to uterus.," *Eur. J. Radiol.*, vol. 73, no. 2, pp. 396–403, Feb. 2010.

[10] L. G. Merckel, L. W. Bartels, M. O. Köhler, H. J. G. D. van den Bongard, R. Deckers, W. P. T. M. Mali, C. A. Binkert, C. T. Moonen, K. G. A. Gilhuijs, and M. A. A. J. van den Bosch, "MR-guided high-intensity focused ultrasound ablation of breast cancer with a dedicated breast platform.," *Cardiovasc. Intervent. Radiol.*, vol. 36, no. 2, pp. 292–301, Apr. 2013.

[11] C. J. Diederich, W. H. Nau, A. B. Ross, P. D. Tyreus, K. Butts, V. Rieke, and G. Sommer, "Catheter-based ultrasound applicators for selective thermal ablation: progress towards MRI-guided applications in prostate," Jul. 2009.

[12] B. Larrat, M. Pernot, J.-F. Aubry, E. Dervishi, R. Sinkus, D. Seilhean, Y. Marie, A.-L. Boch, M. Fink, and M. Tanter, "MR-guided transcranial brain HIFU in small animal models.," *Phys. Med. Biol.*, vol. 55, no. 2, pp. 365–88, Jan. 2010.

[13] N. Lipsman, M. L. Schwartz, Y. Huang, L. Lee, T. Sankar, M. Chapman, K. Hynynen, and A. M. Lozano, "MR-guided focused ultrasound thalamotomy for essential tremor: a proof-of-concept study.," *Lancet Neurol.*, vol. 12, no. 5, pp. 462–8, May 2013.

[14] D. Pajek and K. Hynynen, "Applications of Transcranial Focused Ultrasound Surgery," *Acoust. Today*, vol. 8, no. 4, p. 8, Oct. 2012.

[15] "A Pilot Study of Focused Ultrasound Thalamotomy for Essential Tremor — NEJM." [Online]. Available: http://www.nejm.org/doi/full/10.1056/nejmoa1300962. [Accessed: 12-Aug-2014].

[16] N. M. Hijnen, E. Heijman, M. O. Köhler, M. Ylihautala, G. J. Ehnholm, A. W. Simonetti, and H. Grüll, "Tumour hyperthermia and ablation in rats using a clinical MR-HIFU system equipped with a dedicated small animal set-up.," *Int. J. Hyperthermia*, vol. 28, no. 2, pp. 141–55, Jan. 2012.

[17] R. M. Staruch, M. Ganguly, I. F. Tannock, K. Hynynen, and R. Chopra, "Enhanced drug delivery in rabbit VX2 tumours using thermosensitive liposomes and MRI-controlled focused ultrasound hyperthermia.," *Int. J. Hyperthermia*, vol. 28, no. 8, pp. 776–87, Jan. 2012.

[18] C. van Bree, J. J. Krooshoop, R. C. Rietbroek, J. B. A. Kipp, and P. J. M. Bakker, "Hyperthermia Enhances Tumor Uptake and Antitumor Efficacy of Thermostable Liposomal Daunorubicin in a Rat Solid Tumor," *Cancer Res.*, vol. 56, no. 3, pp. 563–568, Feb. 1996.

[19]   A. Gasselhuber, M. R. Dreher, A. Partanen, P. S. Yarmolenko, D. Woods, B. J. Wood, and D. Haemmerich, "Targeted drug delivery by high intensity focused ultrasound mediated hyperthermia combined with temperature-sensitive liposomes: Computational modelling and preliminary in vivovalidation.," *Int. J. Hyperthermia*, vol. 28, no. 4, pp. 337–48, Jan. 2012.

[20]   S. A. Sapareto and W. C. Dewey, "Thermal dose determination in cancer therapy," *Int. J. Radiat. Oncol. Biol. Phys.*, vol. 10, no. 6, pp. 787–800, 1984.

[21]   B. Hildebrandt, "The cellular and molecular basis of hyperthermia," *Crit. Rev. Oncol. Hematol.*, vol. 43, no. 1, pp. 33–56, Jul. 2002.

[22]   "Cancer Facts & Figures 2010 and NCI Funded Research Portfolio," *Am. Cancer Soc.*, no. September 2010.

[23]   E. Van Cutsem, H. van de Velde, P. Karasek, H. Oettle, W. L. Vervenne, a Szawlowski, P. Schoffski, S. Post, C. Verslype, H. Neumann, H. Safran, Y. Humblet, J. Perez Ruixo, Y. Ma, and D. Von Hoff, "Phase III trial of gemcitabine plus tipifarnib compared with gemcitabine plus placebo in advanced pancreatic cancer.," *J. Clin. Oncol.*, vol. 22, no. 8, pp. 1430–8, Apr. 2004.

[24]   D. Melisi, S. Ishiyama, G. M. Sclabas, J. B. Fleming, Q. Xia, G. Tortora, J. L. Abbruzzese, and P. J. Chiao, "LY2109761, a novel transforming growth factor beta receptor type I and type II dual inhibitor, as a therapeutic approach to suppressing pancreatic cancer metastasis.," *Mol. Cancer Ther.*, vol. 7, no. 4, pp. 829–40, Apr. 2008.

[25]   A. Verma, S. Guha, P. Diagaradjane, A. B. Kunnumakkara, A. M. Sanguino, G. Lopez-Berestein, A. K. Sood, B. B. Aggarwal, S. Krishnan, J. G. Gelovani, and K. Mehta, "Therapeutic significance of elevated tissue transglutaminase expression in pancreatic cancer.," *Clin. Cancer Res.*, vol. 14, no. 8, pp. 2476–83, Apr. 2008.

[26]   T. Shimamura, R. E. Royal, M. Kioi, A. Nakajima, S. R. Husain, and R. K. Puri, "Interleukin-4 cytotoxin therapy synergizes with gemcitabine in a mouse model of pancreatic ductal adenocarcinoma.," *Cancer Res.*, vol. 67, no. 20, pp. 9903–12, Oct. 2007.

[27]   C. J. Bruns, M. Shrader, M. T. Harbison, C. Portera, C. C. Solorzano, K.-W. Jauch, D. J. Hicklin, R. Radinsky, and L. M. Ellis, "Effect of the vascular endothelial growth factor receptor-2 antibody DC101 plus gemcitabine on growth, metastasis and angiogenesis of human pancreatic cancer growing

orthotopically in nude mice.," *Int. J. Cancer*, vol. 102, no. 2, pp. 101–8, Dec. 2002.

[28] J. Grimm, A. Potthast, A. Wunder, and A. Moore, "Magnetic resonance imaging of the pancreas and pancreatic tumors in a mouse orthotopic model of human cancer," *Int. J. Cancer*, vol. 106, no. 5, pp. 806–11, Sep. 2003.

[29] J. H. Cui, U. Kruger, I. Vogel, J. Luttges, D. Henne-Bruns, B. Kremer, and H. Kalthoff, "Intact tissue of gastrointestinal cancer specimen orthotopically transplanted into nude mice," *Hepatogastroenterology*, vol. 45, pp. 2087–2096, 1998.

[30] M. H. Tan and T. M. Chu, "Characterization of the tumorigenic and metastatic properties of a human pancreatic tumor cell line (AsPC-1) implanted orthotopically into nude mice.," *Tumour Biol. J. Int. Soc. Oncodevelopmental Biol. Med.*, vol. 6, pp. 89–98, 1985.

[31] K. P. Olive, M. a Jacobetz, C. J. Davidson, A. Gopinathan, D. McIntyre, D. Honess, B. Madhu, M. a Goldgraben, M. E. Caldwell, D. Allard, K. K. Frese, G. Denicola, C. Feig, C. Combs, S. P. Winter, H. Ireland-Zecchini, S. Reichelt, W. J. Howat, A. Chang, M. Dhara, L. Wang, F. Rückert, R. Grützmann, C. Pilarsky, K. Izeradjene, S. R. Hingorani, P. Huang, S. E. Davies, W. Plunkett, M. Egorin, R. H. Hruban, N. Whitebread, K. McGovern, J. Adams, C. Iacobuzio-Donahue, J. Griffiths, and D. a Tuveson, "Inhibition of Hedgehog signaling enhances delivery of chemotherapy in a mouse model of pancreatic cancer.," *Science*, vol. 324, no. 5933, pp. 1457–61, Jun. 2009.

[32] S. R. Hingorani, L. Wang, A. S. Multani, C. Combs, T. B. Deramaudt, R. H. Hruban, A. K. Rustgi, S. Chang, and D. A. Tuveson, "Trp53 and Kras cooperate to promote chromosomal instability and widely metastatic pancreatic ductal adenocarcinoma in mice," *Cancer Cell*, vol. 7, no. 5, pp. 469–483, 2005.

[33] R. H. Hruban, N. V. Adsay, J. Albores-Saavedra, M. R. Anver, A. V Biankin, G. P. Boivin, E. E. Furth, T. Furukawa, A. Klein, D. S. Klimstra, G. Kloppel, G. Y. Lauwers, D. S. Longnecker, J. Luttges, A. Maitra, G. J. A. Offerhaus, L. Pérez-Gallego, M. Redston, and D. A. Tuveson, "Pathology of genetically engineered mouse models of pancreatic exocrine cancer: consensus report and recommendations.," *Cancer Res.*, vol. 66, no. 1, pp. 95–106, Jan. 2006.

[34] W. Hedrick, D. Hykes, and D. Starchman, "Ultrasound physics and instrumentation," 1995.

[35]   S. Vaezy, M. Andrew, P. Kaczkowski, and L. Crum, "Image-guided acoustic therapy.," *Annu. Rev. Biomed. Eng.*, vol. 3, pp. 375–90, Jan. 2001.

[36]   F. Jolesz and K. Hynynen, "MRI-guided focused ultrasound surgery," *Annu. Rev. Med.*, 2009.

[37]   T. Fjield and K. Hynynen, "The combined concentric-ring and sector-vortex phased array for MRI guided ultrasound surgery," *IEEE Trans. Ultrason. Ferroelectr. Freq. Control*, vol. 44, no. 5, pp. 1157–1167, Sep. 1997.

[38]   V. Frenkel, "Ultrasound mediated delivery of drugs and genes to solid tumors.," *Adv. Drug Deliv. Rev.*, vol. 60, no. 10, pp. 1193–208, Jul. 2008.

[39]   K. Ng and Y. Liu, "Therapeutic ultrasound: its application in drug delivery," *Med. Res. Rev.*, vol. 22, no. 2, pp. 204–223, 2002.

[40]   K. G. Baker, V. J. Robertson, and F. A. Duck, "A review of therapeutic ultrasound: biophysical effects.," *Phys. Ther.*, vol. 81, no. 7, pp. 1351–8, Jul. 2001.

[41]   E. Konofagou, J. Thierman, and K. Hynynen, "A focused ultrasound method for simultaneous diagnostic and therapeutic applications--a simulation study.," *Phys. Med. Biol.*, vol. 46, no. 11, pp. 2967–84, Nov. 2001.

[42]   G. ter Haar, "Therapeutic applications of ultrasound.," *Prog. Biophys. Mol. Biol.*, vol. 93, no. 1–3, pp. 111–29.

[43]   G. ter Haar and C. Coussios, "High intensity focused ultrasound: physical principles and devices," *Int. J. Hyperth.*, vol. 23, no. 2, pp. 89–104, Jan. 2007.

[44]   N. B. Smith and K. Hynynen, "The feasibility of using focused ultrasound for transmyocardial revascularization," *Ultrasound Med. Biol.*, vol. 24, no. 7, pp. 1045–1054, Sep. 1998.

[45]   J. E. Parsons, C. a Cain, G. D. Abrams, and J. B. Fowlkes, "Pulsed cavitational ultrasound therapy for controlled tissue homogenization.," *Ultrasound Med. Biol.*, vol. 32, no. 1, pp. 115–29, Jan. 2006.

[46]   T. D. Khokhlova, M. S. Canney, V. a Khokhlova, O. a Sapozhnikov, L. a Crum, and M. R. Bailey, "Controlled tissue emulsification produced by high intensity focused ultrasound shock waves and millisecond boiling.," *J. Acoust. Soc. Am.*, vol. 130, no. 5, pp. 3498–510, Nov. 2011.

[47] M. S. M. S. Canney, V. a V. A. Khokhlova, O. V. O. V Bessonova, M. R. M. R. Bailey, and L. a L. A. Crum, "Shock-induced heating and millisecond boiling in gels and tissue due to high intensity focused ultrasound," *Ultrasound Med. Biol.*, vol. 36, no. 2, pp. 250–67, Feb. 2010.

[48] T.-Y. Wang, Z. Xu, T. L. Hall, J. B. Fowlkes, and C. A. Cain, "An efficient treatment strategy for histotripsy by removing cavitation memory.," *Ultrasound Med. Biol.*, vol. 38, no. 5, pp. 753–66, May 2012.

[49] C. R. Hill, J. C. Bamber, and G. R. ter Haar, Eds., *Physical Principles of Medical Ultrasonics*. Chichester, UK: John Wiley & Sons, Ltd, 2004.

[50] K. Hynynen, "Biophysics and Technology of Ultrasound Hyperthermia," in *Methods of External Hyperthermic Heating*, M. Gautherie, Ed. Springer Berlin Heidelberg, 1990, pp. 61–115.

[51] G. D. Ludwig, "The Velocity of Sound through Tissues and the Acoustic Impedance of Tissues," *J. Acoust. Soc. Am.*, vol. 22, no. 6, p. 862, Nov. 1950.

[52] H.-L. Liu, N. McDannold, and K. Hynynen, "Focal beam distortion and treatment planning in abdominal focused ultrasound surgery," *Med. Phys.*, vol. 32, no. 5, p. 1270, Apr. 2005.

[53] X. Fan and K. Hynynen, "The effect of wave reflection and refraction at soft tissue interfaces during ultrasound hyperthermia treatments," *J. Acoust. Soc. …*, vol. 91, no. May, pp. 1727–1736, Mar. 1992.

[54] X. Fan, "The effects of curved tissue layers on the power deposition patterns of therapeutic ultrasound beams," *Med. Phys.*, vol. 21, no. 1, p. 25, Jan. 1999.

[55] H.-L. Liu, H. Chang, W.-S. Chen, T.-C. Shih, J.-K. Hsiao, and W.-L. Lin, "Feasibility of transrib focused ultrasound thermal ablation for liver tumors using a spherically curved 2D array: A numerical study," *Med. Phys.*, vol. 34, no. 9, p. 3436, Aug. 2007.

[56] J.-F. Aubry, M. Tanter, M. Pernot, J.-L. Thomas, and M. Fink, "Experimental demonstration of noninvasive transskull adaptive focusing based on prior computed tomography scans," *J. Acoust. Soc. Am.*, vol. 113, no. 1, p. 84, Jan. 2003.

[57] G. T. Clement and K. Hynynen, "A non-invasive method for focusing ultrasound through the human skull," *Phys. Med. Biol.*, vol. 47, no. 8, pp. 1219–1236, Apr. 2002.

[58] H. H. Pennes, "Analysis of tissue and arterial blood temperatures in the resting human forearm. 1948.," *J. Appl. Physiol.*, vol. 85, no. 1, pp. 5–34, Jul. 1998.

[59] M. Borrelli, L. Thompson, C. Cain, and W. Dewey, "Time-temperature analysis of cell killing of BHK cells heated at temperatures in the range of 43.5 C to 57.0 C," *Int. J. ...*, vol. 19, no. February, pp. 389–399, 1990.

[60] W. C. Dewey, "Arrhenius relationships from the molecule and cell to the clinic.," *Int. J. Hyperthermia*, vol. 25, no. 1, pp. 3–20, Feb. 2009.

[61] M. W. Dewhirst, B. L. Viglianti, M. Lora-Michiels, M. Hanson, and P. J. Hoopes, "Basic principles of thermal dosimetry and thermal thresholds for tissue damage from hyperthermia.," *Int. J. Hyperthermia*, vol. 19, no. 3, pp. 267–94, Jul. 2003.

[62] H. Jung, "A Generalized Concept for Cell Killing by Heat," May 2010.

[63] H. Lyngt, O. R. Monge, P. J. Bøhler, and E. K. Rofstad, "Relationships between thermal dose and heat-induced tissue and vascular damage after thermoradiotherapy of locally advanced breast carcinoma," Jul. 2009.

[64] B. E. Lyons, W. G. Obana, J. K. Borcich, R. Kleinman, D. Singh, and R. H. Britt, "Chronic Histological Effects of Ultrasonic Hyperthermia on Normal Feline Brain Tissue," May 2010.

[65] A. Meshorer, S. D. Prionas, L. F. Fajardo, J. L. Meyer, G. M. Hahn, and A. A. Martinez, "The effects of hyperthermia on normal mesenchymal tissues. Application of a histologic grading system.," *Arch. Pathol. Lab. Med.*, vol. 107, no. 6, pp. 328–34, Jun. 1983.

[66] C. Damianou and K. Hynynen, "The effect of various physical parameters on the size and shape of necrosed tissue volume during ultrasound surgery.," *J. Acoust. Soc. Am.*, vol. 95, no. 3, pp. 1641–9, Mar. 1994.

[67] McDannold, K. Hynynen, D. Wolf, G. Wolf, F. Jolesz, and N. McDannold, "MRI evaluation of thermal ablation of tumors with focused ultrasound.," *J. Magn. Reson. Imaging*, vol. 8, no. 1, pp. 91–100, Jan. 1998.

[68] N. J. McDannold, R. L. King, F. A. Jolesz, and K. H. Hynynen, "Usefulness of MR imaging-derived thermometry and dosimetry in determining the threshold for tissue damage induced by thermal surgery in rabbits," *Radiology*, vol. 216, no. 2, pp. 517–23, Aug. 2000.

[69] C. Weidensteiner, B. Quesson, B. Caire-Gana, N. Kerioui, A. Rullier, H. Trillaud, and C. T. W. Moonen, "Real-time MR temperature mapping of rabbit liver in vivo during thermal ablation.," *Magn. Reson. Med.*, vol. 50, no. 2, pp. 322–30, Aug. 2003.

[70] M. Dyson, J. J. B. Pond, B. Woodward, and J. Broadbent, "The production of blood cell stasis and endothelial damage in the blood vessels of chick embryos treated with ultrasound in a stationary wave field," *Ultrasound Med. Biol.*, vol. 1, no. 2, pp. 133–148, Mar. 1974.

[71] W.-S. Chen, T. J. Matula, A. a. Brayman, and L. a. Crum, "A comparison of the fragmentation thresholds and inertial cavitation doses of different ultrasound contrast agents," *J. Acoust. Soc. Am.*, vol. 113, no. 1, p. 643, 2003.

[72] P. P. Chang, P. D. Mourad, S. L. Poliachik, and L. A. Crum, "Thresholds for inertial cavitation in Albunex suspensions under pulsed ultrasound conditions," *IEEE Trans. Ultrason. Ferroelectr. Freq. Control*, vol. 48, no. 1, pp. 161–170, 2001.

[73] W.-S. Chen, A. A. Brayman, T. J. Matula, L. A. Crum, and M. W. Miller, "The pulse length-dependence of inertial cavitation dose and hemolysis," *Ultrasound Med. Biol.*, vol. 29, no. 5, pp. 739–748, May 2003.

[74] H. Cline and J. Schenck, "MR-guided focused ultrasound surgery," *J. Comput. …*, 1992.

[75] K. Hynynen, "MRI-guided noninvasive ultrasound surgery," *Med. Phys.*, vol. 20, no. 1, p. 107, Jan. 1993.

[76] K. Hynynen, C. Damianou, A. Darkazanli, E. Unger, M. Levy, and J. F. Schenck, "On-line MRI monitored noninvasive ultrasound surgery," in *Proceedings of the Annual International Conference of the IEEE Engineering in Medicine and Biology Society*, 1992, vol. 1, pp. 350–351.

[77] H. E. Cline, J. F. Schenck, R. D. Watkins, K. Hynynen, and F. A. Jolesz, "Magnetic resonance-guided thermal surgery," *Magn. Reson. Med.*, vol. 30, no. 1, pp. 98–106, Jul. 1993.

[78] K. Hynynen, A. Chung, T. Fjield, M. Buchanan, D. Daum, V. Colucci, P. Lopath, and F. Jolesz, "Feasibility of using ultrasound phased arrays for MRI monitored noninvasive surgery," *IEEE Trans. Ultrason. Ferroelectr. Freq. Control*, vol. 43, no. 6, pp. 1043–1053, Nov. 1996.

[79] D. R. Daum, N. B. Smith, R. King, and K. Hynynen, "In vivo demonstration of noninvasive thermal surgery of the liver and kidney using an ultrasonic phased array," *Ultrasound Med. Biol.*, vol. 25, no. 7, pp. 1087–1098, Sep. 1999.

[80] E. B. Hutchinson and K. Hynynen, "Intracavitary ultrasound phased arrays for noninvasive prostate surgery," *IEEE Trans. Ultrason. Ferroelectr. Freq. Control*, vol. 43, no. 6, pp. 1032–1042, Nov. 1996.

[81] D. R. Daum, M. T. Buchanan, T. Fjield, and K. Hynynen, "Design and evaluation of a feedback based phased array system for ultrasound surgery.," *IEEE Trans. Ultrason. Ferroelectr. Freq. Control*, vol. 45, no. 2, pp. 431–8, Jan. 1998.

[82] K. Kuroda, A. H. Chung, K. Hynynen, and F. A. Jolesz, "Invited. Calibration of water proton chemical shift with temperature for noninvasive temperature imaging during focused ultrasound surgery," *J. Magn. Reson. Imaging*, vol. 8, no. 1, pp. 175–181, Jan. 1998.

[83] A. H. Chung, K. Hynynen, V. Colucci, K. Oshio, H. E. Cline, and F. A. Jolesz, "Optimization of spoiled gradient-echo phase imaging forin vivo localization of a focused ultrasound beam," *Magn. Reson. Med.*, vol. 36, no. 5, pp. 745–752, Nov. 1996.

[84] N. B. Smith, A. G. Webb, D. S. Ellis, L. J. Wilmes, and W. D. O'Brien, "Non-invasive in vivo temperature mapping of ultrasound heating using magnetic resonance techniques," in *Proceedings of IEEE Ultrasonics Symposium ULTSYM-94*, 1994, vol. 3, pp. 1829–1832 vol.3.

[85] K. Hynynen, O. Pomeroy, D. N. Smith, P. E. Huber, N. J. McDannold, J. Kettenbach, J. Baum, S. Singer, and F. a Jolesz, "MR imaging-guided focused ultrasound surgery of fibroadenomas in the breast: a feasibility study.," *Radiology*, vol. 219, no. 1, pp. 176–85, Apr. 2001.

[86] E. a Stewart, J. Rabinovici, C. M. C. Tempany, Y. Inbar, L. Regan, B. Gostout, B. Gastout, G. Hesley, H. S. Kim, S. Hengst, W. M. Gedroyc, and W. M. Gedroye, "Clinical outcomes of focused ultrasound surgery for the treatment of uterine fibroids.," *Fertil. Steril.*, vol. 85, no. 1, pp. 22–9, Jan. 2006.

[87] J. Vetro and F. Jolesz, "Focused US System for MR Imaging-guided Tumor Ablation'," *Radiology*, pp. 731–737, 1995.

[88] K. Hynynen, a Darkazanli, C. a Damianou, E. Unger, and J. F. Schenck, "The usefulness of a contrast agent and gradient-recalled acquisition in a steady-state imaging sequence for magnetic resonance imaging-guided noninvasive ultrasound surgery.," *Investigative radiology*, vol. 29, no. 10. pp. 897–903, Oct-1994.

[89] E. B. Hutchinson, "Design and optimization of an aperiodic ultrasound phased array for intracavitary prostate thermal therapies," *Med. Phys.*, vol. 23, no. 5, p. 767, May 1996.

[90] I. P. Wharton, I. H. Rivens, G. R. Ter Haar, D. J. Gilderdale, D. J. Collins, J. W. Hand, P. D. Abel, and N. M. deSouza, "Design and development of a prototype endocavitary probe for high-intensity focused ultrasound delivery with integrated magnetic resonance imaging.," *J. Magn. Reson. Imaging*, vol. 25, no. 3, pp. 548–56, Mar. 2007.

[91] R. Salomir, J. Palussière, F. C. Vimeux, J. A. de Zwart, B. Quesson, M. Gauchet, P. Lelong, J. Pergrale, N. Grenier, and C. T. Moonen, "Local hyperthermia with MR-guided focused ultrasound: spiral trajectory of the focal point optimized for temperature uniformity in the target region.," *J. Magn. Reson. Imaging*, vol. 12, no. 4, pp. 571–83, Oct. 2000.

[92] J. D. Hazle, R. J. Stafford, and R. E. Price, "Magnetic resonance imaging-guided focused ultrasound thermal therapy in experimental animal models: correlation of ablation volumes with pathology in rabbit muscle and VX2 tumors.," *J. Magn. Reson. Imaging*, vol. 15, no. 2, pp. 185–94, Feb. 2002.

[93] R. Chopra, L. Curiel, R. Staruch, L. Morrison, and K. Hynynen, "An MRI-compatible system for focused ultrasound experiments in small animal models," *Med. Phys.*, vol. 36, no. 5, p. 1867, Apr. 2009.

[94] C. Damianou, M. Pavlou, O. Velev, K. Kyriakou, and M. Trimikliniotis, "High intensity focused ultrasound ablation of kidney guided by MRI.," *Ultrasound Med. Biol.*, vol. 30, no. 3, pp. 397–404, Mar. 2004.

[95] D. Kopelman, Y. Inbar, A. Hanannel, R. M. Pfeffer, O. Dogadkin, D. Freundlich, B. Liberman, and R. Catane, "Magnetic resonance guided focused ultrasound surgery. Ablation of soft tissue at bone-muscle interface in a porcine model.," *Eur. J. Clin. Invest.*, vol. 38, no. 4, pp. 268–75, Apr. 2008.

[96] J. P. Wansapura, B. L. Daniel, J. Pauly, and K. Butts, "Temperature mapping of frozen tissue using eddy current compensated half excitation RF pulses.," *Magn. Reson. Med.*, vol. 46, no. 5, pp. 985–92, Nov. 2001.

[97] R. Puls, S. Langner, C. Rosenberg, K. Hegenscheid, J. P. Kuehn, K. Noeckler, and N. Hosten, "Laser ablation of liver metastases from colorectal cancer with MR thermometry: 5-year survival.," *J. Vasc. Interv. Radiol.*, vol. 20, no. 2, pp. 225–34, Feb. 2009.

[98] J. A. Moriarty, J. C. Chen, C. M. Purcell, L. C. Ang, R. S. Hinks, R. D. Peters, R. M. Henkelman, D. B. Plewes, M. J. Bronskill, and W. Kucharczyk, "MRI monitoring of interstitial microwave-induced heating and thermal lesions in rabbit brain in vivo," *J. Magn. Reson. Imaging*, vol. 8, no. 1, pp. 128–135, Jan. 1998.

[99] R. M. Botnar, P. Steiner, B. Dubno, P. Erhart, G. K. von Schulthess, and J. F. Debatin, "Temperature quantification using the proton frequency shift technique: In vitro and in vivo validation in an open 0.5 tesla interventional MR scanner during RF ablation.," *J. Magn. Reson. Imaging*, vol. 13, no. 3, pp. 437–44, Mar. 2001.

[100] Q. Zhang, Y.-C. Chung, J. S. Lewin, and J. L. Duerk, "A method for simultaneous RF ablation and MRI," *J. Magn. Reson. Imaging*, vol. 8, no. 1, pp. 110–114, Jan. 1998.

[101] D. L. Parker, "Temperature distribution measurements in two-dimensional NMR imaging," *Med. Phys.*, vol. 10, no. 3, p. 321, May 1983.

[102] N. Bloembergen, E. Purcell, and R. Pound, "Relaxation Effects in Nuclear Magnetic Resonance Absorption," *Phys. Rev.*, vol. 73, no. 7, pp. 679–712, Apr. 1948.

[103] J. Hindman, "Proton resonance shift of water in the gas and liquid states," *J. Chem. Phys.*, 1966.

[104] J. Simpson and H. Carr, "Diffusion and Nuclear Spin Relaxation in Water," *Phys. Rev.*, vol. 111, no. 5, pp. 1201–1202, Sep. 1958.

[105] D. Le Bihan, J. Delannoy, and R. L. Levin, "Temperature mapping with MR imaging of molecular diffusion: application to hyperthermia.," *Radiology*, vol. 171, no. 3, pp. 853–7, Jun. 1989.

[106] B. Denis de Senneville, B. Quesson, and C. T. W. Moonen, "Magnetic resonance temperature imaging.," *Int. J. Hyperthermia*, vol. 21, no. 6, pp. 515–31, Sep. 2005.

[107] V. Rieke and K. Butts Pauly, "MR thermometry.," *J. Magn. Reson. Imaging*, vol. 27, no. 2, pp. 376–90, Feb. 2008.

[108] R. Brenner, T. Metens, M. Bali, P. Demetter, and C. Matos, "Pancreatic neuroendocrine tumor: added value of fusion of T2-weighted imaging and high b-value diffusion-weighted imaging for tumor detection.," *Eur. J. Radiol.*, vol. 81, no. 5, pp. e746–9, May 2012.

[109] D. Le Bihan, E. Breton, and D. Lallemand, "MR imaging of intravoxel incoherent motions: application to diffusion and perfusion in neurologic disorders," …, pp. 401–407, 1986.

[110] T. Yoshikawa, "ADC measurement of abdominal organs and lesions using parallel imaging technique," *Am. J. …*, vol. 187, pp. 1521–1530, 2006.

[111] H. Lyng, "Measurement of cell density and necrotic fraction in human melanoma xenografts by diffusion weighted magnetic resonance imaging," *Magn. Reson. …*, vol. 43, pp. 828–836, 2000.

[112] A. Dzik-Jurasz, C. Domenig, and M. George, "Diffusion MRI for prediction of response of rectal cancer to chemoradiation," *Lancet*, vol. 360, pp. 307–308, 2002.

[113] H. C. Thoeny, F. De Keyzer, F. Chen, Y. Ni, W. Landuyt, E. K. Verbeken, and H. Bosmans, "Imaging in Monitoring the Effect of a Vascular Targeting Agent on Rhabdomyosarcoma in Rats," *Radiology*, vol. 234, pp. 756–64, 2005.

[114] S. H. Young and E. Rozengurt, "Crosstalk between insulin receptor and G protein-coupled receptor signaling systems leads to Ca^2+ oscillations in pancreatic cancer PANC-1 cells," *Biochem. Biophys. Res. Commun.*, vol. 401, pp. 154–158, 2010.

[115] A. Neesse, P. Michl, K. Frese, and C. Feig, "Stromal biology and therapy in pancreatic cancer," *Gut*, vol. 60, pp. 861–868, 2011.

[116] J. Mollenhauer, I. Roether, and H. Kern, "Distribution of extracellular matrix proteins in pancreatic ductal adenocarcinoma and its influence on tumor cell proliferation in vitro," *Pancreas*, vol. 2, pp. 14–24, 1987.

[117] T. Imamura, H. Iguchi, and T. Manabe, "Quantitative analysis of collagen and collagen subtypes I, III, and V in human pancreatic cancer, tumor-associated chronic pancreatitis, and alcoholic," *Pancreas*, vol. 11, pp. 357–364, 1995.

[118] G. S. Seo, J. Aoki, H. Moriya, O. Karakida, S. Sone, H. Hidaka, and T. Katsuyama, "Hyaline cartilage: in vivo and in vitro assessment with magnetization transfer imaging.," *Radiology*, vol. 201, no. 2, pp. 525–30, Nov. 1996.

[119] W. Li, L. Hong, L. Hu, and R. Magin, "Magnetization transfer imaging provides a quantitative measure of chondrogenic differentiation and tissue development," *Tissue Eng. Part C …*, vol. 16, pp. 1407–1415, 2010.

[120] A. M. Aisen, K. Doi, and S. D. Swanson, "Detection of liver fibrosis with magnetic cross-relaxation.," *Magn. Reson. Med.*, vol. 31, no. 5, pp. 551–6, May 1994.

[121] S. P. Li and A. R. Padhani, "Tumor response assessments with diffusion and perfusion MRI.," *J. Magn. Reson. Imaging*, vol. 35, no. 4, pp. 745–63, Apr. 2012.

[122] P. Tofts, G. Brix, D. Buckley, and J. Evelhoch, "Estimating kinetic parameters from dynamic contrast-enhanced T 1-weighted MRI of a diffusable tracer: standardized quantities and symbols," *J. Magn. Reson. Imaging*, vol. 232, pp. 223–232, 1999.

[123] a. D. Bangham, M. M. Standish, and J. C. Watkins, "Diffusion of univalent ions across the lamellae of swollen phospholipids," *J. Mol. Biol.*, vol. 13, no. 1, pp. 238–IN27, Aug. 1965.

[124] M. M. H. M. Gaber, N. N. Z. Wu, K. Hong, S. K. Huang, M. W. Dewhirst, and D. Papahadjopoulos, "Thermosensitive liposomes: extravasation and release of contents in tumor microvascular networks," *Int. J. …*, vol. 36, no. 5, pp. 1177–1187, 1996.

[125] C. Safinya and K. EWERT, "Liposomes derived from molecular vases," *Nature*, vol. 489, no. 20, pp. 8–10, 2012.

[126] L. Zhang, F. X. Gu, J. M. Chan, A. Z. Wang, R. S. Langer, and O. C. Farokhzad, "Nanoparticles in medicine: therapeutic applications and developments.," *Clin. Pharmacol. Ther.*, vol. 83, no. 5, pp. 761–9, May 2008.

[127] D. Lasic and D. Papahadjopoulos, *Medical applications of liposomes*. Elsevier, 1998, p. 779.

[128] S. B. Kaye, "Liposomes—Problems and promise as selective drug carriers," *Cancer Treat. Rev.*, vol. 8, no. 1, pp. 27–50, Mar. 1981.

[129] G. Gregoriadis, "The carrier potential of liposomes in biology and medicine (first of two parts).," *N. Engl. J. Med.*, vol. 295, no. 13, pp. 704–10, Sep. 1976.

[130] W. J. M. Mulder, G. J. Strijkers, G. a F. van Tilborg, A. W. Griffioen, and K. Nicolay, "Lipid-based nanoparticles for contrast-enhanced MRI and molecular imaging.," *NMR Biomed.*, vol. 19, no. 1, pp. 142–64, Feb. 2006.

[131] S. Zhang, H.-J. Sun, A. D. Hughes, R.-O. Moussodia, A. Bertin, Y. Chen, D. J. Pochan, P. a Heiney, M. L. Klein, and V. Percec, "Self-assembly of amphiphilic Janus dendrimers into uniform onion-like dendrimersomes with predictable size and number of bilayers.," *Proc. Natl. Acad. Sci. U. S. A.*, vol. 111, no. 25, pp. 9058–63, Jun. 2014.

[132] K. M. Laginha, S. Verwoert, G. J. R. Charrois, and T. M. Allen, "Determination of doxorubicin levels in whole tumor and tumor nuclei in murine breast cancer tumors," *Clin. Cancer Res.*, vol. 11, no. 19 Pt 1, pp. 6944–9, Oct. 2005.

[133] S. Bandak, D. Goren, and A. Horowitz, "Pharmacological studies of cisplatin encapsulated in long-circulating liposomes in mouse tumor models," *Anticancer. Drugs*, 1999.

[134] T. M. Allen, M. S. Newman, M. C. Woodle, E. Mayhew, and P. S. Uster, "Pharmacokinetics and anti-tumor activity of vincristine encapsulated in sterically stabilized liposomes," *Int. J. Cancer*, vol. 62, no. 2, pp. 199–204, Jul. 1995.

[135] R. Krishna, M. S. Webb, G. St Onge, and L. D. Mayer, "Liposomal and nonliposomal drug pharmacokinetics after administration of liposome-encapsulated vincristine and their contribution to drug tissue distribution properties.," *J. Pharmacol. Exp. Ther.*, vol. 298, no. 3, pp. 1206–12, Sep. 2001.

[136] S. C. White, P. Lorigan, G. P. Margison, J. M. Margison, F. Martin, N. Thatcher, H. Anderson, and M. Ranson, "Phase II study of SPI-77 (sterically stabilised liposomal cisplatin) in advanced non-small-cell lung cancer.," *Br. J. Cancer*, vol. 95, no. 7, pp. 822–8, Oct. 2006.

[137] C. R. Dass, T. L. Walker, M. A. Burton, and E. E. Decruz, "Enhanced Anticancer Therapy Mediated by Specialized Liposomes," *J. Pharm. Pharmacol.*, vol. 49, no. 10, pp. 972–975, Oct. 1997.

[138] A. Schroeder, R. Honen, K. Turjeman, A. Gabizon, J. Kost, and Y. Barenholz, "Ultrasound triggered release of cisplatin from liposomes in murine tumors.," *J. Control. Release*, vol. 137, no. 1, pp. 63–8, Jul. 2009.

[139] P. Shum, J.-M. Kim, and D. H. Thompson, "Phototriggering of liposomal drug delivery systems," *Adv. Drug Deliv. Rev.*, vol. 53, no. 3, pp. 273–284, Dec. 2001.

[140] H. Karanth and R. S. R. Murthy, "pH-sensitive liposomes--principle and application in cancer therapy.," *J. Pharm. Pharmacol.*, vol. 59, no. 4, pp. 469–83, Apr. 2007.

[141] E. Evans and D. Needham, "Physical properties of surfactant bilayer membranes: thermal transitions, elasticity, rigidity, cohesion and colloidal interactions," *J. Phys. Chem.*, vol. 91, no. 16, pp. 4219–4228, Jul. 1987.

[142] L. Cruzeiro-Hansson and O. Mouritsen, "Passive ion permeability of lipid membranes modelled via lipid-domain interfacial area," *Biochim. Biophys. Acta (BBA)- …*, 1988.

[143] D. Papahadjopoulos, K. Jacobson, S. Nir, and I. Isac, "Phase transitions in phospholipid vesicles fluorescence polarization and permeability measurements concerning the effect of temperature and cholesterol," *Biochim. Biophys. …*, 1973.

[144] H. Grüll and S. Langereis, "Hyperthermia-triggered drug delivery from temperature-sensitive liposomes using MRI-guided high intensity focused ultrasound," *J. Control. Release*, vol. 161, no. 2, pp. 317–27, Jul. 2012.

[145] M. Ruocco, D. Siminovitch, and R. Griffin, "Comparative study of the gel phases of ether-and ester-linked phosphatidylcholines," *Biochemistry*, 1985.

[146] A. Blume, "A comparative study of the phase transitions of phospholipid bilayers and monolayers," *Biochim. Biophys. Acta (BBA)-Biomembranes*, 1979.

[147] J. Weinstein, R. Magin, M. Yatvin, and D. Zaharko, "Liposomes and local hyperthermia: selective delivery of methotrexate to heated tumors," *Science (80-.).*, vol. 204, no. 4389, pp. 188–191, 1979.

[148] Y. Zou, M. Ueno, M. Yamagishi, I. Horikoshi, I. Yamashita, K. Tazawa, and X. Gu, "Targeting Behavior of Hepatic Artery Injected Temperature Sensitive Liposomal Adriamycin on Tumor-Bearing Rats," *Sel. Cancer Ther.*, vol. 6, no. 3, pp. 119–127, Jan. 1990.

[149] M. B. Yatvin, H. Muhlensiepen, W. Porschen, J. N. Weinstein, and L. E. Feinendegen, "Selective Delivery of Liposome-associated cis-Dichlorodiammineplatinum(II) by Heat and Its Influence on Tumor Drug Uptake and Growth," *Cancer Res.*, vol. 41, no. 5, pp. 1602–1607, May 1981.

[150] S. Unezaki, K. Maruyama, N. Takahashi, M. Koyama, T. Yuda, A. Suginaka, and M. Iwatsuru, "Enhanced Delivery and Antitumor Activity of Doxorubicin Using Long-Circulating Thermosensitive Liposomes Containing Amphipathic Polyethylene Glycol in Combination with Local Hyperthermia," *Pharm. Res.*, vol. 11, no. 8, pp. 1180–1185, Aug. 1994.

[151] Y. Nibu, T. Inoue, and I. Motoda, "Effect of headgroup type on the miscibility of homologous phospholipids with different acyl chain lengths in hydrated bilayer," *Biophys. Chem.*, vol. 56, no. 3, pp. 273–280, Nov. 1995.

[152] M. H. Gaber, K. Hong, S. K. Huang, and D. Papahadjopoulos, "Thermosensitive Sterically Stabilized Liposomes: Formulation and in Vitro Studies on Mechanism of Doxorubicin Release by Bovine Serum and Human Plasma," *Pharm. Res.*, vol. 12, no. 10, pp. 1407–1416, Oct. 1995.

[153] D. Needham, G. Anyarambhatla, G. Kong, and M. W. M. Dewhirst, "A new temperature-sensitive liposome for use with mild hyperthermia: characterization and testing in a human tumor xenograft model," *Cancer Res.*, vol. 60, no. 5, pp. 1197–1201, 2000.

[154] G. Kong, G. Anyarambhatla, W. P. Petros, R. D. Braun, O. M. Colvin, D. Needham, and M. W. Dewhirst, "Efficacy of liposomes and hyperthermia in a human tumor xenograft model: importance of triggered drug release," *Cancer Res.*, vol. 60, no. 24, pp. 6950–7, Dec. 2000.

[155] D. L. Bratton, R. Adron Harris, K. L. Clay, and P. M. Henson, "Effects of platelet activating factor and related lipids on phase transition of dipalmitoylphosphatidylcholine," *Biochim. Biophys. Acta - Biomembr.*, vol. 941, no. 1, pp. 76–82, Jun. 1988.

[156] M. L. Matteucci, G. Anyarambhatla, G. Rosner, C. Azuma, P. E. Fisher, M. W. Dewhirst, D. Needham, and D. E. Thrall, "Hyperthermia increases accumulation

of technetium-99m-labeled liposomes in feline sarcomas.," *Clin. Cancer Res.*, vol. 6, no. 9, pp. 3748–55, Sep. 2000.

[157] D. Needham and M. W. Dewhirst, "The development and testing of a new temperature-sensitive drug delivery system for the treatment of solid tumors.," *Adv. Drug Deliv. Rev.*, vol. 53, no. 3, pp. 285–305, Dec. 2001.

[158] C. D. Landon, J.-Y. Park, D. Needham, and M. W. Dewhirst, "Nanoscale Drug Delivery and Hyperthermia: The Materials Design and Preclinical and Clinical Testing of Low Temperature-Sensitive Liposomes Used in Combination with Mild Hyperthermia in the Treatment of Local Cancer.," *Open Nanomed. J.*, vol. 3, pp. 38–64, Jan. 2011.

[159] L. M. Ickenstein, M. C. Arfvidsson, D. Needham, L. D. Mayer, and K. Edwards, "Disc formation in cholesterol-free liposomes during phase transition," *Biochim. Biophys. Acta - Biomembr.*, vol. 1614, no. 2, pp. 135–138, Aug. 2003.

[160] A. Gasselhuber, M. R. Dreher, A. Negussie, B. J. Wood, F. Rattay, and D. Haemmerich, "Mathematical spatio-temporal model of drug delivery from low temperature sensitive liposomes during radiofrequency tumour ablation," *Int. J. Hyperthermia*, vol. 26, no. 5, pp. 499–513, Jan. 2010.

[161] M. C. Sandström, L. M. Ickenstein, L. D. Mayer, and K. Edwards, "Effects of lipid segregation and lysolipid dissociation on drug release from thermosensitive liposomes.," *J. Control. Release*, vol. 107, no. 1, pp. 131–42, Sep. 2005.

[162] B. Banno, L. M. Ickenstein, G. N. C. Chiu, M. B. Bally, J. Thewalt, E. Brief, and E. K. Wasan, "The functional roles of poly(ethylene glycol)-lipid and lysolipid in the drug retention and release from lysolipid-containing thermosensitive liposomes in vitro and in vivo.," *J. Pharm. Sci.*, vol. 99, no. 5, pp. 2295–308, May 2010.

[163] L. Lindner, M. Eichhorn, and H. Eibl, "Novel temperature-sensitive liposomes with prolonged circulation time," *Clin. Cancer Res.*, pp. 2168–2178, 2004.

[164] M. Hossann, M. Wiggenhorn, A. Schwerdt, K. Wachholz, N. Teichert, H. Eibl, R. D. Issels, and L. H. Lindner, "In vitro stability and content release properties of phosphatidylglyceroglycerol containing thermosensitive liposomes.," *Biochim. Biophys. Acta*, vol. 1768, no. 10, pp. 2491–9, Oct. 2007.

[165] A. H. Negussie, P. S. Yarmolenko, A. Partanen, A. Ranjan, G. Jacobs, D. Woods, H. Bryant, D. Thomasson, M. W. Dewhirst, B. J. Wood, and others,

"Formulation and characterisation of magnetic resonance imageable thermally sensitive liposomes for use with magnetic resonance-guided high intensity focused ultrasound," *Int. J. Hyperth.*, vol. 27, no. 2, pp. 140–155, 2011.

[166] A. Ranjan, G. C. Jacobs, D. L. Woods, A. H. Negussie, A. Partanen, P. S. Yarmolenko, C. E. Gacchina, K. V Sharma, V. Frenkel, B. J. Wood, and M. R. Dreher, "Image-guided drug delivery with magnetic resonance guided high intensity focused ultrasound and temperature sensitive liposomes in a rabbit Vx2 tumor model.," *J. Control. Release*, vol. i, Dec. 2011.

[167] M. L. Hauck, S. M. LaRue, W. P. Petros, J. M. Poulson, D. Yu, I. Spasojevic, A. F. Pruitt, A. Klein, B. Case, D. E. Thrall, D. Needham, and M. W. Dewhirst, "Phase I trial of doxorubicin-containing low temperature sensitive liposomes in spontaneous canine tumors.," *Clin. Cancer Res.*, vol. 12, no. 13, pp. 4004–10, Jul. 2006.

[168] R. Poon, "Lyso-thermosensitive liposomal doxorubicin: a novel approach to enhance efficacy of thermal ablation of liver cancer," *Expert Opin. Pharmacother*, vol. 10, no. 2, pp. 333–343, 2009.

[169] R. P. Julie Locklin, Steven Libutti, Ziv Neeman, Matt Dreher, "Imaging features in patients undergoing liver RFA puls Heat Deployed Nanoparticles," *SIR-Society Interv. Radiol. Conf.*, 2008.

[170] M. de Smet, E. Heijman, S. Langereis, N. Hijnen, and H. Grüll, "Magnetic resonance imaging of high intensity focused ultrasound mediated drug delivery from temperature sensitive liposomes; An in vivo proof-of-concept study," *J. Control. Release*, vol. 150, no. 1, pp. 102–110, 2010.

[171] C. Perez and S. Sapareto, "Thermal Dose Expression in Clinical Hyperthermia and Correlation with Tumor Response/Control," *Cancer Res.*, 1984.

[172] C. W. Song, M. S. Kang, J. G. Rhee, and S. H. Levitt, "Effect of hyperthermia on vascular function in normal and neoplastic tissues," *Ann. N. Y. Acad. Sci.*, vol. 335, no. 1 Thermal Chara, pp. 35–47, Mar. 1980.

[173] T. Dudar and R. Jain, "Differential response of normal and tumor microcirculation to hyperthermia," *Cancer Res.*, pp. 605–612, 1984.

[174] C. Song, "Effect of Local Hyperthermia on Blood Flow and Microenvironment : A Review," *Cancer Res.*, 1984.

[175] C. W. Song, A. Lokshina, J. G. Rhee, M. Patten, and S. H. Levitt, "Implication of blood flow in hyperthermic treatment of tumors.," *IEEE Trans. Biomed. Eng.*, vol. 31, no. 1, pp. 9–16, Jan. 1984.

[176] M. R. Horsman and J. Overgaard, "Can mild hyperthermia improve tumour oxygenation?," Jul. 2009.

[177] R. K. Jain, "Transport of molecules across tumor vasculature," *CANCER METASTASIS Rev.*, vol. 6, no. 4, pp. 559–593, Dec. 1987.

[178] G. Kong and M. W. Dewhirst, "Review Hyperthermia and liposomes," *Int. J. Hyperth.*, vol. 15, no. 5, pp. 345–370, Jan. 1999.

[179] P. Wust, B. Hildebrandt, and G. Sreenivasa, "Hyperthermia in combined treatment of cancer," *Lancet Oncol.*, pp. 487–497, 2002.

[180] A. Ponce, B. Viglianti, and D. Yu, "Magnetic resonance imaging of temperature-sensitive liposome release: drug dose painting and antitumor effects," *J. Natl. Cancer Inst.*, vol. 99, no. 1, pp. 53–63, 2007.

[181] S. Dromi, V. Frenkel, A. Luk, B. Traughber, M. Angstadt, M. Bur, J. Poff, J. Xie, S. K. Libutti, K. C. P. Li, and B. J. Wood, "Pulsed-high intensity focused ultrasound and low temperature-sensitive liposomes for enhanced targeted drug delivery and antitumor effect.," *Clin. Cancer Res.*, vol. 13, no. 9, pp. 2722–7, May 2007.

[182] P. R. Patel, A. Luk, A. Durrani, S. Dromi, J. Cuesta, M. Angstadt, M. R. Dreher, B. J. Wood, and V. Frenkel, "In vitro and in vivo evaluations of increased effective beam width for heat deposition using a split focus high intensity ultrasound (HIFU) transducer.," *Int. J. Hyperthermia*, vol. 24, no. 7, pp. 537–49, Nov. 2008.

[183] B. E. O'Neill and K. C. P. Li, "Augmentation of targeted delivery with pulsed high intensity focused ultrasound.," *Int. J. Hyperthermia*, vol. 24, no. 6, pp. 506–20, Sep. 2008.

[184] A. Partanen, P. S. Yarmolenko, A. Viitala, S. Appanaboyina, D. Haemmerich, A. Ranjan, G. Jacobs, D. Woods, J. Enholm, B. J. Wood, and M. R. Dreher, "Mild hyperthermia with magnetic resonance-guided high-intensity focused ultrasound for applications in drug delivery.," *Int. J. Hyperthermia*, vol. 28, no. 4, pp. 320–36, Jan. 2012.

[185] R. Staruch, R. Chopra, and K. Hynynen, "Localised drug release using MRI-controlled focused ultrasound hyperthermia.," *Int. J. Hyperthermia*, vol. 27, no. 2, pp. 156–71, Jan. 2011.

[186] T. Ichikawa, S. M. Erturk, U. Motosugi, H. Sou, H. Iino, T. Araki, and H. Fujii, "High-b value diffusion-weighted MRI for detecting pancreatic adenocarcinoma: preliminary results.," *AJR. Am. J. Roentgenol.*, vol. 188, no. 2, pp. 409–14, Feb. 2007.

[187] T. Niwa, M. Ueno, S. Ohkawa, T. Yoshida, T. Doiuchi, K. Ito, and T. Inoue, "Advanced pancreatic cancer: the use of the apparent diffusion coefficient to predict response to chemotherapy.," *Br. J. Radiol.*, vol. 82, no. 973, pp. 28–34, Jan. 2009.

[188] R. Fattahi, N. C. Balci, W. H. Perman, E. C. Hsueh, S. Alkaade, N. Havlioglu, and F. R. Burton, "Pancreatic diffusion-weighted imaging (DWI): comparison between mass-forming focal pancreatitis (FP), pancreatic cancer (PC), and normal pancreas.," *J. Magn. Reson. Imaging*, vol. 29, no. 2, pp. 350–6, Feb. 2009.

[189] Z. He, J. L. Evelhoch, R. M. Mohammad, N. V Adsay, G. R. Pettit, V. K. Vaitkevicius, and F. H. Sarkar, "Magnetic resonance imaging to measure therapeutic response using an orthotopic model of human pancreatic cancer," *Pancreas*, vol. 21, no. 1, pp. 69–76, Jul. 2000.

[190] H. Poptani, U. Duvvuri, C. G. Miller, A. Mancuso, S. Charagundla, N. W. Fraser, J. D. Glickson, J. S. Leigh, and R. Reddy, "T1ρ imaging of murine brain tumors at 4 T.," *Acad. Radiol.*, vol. 8, pp. 42–47, 2001.

[191] J. L. Evelhoch, R. J. Gillies, G. S. Karczmar, J. A. Koutcher, R. J. Maxwell, O. Nalcioglu, N. Raghunand, S. M. Ronen, B. D. Ross, and H. M. Swartz, "Applications of magnetic resonance in model systems: cancer therapeutics.," *Neoplasia*, vol. 2, no. 1–2, pp. 152–65.

[192] C. A. Schneider, W. S. Rasband, and K. W. Eliceiri, "NIH Image to ImageJ: 25 years of image analysis," *Nat. Methods*, vol. 9, no. 7, pp. 671–675, Jun. 2012.

[193] W. Li, Z. Zhang, J. Nicolai, G.-Y. Yang, R. a Omary, and A. C. Larson, "Magnetization transfer MRI in pancreatic cancer xenograft models," *Magn. Reson. Med.*, vol. 000, pp. 1–7, Dec. 2011.

[194] D. D. Von Hoff, R. Korn, and S. Mousses, "Pancreatic cancer--could it be that simple? A different context of vulnerability.," *Cancer Cell*, vol. 16, no. 1, pp. 7–8, Jul. 2009.

[195] D. Li, K. Xie, R. Wolff, and J. Abbruzzese, "Pancreatic cancer.," *Lancet*, vol. 363, no. 9414, pp. 1049–57, Mar. 2004.

[196] Burris, HA, M. Moore, J. Andersen, M. Green, M. Rothenberg, M. Modiano, M. Cripps, R. Portenoy, A. Storniolo, P. Tarassoff, R. Nelson, F. Dorr, C. Stephens, and D. Von Hoff, "Improvements in survival and clinical benefit with gemcitabine as first- line therapy for patients with advanced pancreas cancer: a randomized trial," *J. Clin. Oncol.*, vol. 15, no. 6, pp. 2403–2413, Jun. 1997.

[197] M. Tempero, W. Plunkett, V. Ruiz Van Haperen, J. Hainsworth, H. Hochster, R. Lenzi, and J. Abbruzzese, "Randomized phase II comparison of dose-intense gemcitabine: thirty-minute infusion and fixed dose rate infusion in patients with pancreatic adenocarcinoma.," *J. Clin. Oncol.*, vol. 21, no. 18, pp. 3402–8, Sep. 2003.

[198] T. M. Allen and P. R. Cullis, "Drug delivery systems: entering the mainstream.," *Science*, vol. 303, no. 5665, pp. 1818–22, Mar. 2004.

[199] Y. Bae and K. Park, "Targeted drug delivery to tumors: myths, reality and possibility," *J. Control. release*, vol. 153, no. 3, pp. 198–205, 2011.

[200] T. Corbett, B. Roberts, and W. Leopold, "Induction and chemotherapeutic response of two transplantable ductal adenocarcinomas of the pancreas in C57BL/6 mice," *Cancer Res.*, pp. 717–726, 1984.

[201] A. M. Al-Abd, N. H. Kim, S.-C. Song, S. J. Lee, and H.-J. Kuh, "A simple HPLC method for doxorubicin in plasma and tissues of nude mice.," *Arch. Pharm. Res.*, vol. 32, no. 4, pp. 605–11, Apr. 2009.